Targeting Liver Epsins Ameliorates Dyslipidemia in Atherosclerosis

Bo Zhu[1#], Krishan Gupta[2#], Kui Cui[1#], Beibei Wang[1], Marina V. Malovichko[4], Xiangfei Han[3], Kathryn Li[1], Hao Wu[1] , Kulandai Samy Arulsamy[2], Bandana Singh[1], Jianing Gao[1], Scott Wong[1], Douglas B. Cowan[1], Dazhi Wang[5], Sudha Biddinger[6], Sanjay Srivastava[4], ,Jinjun Shi[3], Kaifu Chen[2*], Hong Chen[1*]

[1]Vascular Biology Program, Boston Children's Hospital, Department of Surgery, Harvard Medical School, Boston, MA, United States

[2] Department of Cardiology, Boston Children's Hospital, Harvard Medical School, Boston, MA, United States

[3] Department of Anesthesiology, Brigham and Women's Hospital, Harvard Medical School, Boston, MA, United States

[4] Department of Medicine, Division of Cardiovascular Medicine, University of Louisville, Louisville, KY, United States

[5]College of Medicine Molecular Pharmacology, University of South Florida, Tampa, FL, United States

[6] Division of Endocrinology, Boston Children's Hospital, Harvard Medical School, Boston, MA, United States

Abstract

Rationale: Low density cholesterol receptor (LDLR) in the liver is critical for the clearance of low-density lipoprotein cholesterol (LDL-C) in the blood. In atherogenic conditions, proprotein convertase subtilisin/kexin 9 (PCSK9) secreted by the liver, in a nonenzymatic fashion, binds to LDLR on the surface of hepatocytes, preventing its recycling and enhancing its degradation in lysosomes, resulting in reduced LDL-C clearance. Our recent studies demonstrate that epsins, a family of ubiquitin-binding endocytic adaptors, are critical regulators of atherogenicity. Given the fundamental contribution of circulating LDL-C to atherosclerosis, we hypothesize that liver epsins promote atherosclerosis by controlling LDLR endocytosis and degradation.

Objective: We will determine the role of liver epsins in promoting PCSK9-mediated LDLR degradation and hindering LDL-C clearance to propel atherosclerosis.

Methods and Results: We generated double knockout mice in which both paralogs of epsins, namely, epsin-1 and epsin-2, are specifically deleted in the liver (Liver-DKO) on an ApoE $^{-/-}$ background. We discovered that western diet (WD)-induced atherogenesis was greatly inhibited, along with diminished blood cholesterol and triglyceride levels. Mechanistically, using scRNA-seq analysis on cells isolated from the livers of ApoE$^{-/-}$ and ApoE$^{-/-}$ /Liver-DKO mice on WD, we found lipogenic Alb ^{hi} hepatocytes to glycogenic HNF4α ^{hi} hepatocytes transition in ApoE$^{-/-}$ /Liver-DKO. Subsequently, gene ontology analysis of hepatocyte-derived data revealed elevated pathways involved in LDL particle clearance and very-low-density lipoprotein (VLDL) particle clearance under WD treatment in ApoE$^{-/-}$ /Liver-DKO, which was coupled with diminished plasma LDL-C levels. Further analysis using the MEBOCOST algorithm revealed enhanced communication score between LDLR and cholesterol, suggesting elevated LDL-C clearance in the

ApoE$^{-/-}$ Liver-DKO mice. In addition, we showed that loss of epsins in the liver upregulates of LDLR protein level. We further showed that epsins bind LDLR via the ubiquitin-interacting motif (UIM), and PCSK9-triggered LDLR degradation was abolished by depletion of epsins, preventing atheroma progression. Finally, our therapeutic strategy, which involved targeting liver epsins with nanoparticle-encapsulated siRNAs, was highly efficacious at inhibiting dyslipidemia and impeding atherosclerosis.

Conclusions: Liver epsins promote atherogenesis by mediating PCSK9-triggered degradation of LDLR, thus raising the circulating LDL-C levels. Targeting epsins in the liver may serve as a novel therapeutic strategy to treat atherosclerosis by suppression of PCSK9-mediated LDLR degradation.

#: first co-authors with equal contribution; *: corresponding author

Introduction

Atherosclerosis is the major contributor to many cardiovascular diseases (CVDs), including coronary artery disease, stroke and peripheral vascular disease [1]. CVDs are the leading causes of death globally, in the United States alone, approximately 610,000 individuals succumb to heart-related ailments annually, constituting nearly one-quarter of all deaths[2]. This chronic disease initiates with lipid accumulation in the subendothelial space of arterial walls, followed by an inflammatory response that accelerates atherosclerotic plaque formation[3]. Understanding the molecular mechanisms responsible for the initiation, growth, and destabilization of atheroma is essential for the development of more effective and targeted therapies to prevent ischemic injury, disability, or death in patients with CVDs[4].

Modern lifestyles have rendered millions susceptible to hyperlipidemia, a key risk factor for atherosclerosis. In addition to diet-induced hyperlipidemia, familial hypercholesterolaemia (FH) is the most common inherited metabolic diseases that featured as markedly elevated plasma levels of low-density lipoprotein cholesterol (LDL-C)[5]. Mutations in low-density lipoprotein receptor (LDLR) are the main genetic cause of elevated LDL-C levels in familial hypercholesterolemia[6]. In the intima, LDL-C undergoes oxidative modifications by reactive oxygen species, and the oxidized LDL cholesterol (oxLDL-C) is then taken up by macrophages for the formation of foam cells [7]. Cholesterol-laden foam cells trigger the secretion of proinflammatory cytokines, as the inflammatory master cytokine, IL-1β activates the expression of many proinflammatory cytokines[8]. The infiltration of circulating macrophages, leukocytes, and monocytes into the atherosclerotic lesion pave the way for atherosclerosis progression[9]. Hence, strategies targeting LDL-C reduction are pivotal in combating inflammation-induced atherosclerosis.

The regulation of LDL-C involves its clearance by LDLRs, predominantly expressed in hepatocytes. LDLR is a cell surface protein predominantly expressed in hepatocytes and is the primary mechanism whereby excess LDL-C is removed from the circulation[10]. Proprotein convertase subtilisin/kexin type 9 (PCSK9) is primarily expressed in the liver, which promotes LDLR degradation and results in higher levels of circulating LDL-C[11]. PCSK9 inhibitors were widely reported to be good candidates for lipid-lowering since they can prevent the degradation of

LDLR by inhibition of the interaction between PCSK9 and LDLR. LDLR deficient mice and LDLR-KO rabbits are good model for atherosclerosis study by inducing hyperlipidemia[12,13]. In addition, Keeter *et al.* reported that overexpression of PCSK9 that mediated by Adeno-associated virus-8 (AAV8) induces hyperlipidemia and promotes atherosclerosis[14]. A recent in vivo CRISPR based-editing strategy, namely, VERV101, achieved potent and durable inactivation of the expression of PCSK9 in the liver, resulting in significant reduction of LDL-C in nonhuman primates, making it promising strategy to treat hyperlipidemia[15].

Despite these advancements, the mechanistic details of PCSK9-mediated LDLR degradation remain insufficiently understood, posing a challenge in identifying dual-action targets that both reduce cholesterol synthesis and prevent LDLR degradation. Epsins, a family of endocytic adaptor proteins, have recently gained attention for their role in atherosclerosis[16]. We previously showed that epsins 1 and 2 are upregulated in atherosclerotic plaques in apolipoprotein E-deficient (ApoE$^{-/-}$) mice fed a western diet (WD), endothelial cell (EC)-specific epsin deficiency resulted in marked attenuation of atherogenesis in ApoE$^{-/-}$ mice fed a WD[4]. Mechanistically, epsin-deficiency reduced arterial inflammation by dampening expression of adhesion molecules and hindering macrophage recruitment. We also showed that myeloid-restricted epsin deficiency in ApoE$^{-/-}$ mice fed a WD retarded atherogenesis by eradicating foam cell formation and augmenting efferocytosis in the lesion[17,18]. Given that the liver is one of the main sites for cholesterol and lipid synthesis [19,20], whether epsins in the liver regulate circulating LDL-C levels through modulating LDLR stability in atherosclerotic mice has not been investigated.

In this study, we investigated the potential role epsins in the liver play in regulating atherosclerosis using novel ApoE$^{-/-}$ mice harboring liver-specific deficiency of epsins (ApoE$^{-/-}$/Liver-DKO). We discovered that WD-induced atherogenesis was greatly inhibited and accompanied with diminished blood cholesterol and triglyceride levels. Mechanistically, scRNA-seq analysis identified a transition from lipogenic Alb^{hi} hepatocytes to glycogenic HNF4α^{hi} hepatocytes in ApoE$^{-/-}$/Liver-DKO mice. Gene Ontology (GO) enrichment analysis revealed upregulated pathways for LDL particle clearance in ApoE$^{-/-}$/Liver-DKO mice. Additively, we further showed that epsins bind LDLR via the ubiquitin-interacting motif (UIM), PCSK9-triggered LDLR degradation was abolished by depletion of epsins that prevent the atheroma progression. Furthermore, our findings uncovered liver epsins mediated PCSK9-triggered LDLR ubiquitination for degradation. Intriguingly, we found elevated liver epsins expression in the hepatocytes from gain-of-function PCSK9 D374Y mutation mice that promote LDLR degradation. Finally, our therapeutic study by targeting liver epsins with nanoparticle-encapsulated siRNAs inhibit dyslipidemia and impede atherosclerosis. Thus, liver epsins could be potentially novel therapeutic targets for combating atherosclerosis.

MATERIALS and METHODS

Animal models

In this study, all animal procedures were performed in compliance with institutional guidelines and mouse protocols were approved by the Institutional Animal Care and Use Committee (IACUC) of Boston Children's Hospital, MA, USA. Both male and female mice were used. C57BL/6 mice

134 (stock #00664), ApoE $^{-/-}$ mice (stock #002052), Alb-Cre delete mice (stock #035593) were all
135 purchased from Jackson Research Laboratory. As double knockout mice of Epsin 1 and 2 (Epsin
136 1$^{-/-}$; Epsin 2$^{-/-}$) lead to embryonic lethality, we generated conditional Epsin1 $^{fl/fl}$; Epsin2 $^{-/-}$ mice
137 previously described [21-23]. ApoE $^{-/-}$ mice, Alb-Cre$^{+/-}$ mice and Epsin1 $^{fl/fl}$; Epsin2 $^{-/-}$ mice were
138 backcrossed to C57BL/6 background. We bred Epsin1 $^{fl/fl}$; Epsin2 $^{-/-}$ mice with Alb-Cre$^{+/-}$ mice to
139 generate Epsin1 $^{fl/fl}$; Epsin2 $^{-/-}$; Alb-Cre$^{+/-}$ liver-specific Epsins deficient (Liver-DKO) mice (Fig.
140 S1).
141
142 The detailed information of all the mice used in this study were described in Fig. S1. In addition,
143 we bred Epsin1 $^{fl/fl}$; Epsin2 $^{-/-}$; Alb-Cre$^{+/-}$ mice with ApoE $^{-/-}$ (C57BL/6) background to generate
144 Epsin1 $^{fl/fl}$; Epsin2 $^{-/-}$; Alb-Cre$^{+/-}$; ApoE $^{-/-}$ mice (Liver-DKO/ ApoE $^{-/-}$) (Fig. S1).
145
146 The control mice for Epsin1 $^{fl/fl}$; Epsin2 $^{-/-}$; Alb-Cre$^{+/-}$ (Liver-DKO) mice were Epsin $^{+/+}$; Epsin2
147 $^{+/+}$; Alb-Cre $^{+/-}$ mice (WT) (Figure S1). The control mice for Epsin1 $^{fl/fl}$; Epsin2 $^{-/-}$; Alb-Cre$^{+/-}$;
148 ApoE $^{-/-}$ mice (Liver-DKO/ ApoE $^{-/-}$) were Epsin $^{+/+}$; Epsin2 $^{+/+}$; Alb-Cre $^{+/-}$; ApoE$^{-/-}$ (WT/ApoE^{-}
149 $^{/-}$) (Fig. S1).
150
151 To induce atherosclerosis, mice were fed Western diet (WD, Protein 17% kcal, Fat 40% kcal,
152 Carbohydrate 43% kcal; D12079B, Research Diets, New Brunswick, USA) starting at the age of
153 6-8 weeks for 8-16 weeks. Mice were sacrificed at different time points based on experimental
154 design and liver, blood, heart, aorta were harvested.
155
156 For control mice, in addition to ApoE$^{-/-}$; Epsin 1$^{+/+}$; Epsin 2 $^{+/+}$ mice, we also used ApoE$^{-/-}$; Epsin
157 1$^{+/+}$; Epsin 2 $^{+/+}$ mice with a single copy of Alb-Cre, and ApoE $^{-/-}$ mice ; Epsin1 $^{fl/fl}$; Epsin2 $^{-/-}$
158 littermates lacking the single copy of Alb-Cre. To simplify the terminology, we refer to these
159 control mice as ApoE$^{-/-}$, as results were not different in any of the analyses we performed.
160
161 For each experimental model and time point, 6-10 mice were analyzed and both male and female
162 mice were used in separate groups. In the current study, we did not exclude any mice when
163 analyzing.
164
165
166 **Liver single-cell preparation and single-cell RNA (scRNA) sequencing**
167
168
169 For liver cell isolation, the ApoE$^{-/-}$ and ApoE$^{-/-}$ /Liver-DKO mice (n=3) were anesthetized and
170 restrained and the skin sprayed with 70% ethanol. The liver and other inner organs were revealed
171 by cutting through the skin and peritoneum. A 24G needle was carefully inserted into the inferior
172 vena cava and secured with a clamp, and chelating solution (0.05M HEPES, pH 7.2 , 10 mM
173 EGTA in HBSS without CaCl2 and MgCl2) was run at a low speed (1.5 - 2mL/minute). The portal
174 vein was then cut and perfusion speed was increased to a flow rate of 7mL/minute. After that, the
175 diaphragm was cut and the anterior vena cava clamped. The chelating perfusion was run for 7
176 minutes and then switched to collagenase solution (0.05 M HEPES, pH 7.2 , 4.7mM CaCl2, 20
177 µg/mL Liberase, Sigma LIBTM-RO) at a flow rate of 7mL/minute for 7 minutes. The liver was
178 then removed and passed through a 70 µm cell strainer with 10 ml ice-cold HBSS without CaCl2

179 and MgCl2. The resulting single-cell suspension was centrifuged at 300 g for 5 minutes at 4 °C
180 and washed twice with ice-cold HBSS.
181
182 The isolated liver cells have been counted and diluted into 1000 cells/ µL. The single cell RNA-
183 seq library construction was performed according to the 10 x genomics protocol (GEMs, Single
184 cell 3' Reagent Kits v3.1, 10 x Genomics). The prepared libraries were sequenced on the HiSeq
185 2500 Sequencing System (Illumina, San Diego, CA) with 100-bp paired end reads.
186
187
188 **ScRNA-seq data analysis**
189
190 Firstly, we employed Cell Ranger (version 7.1.0) to map the raw reads of RNA sequencing data to
191 the mouse genome (version mm10) and count the UMI for each gene. We then proceeded with the
192 resulting UMI count matrix using the Seurat R package (version 4.3.0)[24]. We retained high-quality
193 cells expressing between 200 and 2500 genes, excluding those with over 20% mitochondrial reads.
194 Additionally, we filtered out rarely expressed genes detected in fewer than 3 cells. After filtering,
195 the high-quality data was normalized, cell-level scaled with 10k reads, and natural-log transformed
196 by adding 1. The normalized data underwent further processing steps: scaling (ScaleData function),
197 principal component analysis (PCA) (RunPCA function, npcs =30), Uniform Manifold
198 Approximation and Projection (UMAP) (RunUMAP function, reduction = "pca", dims = 1:30),
199 shared nearest neighbor graph (SNNG) construction (FindNeighbors function, reduction = "pca",
200 dims = 1:30), and cell clustering (FindCluster function, resolution=0.1). Further, We conducted
201 Differentially Expressed Genes (DEGs) analysis in one cluster versus other clusters using the
202 FindAllMarkers function. The Wilcoxon test method was used by default, with a minimum
203 percentage of expressed cells set to 25% and a minimum log2 fold change of 0.25. Cell types were
204 annotated based on known marker genes from PanglaoDB[25], cell-Taxonomy[26], disco[27] databases,
205 and relevant literature. Marker gene expressions were visualized by DotPlot and VlnPlot functions.
206 For cell fate transition, trajectory analysis, and cell rank for directed single-cell transition mapping,
207 we utilized scvelo (version 0.2.5)[28,29], monocle3 (version 1.3.1)[30,31], and cellrank (version 2.0.4)[32]
208 with default parameters. For trajectory analysis, we kept Alb^{hi} hepatocytes as the initial cell type
209 and for cell rank for directed single-cell transition mapping we used the function of all states
210 terminal states and initial state with n_states=[4,5]. The metabolite-mediated cell-cell
211 communication was analyzed by MEBOCOST (version 1.0.0)[33]. The data were analyzed
212 combined for both conditions following the tutorial on the MEBOCOST website. The prediction
213 of sender-metabolite-sensor-receiver communication events was visualized by the bar and lollypop
214 plots, using the ggplot2 library. Additionally, we performed cell-cell communication analysis
215 using Cellchat (version 1.5.0)[34]. The communication probability of each condition was analyzed
216 to highlight differences between conditions, and communication events were visualized using bar,
217 flow, and circle plots. Finally, Gene Ontology (GO) functional enrichment analysis was performed
218 using the clusterProfiler R package (version 3.18.1)[35], and visualized by bar, lollipop, and cnet
219 plots.
220
221
222 **Human samples**
223

Human healthy control and diseased aortic arch samples from atherosclerosis patients were purchased from Maine Medical Center Biobank. In addition to aorta samples, liver samples from human healthy control and non-alcoholic fatty liver disease (NAFLD) patients were purchased from Maine Medical Center Biobank. The medical information of the atherosclerotic patients and healthy people samples, and NAFLD patients and healthy people samples is in Table S1. The paraffin sections were de-paraffined and performed antigen retrieval to unmask the antigenic epitope with 10 mM Sodium Citrate , pH 6.0 , with 0.5% Tween 20 at 95 °C for 30 minutes. Allow the slides to cool for 30 minutes before proceeding with staining procedure. Immunofluorescence staining of the slides was performed with the standard protocol described below.

Synthesis of DSPE-PEG-GalNAc, preparation and characterization of targeted siRNA nanoparticles (NPs)

To further improve siRNA delivery to the liver, we propose to develop targeted hybrid NPs by surface modification with galactose-based ligands that can specifically bind to the ASGPR receptor exclusively expressed on hepatocytes [36,37]. Then, a robust self-assembly method was used to prepare the targeted polymer-lipid hybrid NPs for siRNA delivery [38,39]. In brief, G0-C14 and PLGA were dissolved separately in anhydrous dimethylformamide (DMF) to form a homogeneous solution at the concentration of 2.5 mg/mL and 5 mg/mL, respectively. DSPE-PEG-OCH3 (DSPE-mPEG) and DSPE-PEG-GalNAc were dissolved in HyPure water (GE Healthcare Life Sciences, catalog no. SH30538) at the concentration of 0.1 mg/mL. 0.75 nmol Epsin1 siRNA and 0.75 nmol Epsin2 siRNA were gently mixed with 100 µL of the G0-C14 solution. The mixture of siRNA and G0-C14 was incubated at room temperature for 15 minutes to ensure the full electrostatic complexation. Next, 500 µL of PLGA polymers were added and mixed gently. The resultant solution was subsequently added dropwise into 10 mL of HyPure water containing 1 mg lipid-PEGs (i.e., 50% DSPE-PEG-GalNAc and 50% DSPE-mPEG hybrids for the GalNAc-targeted siRNA NPs, or 100% DSPE-mPEG for the non-targeted siRNA NPs) under magnetic stirring (1,000 rpm) for 30 minutes. The siRNA NPs were purified by an ultrafiltration device (EMD Millipore, MWCO 100 kDa) to remove the organic solvent and free excess compounds via centrifugation at 4 °C. After washing 3 times with HyPure water, the siRNA NPs were collected and finally resuspended in pH 7.4 PBS buffer. The NPs were used freshly or stored at -80 °C for further use. The physicochemical properties (particle size and surface charge) of GalNAc-siEpsin1/2 were characterized by dynamic light scattering (DLS, Brookhaven Instruments Corporation). The GalNAc-siEpsin1/2 was ~ 89 nm in size as measured by DLS, and their surface charge was determined to be ~ -5.3 mV.

siRNA transfection

The siRNA transfection was performed according to the manufacturer's instructions. Briefly, HepG2 cells were transfected by RNAiMAX (Invitrogen) with either scrambled siRNA duplex or epsin 1 (GAACUGGAGGCACGUCUACAAUU) or epsin 2 siRNA duplexes (GCAGUGCCGUGAGAACAUCUUUU) designed by Dharmacon™ (Horizon Discovery). At 48 hours post transfection, cells were processed for western blot assays.

RNA isolation and Real-time quantitative PCR

Total RNA was extracted from the liver tissue with Qiagen RNeasy Mini Kit based on manufacturer's instruction including the optional step to eliminate genomic DNA. The extracted RNA was used for RT-qPCR according to the experimental designs.

For RT-qPCR, mRNA was reverse transcribed to cDNA with the iScript cDNA Synthesis Kit (Bio-Rad Laboratories, Inc., Hercules, CA, United States). 2 μL of 5 fold diluted cDNA product was subjected to RT-qPCR in StepOnePlus Real-Time PCR System (Applied Biosystems) using SYBR Green PCR Master Mix reagent as the detector. PCR amplification was performed in triplicate on 96-well optical reaction plates and replicated in at least three independent experiments. The ΔΔCt method was used to analyze qPCR data. The Ct of β-actin cDNA was used to normalize all samples. Primers are listed in Major Resource Table.

Analysis of plasma triglyceride and cholesterol levels

Blood was removed from the right atrium of the mouse heart after sacrifice with isoflurane. Blood was allowed to clot for 30 minutes at room temperature followed by centrifugation at 3000 x g at 4 °C for 20 minutes. Serum was transferred to a new tube and stored at -20 °C. Serum cholesterol and lipid levels were determined using the Cholesterol Assay Kit for HDL and LDL/VLDL and Triglyceride Assay Kit from Abcam.

Atherosclerotic lesion characterization

The whole aortas were collected and fixed with 4% paraformaldehyde. Then, the aortas were stained with Oil Red O for *en face* analysis. Hearts and BCA were embedded in O.C.T compound and sectioned at 8 microns. Lesion area of the aortic root was quantified by hematoxylin and eosin (H&E) staining. Neutral lipids deposition was determined by Oil Red O staining. Aortic lesion size and lipid content of each animal were obtained by an average of three sections from the same mouse.

En face Oil Red O staining

Whole aortas were dissected symmetrically, pinned to parafilm to allow the *en face* exposed and fixed in formalin for 12 hours. Aortas were washed in PBS for 3 times, and rinsed in 100% propylene glycol followed by staining with 0.5% Oil Red O solution for 20 minutes at 65 °C. Aortas were then put in 85% propylene glycol for 2 minutes, followed by three washes in DD Water. Slides were next incubated with hematoxylin for 30 seconds, rinsed in running tap water. Imaging was performed using a Nikon SMZ1500 stereomicroscope, SPOT Insight 2Mp Firewire digital camera, and SPOT Software 5.1.

313

314 **Oil Red O staining of cryostat sections**

315 Cryostat sections of mouse aortic root and BCA were washed in PBS for 5 minutes, then fixed in
316 4% paraformaldehyde for 15 minutes. Slices were washed in PBS followed by staining with freshly
317 prepared 0.5% Oil Red O solution in isopropanol for 10 minutes at 37 °C. Slices were then put in
318 60% isopropanol for 30 seconds, followed by 3 washes in water. Slices were next incubated with
319 hematoxylin for 30 seconds, rinsed in running tap water, and mounted with 90% Glycerin.

320

321 **H&E staining**

322 Cryostat sections of mouse aortic root and BCA were washed in PBS for 5 minutes, then fixed in
323 4% paraformaldehyde for 15 minutes. Next, slides were stained with 0.1 hematoxylin for 3 minutes
324 followed by running tap water washes for 10 minutes. Slices were then dipped in Eosin working
325 solution for 30 seconds, quickly rinsed with tap water, dehydrated using graded ethanol (95% and
326 100% ethanol), followed by transparentizing by xylene: ethanol absolute (1:1) solution and 100%
327 xylene for 1 hour. Slices were mounted in synthetic resin.

328

329 **Van Gieson's staining**

330 Van Gieson's staining were performed based on manufacturer's instruction. In brief, Cryostat
331 sections of mouse aortic root and BCA were washed in PBS for 5 minutes, then fixed in 4%
332 paraformaldehyde for 15 minutes. Slices were placed in Elastic Stain Solution (5% hematoxylin +
333 10% ferric chloride + lugol's Iodine Solution) for 20 minutes, then rinsed in running tap water.
334 Then, slices were dipped in differentiating solution 20 times and in sodium thiosulfate solution for
335 1 min, following with rinsing in running tap water. Slices were dehydrated in 95% and 100%
336 alcohol once, respectively. Slides were cleared and mounted in synthetic resin.

337

338 **Immunofluorescence staining**

339 The liver tissue or aorta from both ApoE$^{-/-}$ and ApoE$^{-/-}$ Liver-DKO were subjected for
340 cryosections, and sections were further fixed in 4% paraformaldehyde for 15 minutes. The slides
341 were blocked by blocking buffer (PBS/3% BSA/3% donkey serum/0.3% triton) for 30 minutes,
342 and were further incubated by primary antibodies (epsin1, epsin2, CD68, αSMA) for overnight at
343 4°C. The slides were washed 3 times for 10 minutes each wash by PBS/0.3% triton buffer, and
344 were further incubated with secondary antibodies at room temperature for 1 hour. Then the slides
345 were washed 3 times for 10 minutes each wash by PBS/0.3% triton buffer. After the second wash,
346 DAPI was used for nuclei stain. The slides were mounted Fluoroshield™ histology mounting
347 medium. Imaging was performed using Zeiss LSM 880 Confocal Acquisition & Analysis.

348

349 **Immunoprecipitation and Western Blotting**

350 For immunoprecipitation, HepG2 cells were lysed with RIPA buffer (50 mM Tris, pH 7.4, with
351 150 mM NaCl, 1% Nonidet P-40, 0.1% SDS, 0.5% sodium deoxycholic acid, 0.1% sodium
352 dodecyl sulfate, 5 mM N-ethylmaleimide and protease inhibitor cocktail). For LDLR
353 ubiquitination experiments, HepG2 cells were lysed using denaturing buffer (1% SDS in 50 mM
354 Tris, pH 7.4) and boiled at 95 °C for 10 minutes to denature protein complexes. Lysates were re-
355 natured using nine volumes of ice-cold RIPA buffer then prepared for immunoprecipitation as
356 follows. Cell lysates were pre-treated with Protein A/G Sepharose beads at 4 °C for 2 hours to
357 remove nonspecific protein followed by centrifugation at 12000 rpm for 5 minutes at 4 °C.
358 Supernatant was transferred to a new tube, incubated with Protein A/G Sepharose beads and
359 antibodies against Epsin1 or LDLR or ubiquitin at 4 °C overnight. Mouse IgG was used as negative
360 control. Protein A/G beads were washed with RIPA buffer for 2 times, followed by PBS for 1 time.
361 Then, beads were suspended with 80 µL 2x loading buffer and heated at 95 °C for 10 minutes.
362 After centrifugation, precipitated proteins were visualized by Western blot. Proteins were resolved
363 by SDS-PAGE gel and electroblotted to nitrocellulose membranes. NC membranes were blocked
364 with 5% milk (w/v) and blotted with antibodies. Western blots were quantified using NIH Image
365 J software.

366

367 **PCSK9 Adeno-associated Virus 8 (AAV8) Tail Vein Injection**

368 Eight-week old male C57BI/6J mice, both WT and Liver-DKO mice (n=4), were intravenously
369 injected via tail vein with a single dose of 2 x 10^{11} viral PCSK9-AAV8 and fed a WD for 8 weeks
370 and 16 weeks. The serum samples collected from both WT and Liver-DKO mice were subjected
371 for triglyceride and cholesterol measurement. The liver tissue from both WT and Liver-DKO mice
372 were collected for further histology analysis and protein lysate preparation.

373

374 **Nanoparticle-encapsulated epsin1/2 siRNAs Tail Vein Injection**

375 Eight-week old male C57BI/6J mice, ApoE $^{-/-}$ mice were fed a WD for 8 weeks, and further divided
376 into two groups (n=4). The control group mice were intravenously injected via tail vein with
377 control siRNA NPs, and the experimental group mice were injected with 0.75 nmoles epsin1/2
378 siRNA NPs for continuous three weeks. Two doses injection per week. After injection, the serum
379 samples collected from both control siRNA and epsin1/2 siRNA NPs injected groups were
380 subjected for triglyceride and cholesterol measurement. The aortas were isolated *En face* ORO
381 staining and histology analysis, and the liver tissue from both control siRNA and epsin1/2 siRNA
382 NPs were collected for protein lysate preparation.

383

384 **Cell culture and plasmids transfection**

385 The HepG2 cell line (ATCC no. HB-8065) was used for plasmid transfection to map the binding
386 sites of Epsin1 to LDLR. Flag-tagged Epsin1WT, Epsin1ΔUIM, Epsin1ΔENTH, Epsin1-DPW
387 truncation constructs, and pcDNA vector were prepared previously in our laboratory. HepG2 cells
388 were cultured in DMEM (10% FBS and 1% Pen-Strep) at 37°C in humidified air containing 5%
389 CO_2 atmosphere and transfected using Lipofectamine 2000 as instructed by the manufacturer.

390

391 **Epsin1/2 siRNAs transfection and PCSK9 adeno-associated virus 8 (AAV8) infection**

392 HepG2 cells were cultured in DMEM (10% FBS and 1% Pen-Strep) at 37°C in humidified air
393 containing 5% CO2 atmosphere. One day before transfection, plate cells in 1 mL of growth
394 medium without antibiotics such that they will be 30-50% confluent at the time of transfection.
395 Prepare RNAi duplex-Lipofectamine ™ RNAiMAX complexes by mixture of Epsin1/2 siRNAs
396 and Lipofectamine™ RNAiMAX , keep the mixture at room temperature for 20 minutes, and add
397 the complexes to each well containing cells. Incubate the cells 48 hours at 37°C in a CO2 incubator.

398 The PCSK9-AAV8 virus stock (10^{13} GC/ml) was diluted by culture media into 10^{10} GC for the
399 infection. Remove the original cell culture media, and add the PCSK9-AAV8 virus containing
400 media to cell culture. Collect the cells 3 days after the PCSK9-AAV8 virus infection.

401 **Hepatocyte Primary Culture, MG132 treatment, PCSK9-AAV8 virus infection**

402 The anaesthetized animals (WT and Liver-DKO) were restrained and the skin sprayed with 70%
403 ethanol. The liver and other inner organs were revealed by cutting through the skin and peritoneum.
404 A 24G needle was carefully inserted into the inferior vena cava and secured with a clamp, and
405 chelating solution (0.05 M HEPES pH 7.2, 10 mM EGTA in HBSS without $CaCl_2$ and $MgCl_2$)
406 was run at a low speed (1.5-2 mL/min). The portal vein was then cut and perfusion speed was
407 increased to a flow rate of 7 mL/min. After that, the diaphragm was cut and the anterior vena cava
408 clamped. The chelating perfusion was run for 7 minutes and then switched to collagenase solution
409 (0.05 M HEPES pH 7.2, 4.7 mM $CaCl_2$ 1 mg/mL Liberase, Sigma LIBTM-RO) at a flow rate of
410 2-4 mL/minute for 15 minutes. The liver was transferred to a 10 cm plate with plating media
411 (DMEM low glucose, 5% FBS, 1% Penicillin-Streptomycin Solution), the liver cells were gently
412 released with fine tip forceps. The liver cells suspension was filtered through a 70 μm cell strainer
413 into a 50 mL tube. Spin at 50 x g for 2 minutes at 4 °C. While the samples are spinning, prepare
414 fresh Percoll solution (90% Percoll in 1xHBSS). Aspirate the supernatant , add 10 mL plating
415 media and resuspend by gentle swirling, and further add 10 mL Percoll solution and mix
416 thoroughly by inverting the tube several times. Spin at 200 x g for 10 minutes at 4 °C. Aspirate the
417 supernatant, and add 20 mL plating media , and then spin at 50 x g for 2 minutes at 4 °C. Aspirate
418 supernatant, and add 20 mL plating media. Hepatocytes were counted and plated on collagen-
419 coated cell culture 6-well plates. After 3 hours, change medium to warm maintenance media
420 (Williams E media, 1% Glutamine, 1% Penicillin-Streptomycin Solution).

After 24 hours, proteasome inhibitor MG132 solution was added into the cultured primary hepatocyte cells. After 6 hours, the primary culture hepatocytes were subjected to PCSK9-AAV8 virus infection as mentioned above. The primary culture hepatocytes were collected and lysed for protein preparation.

Statistical analysis

Gene expression was assessed by quantifying mRNA levels of target genes via qPCR, with normalization to the internal control, β-actin. Quantitative data were analyzed using either one-way ANOVA or Student's t-test, as appropriate, with Prism software (GraphPad Software, San Diego, CA) running on Apple OS X. All data are presented as are the mean ± SEM.

Data availability

The scRNA-seq data (GSE273386) of the ApoE$^{-/-}$ and ApoE$^{-/-}$ /Liver-DKO are available at the Gene Expression Omnibus. The scRNA-seq data (GSE254971) for D374Y mCherry-APOB mice is available in published paper entitled "Kupffer cells dictate hepatic responses to the atherogenic dyslipidemic insult" (https://doi.org/10.1038/s44161-024-00448-6). Source data are provided with this paper.

Results

Elevated Epsin1 and Epsin2 Expression in Atherosclerotic Patients.

In this study, we measured the protein expression of epsin1 and epsin2 between healthy control and atherosclerotic patients by immunofluorescence staining. Intriguingly, we found significantly elevated expression of epsin1 and epsin2 protein in diseased aortic arch samples (Fig.S2A-C). As expected, we found dramatically increased CD68 protein expression in atherosclerotic patients (Fig.S2A, 2B), suggests more macrophages accumulation and more atherosclerotic lesion in patients. Especially, we discovered significantly higher colocalization between epsin1 and CD68, and higher overlay percentage between epsin2 and CD68 in the macrophages in atherosclerotic patients than healthy control (Fig.S2A-C).

Diminished LDLR and HNF4α but Elevated Epsin1 and Epsin2 Expression in the Liver from WD-fed Mice and NAFLD Patients

In addition to aorta, we found significantly elevated expression of both epsin1 and epsin2 proteins in the liver from WD-fed mice (Fig.4B, 4C), but with significantly diminished expression of LDLR protein in the liver from WD-fed mice (Fig.4B, 4C). It is reported that atherosclerosis and NAFLD are two sides of the same coin[3], therefore, we have evaluated the protein expression of epsin1, epsin2, LDLR and HNF4α in the liver between healthy control and NAFLD patients. Intriguingly, we also found significantly elevated epsin1 and epsin2 expression in the liver from NAFLD

464 patients (Fig.S3A, 3B), but with dramatically diminished LDLR expression in the liver from
465 NAFLD patients (Fig.S3A, 3B). In addition, we detected markedly diminished HNF4α in NAFLD
466 patients both at protein and mRNA levels (Fig.S4 A-C).
467

468 **Epsins Depletion in the Liver Inhibits Atherogenesis and Reduces Lipid Levels**

469 In this study, we explored the role of hepatic epsins in atherosclerosis by employing liver-specific
470 epsins-deficient mice (ApoE$^{-/-}$/Liver-DKO) and compared their phenotypic outcomes to ApoE$^{-/-}$
471 controls. Our results demonstrated that epsins depletion significantly inhibited western diet (WD)-
472 induced atherogenesis (Fig. 5A). Specifically, the ApoE$^{-/-}$/Liver-DKO mice exhibited markedly
473 reduced atherosclerotic lesion formation, as evidenced by decreased plaque size and lipid
474 accumulation in the arterial walls compared to the ApoE-/- controls (Fig. 5B). These findings
475 indicate that liver epsins play a crucial role in the pathogenesis of atherosclerosis.

476 Plasma cholesterol and triglyceride (TG) levels, measured by Wako enzymatic and TG Infinity
477 kits, showed decreases resulting from loss of hepatic epsins in mice injected with PCSK9-AAV8
478 ($2x10^{11}$ genomes) and fed a WD for 8 weeks. We found significantly diminished TG and plasma
479 cholesterol levels in WD-fed Liver-DKO mice after PCSK9-AAV8 injection (Fig.5C). Additively,
480 quantitative analysis revealed that the ApoE$^{-/-}$/Liver-DKO mice had significantly lower plasma
481 cholesterol and triglyceride levels than those in ApoE$^{-/-}$ mice (Fig. 5D). These reductions in lipid
482 levels are indicative of improved lipid metabolism and clearance in the absence of hepatic epsins,
483 suggesting that liver epsins contribute to hyperlipidemia in atherosclerosis. In addition, we found
484 significantly reduced hepatic lipid accumulation in ApoE-/-/Liver-DKO mice by Oil Red O
485 staining (Fig.5E). The reduced lipid levels were also associated with decreased systemic
486 inflammation, as shown by lower levels of pro-inflammatory cytokines in the serum of ApoE-/-
487 /Liver-DKO mice (Data not shown).
488

489 **Single-Cell RNA Sequencing Identified Lipogenic Alb^{hi} Hepatocyte and Glycogenic HNF4α**
490 **^{hi} Hepatocytes**

491 To understand the cellular mechanisms underlying the observed phenotypic changes, we
492 performed single-cell RNA sequencing (scRNA-seq) on liver tissues from both ApoE$^{-/-}$ and ApoE^{-}
493 $^{/-}$/Liver-DKO mice (Fig. 1A). The Uniform Manifold Approximation and Projection (UMAP)
494 visualization revealed different cell types in the liver based on cell type-specific gene markers and
495 their corresponding expression between ApoE$^{-/-}$ and ApoE$^{-/-}$/Liver-DKO mice (Fig.S6A, S6B).
496 Further, the scRNA-seq analysis revealed distinct hepatocyte populations in the livers between
497 ApoE$^{-/-}$ and ApoE$^{-/-}$/Liver-DKO mice, highlighting the heterogeneity of hepatocyte cell
498 populations. UMAP visualization of hepatocytes illustrated a clear separation of different
499 subcluster hepatocytes between of ApoE$^{-/-}$ and ApoE$^{-/-}$/Liver-DKO mice (Fig. 1B), including HC
500 HNF4α ^{hi}, HC1 Alb^{hi}, HC2 Alb^{hi} , HC3 Alb^{hi}, indicating significantly transcriptional
501 reprogramming in the absence of epsins. The hepatocyte markers for hepatocytes clustering are
502 highlighted in the dotplot (Fig.1C).

503 Intriguingly, we identified significantly elevated HNF4α expression in the HNF4α^{hi} hepatocytes
504 in ApoE$^{-/-}$/Liver-DKO mice (Fig.1D, 1E). In addition, we found higher mean HNF4α expression
505 in HC HNF4α^{hi}, HC1 Alb^{hi}, HC2 Alb^{hi}, HC3 Alb^{hi} in ApoE$^{-/-}$/Liver-DKO than ApoE$^{-/-}$ (Fig.1F).
506 Especially, we discovered that Alb^{hi} hepatocytes have lower expression of apolipoprotein genes,
507 such as *Apob*, *Apoa4* , but with their higher expression in HNF4α^{hi} hepatocytes (Fig.1F-H,
508 Fig.S11), indicating more effective LDL cholesterol clearance in HNF4α^{hi} hepatocytes that
509 transported by ApoB and ApoA4 proteins. The lipogenic genes, such as *Acaca*, *Scd1*, have their
510 higher expression in HC3 Alb^{hi} hepatocytes but lower expression in HNF4α^{hi} hepatocytes
511 (Fig.S11). Especially, HNF4α^{hi} hepatocytes have higher expression of glycogenic genes, such as
512 *Pgm1*, *Gys2*, *Ugp2*, but with their lower expression in Alb^{hi} hepatocytes (Fig.S11), suggests
513 increased glycogenesis in HNF4α^{hi} hepatocytes. Therefore, Alb^{hi} hepatocytes prone to lipogenesis
514 in the liver, while HNF4α^{hi} hepatocytes have preference for glycogenesis. In addition, in the whole
515 liver, the elevated glycogenic genes expression and diminished lipogenic genes expression in
516 ApoE$^{-/-}$/Liver-DKO that have been validated by RT-qPCR (Fig.S10A, S10B).

517 Notably, the ApoE$^{-/-}$/Liver-DKO mice exhibited elevated gene expression related to LDL particle
518 clearance and decreased expression related to fatty acid synthesis (Fig. 1D, 2E). Real-time
519 quantitative PCR (RT-qPCR) further validated the single-cell RNA sequencing findings (Fig. 1E,
520 2F). These transcriptional changes reflect a shift towards improved lipid metabolism and clearance
521 in the absence of hepatic epsins. Especially, we found elevated cardiovascular disease (CAD)
522 protective score that from lipogenic Alb^{hi} hepatocytes to glycogenic HNF4α^{hi} hepatocytes
523 (Fig.1G).

524 **Lipogenic Alb^{hi} Hepatocytes to Glycogenic HNF4α^{hi} Hepatocytes Transition in ApoE$^{-/-}$**
525 **Liver-DKO, and HNF4α^{hi} Hepatocytes are Protective that with Higher CAD Protective**
526 **Score under Western Diet Treatment.**
527
528 We performed single cell transcriptome analysis for the liver cells from both ApoE$^{-/-}$ and ApoE$^{-/-}$
529 Liver-DKO under western diet treatment, and the workflow for libraries preparation of scRNA-
530 seq has been illustrated (Fig.1A). After hepatocyte-derived data analysis, we isolated four different
531 hepatocyte clusters, including HC1 Alb^{hi}, HC2 Alb^{hi}, HC3 Alb^{hi}, and HC HNF4α^{hi} (Fig.1B), and
532 their cell proportions in the liver are highlighted (Fig.S1A). Intriguingly, we found lower
533 proportion of lipogenic Alb^{hi} hepatocytes but higher proportion of glycogenic HNF4α^{hi}
534 hepatocytes in ApoE$^{-/-}$/Liver-DKO mice (Fig.S1A). Correspondingly, Gene Ontology (GO)
535 enrichment analysis revealed upregulated pathways for LDL particle clearance and downregulated
536 pathways for glycolytic process in different type of hepatocytes in the ApoE$^{-/-}$/Liver-DKO mice
537 (Fig. 2A, 2B; Fig.S8A-G). These pathways were significantly enriched compared to the ApoE$^{-/-}$
538 controls, suggesting improved LDL-C clearance in the absence of hepatic epsins. Correspondingly,
539 LDLR-cholesterol communication pathways were also enhanced, as evidenced by increased
540 signaling interactions in the ApoE$^{-/-}$/Liver-DKO mice (Fig. 2C, 2D). This enhancement in LDL-C
541 clearance mechanisms likely contributes to the reduced atherogenesis observed in these mice.
542 Consequently, we found elevated expression of genes involved in LDL-C clearance in the liver in
543 ApoE$^{-/-}$/Liver-DKO mice (Fig.2E, 2F). The hepatocyte markers for hepatocyte subcluster are
544 shown in dotplot (Fig.1C). Intriguingly, in HNF4α^{hi} hepatocytes, we also discovered significantly
545 elevated HNF4α expression in ApoE$^{-/-}$ Liver-DKO that have been validated at both mRNA and
546 protein levels (Fig.1D-G), also diminished expression of lipogenesis genes , such as Acaca and

547 Scd1, and gene for lipid uptake, Fabp1, but elevated gene expression of lipoprotein clearance,
548 including Apoa4 and Ldlr (Fig.1D, 1E). Especially, we found HNF4α^{hi} hepatocytes are protective
549 in ApoE$^{-/-}$ Liver-DKO, the CAD protective score is positively associated with HNF4α expression
550 in ApoE$^{-/-}$ Liver-DKO (Fig.1G).
551

552 Further analysis identified a transition from lipogenic Alb^{hi} hepatocytes to glycogenic HNF4α^{hi}
553 hepatocytes in the ApoE$^{-/-}$/Liver-DKO mice (Fig. S1B-F). Correlate to this transition, lipogenic
554 genes, such as *Acaca*, *Scd1*, *Acly*, *Hmgcr*, *Fasn*, show diminished expression in the hepatocytes in
555 ApoE$^{-/-}$/Liver-DKO (Fig.S7A), while show elevated expression of apolipoprotein genes, such as
556 Apoa4 and Apob, which is positively associated with HNF4α expression (Fig.S7B). RNA velocity
557 and CellRank analyses supported these dynamic shifts, demonstrating an increased propensity for
558 hepatocyte differentiation towards a glycogenic state in the absence of hepatic epsins (Fig. S1B-
559 F). This transition is likely a compensatory mechanism to enhance glucose metabolism and reduce
560 lipid synthesis, contributing to the reduced lipid levels observed in the ApoE$^{-/-}$/Liver-DKO mice.
561 In addition, by single cell RNA-seq, under normal chow, we also discovered downregulated genes
562 involved in lipogenesis and lipid uptake, such as *Acaca*, *Scd1*, and *Fabp1*, but genes respond for
563 lipoprotein clearance, including *Apoa4*, *Apob*, *Apoc1*, are significantly upregulated in Liver-DKO
564 (Data not shown). Similarly, by comparison of cardiovascular diseases (CAD) susceptible genes
565 expression that were reported by GWAS analysis expression between WT and Liver-DKO, with
566 particularly emphasize on genes that participate in low-density lipoprotein particles removal [40].
567 We found significantly higher CAD protective score in the hepatocytes in Liver-DKO compared
568 with WT (Data not shown). Furthermore, both the RNA velocity and CellRank analyses showed
569 that higher probability from lipogenic Alb^{hi} hepatocytes to glycogenic HNF4α^{hi} hepatocytes
570 transition in Liver-DKO than WT (Data not shown).

571
572
573 **HNF4α^{hi} Hepatocytes in ApoE$^{-/-}$ Liver-DKO have Upregulated Low-density Lipoprotein**
574 **Particle Clearance and Glycogen Biosynthesis Compared with ApoE$^{-/-}$ under Western Diet**
575 **Treatment.**
576
577 Mechanistically, by Gene Ontology (GO) analysis, we found upregulated plasma lipoprotein
578 oxidation and elevated low-density lipoprotein particle clearance, but with downregulated
579 glycolytic process in ApoE$^{-/-}$ Liver-DKO (Fig2A, 2B). Similarly, we also found upregulated of
580 pathways involved in LDL-C particle clearance in Liver-DKO under normal chow (Data not
581 shown). Furthermore, we performed cell-cell communication analysis, we found significantly
582 upregulated *Rorα* and *Sdc4* associated pathways in ApoE$^{-/-}$ Liver-DKO, which inhibit lipogenesis
583 in the liver[41] (Fig.2C; Fig.S9A). Similarly, under normal chow, by cell-cell communication
584 analysis, and found *Sdc4* and *Nr1h3* pathways, which are reported to reduce steatosis [42,43], are
585 upregulated in Liver-DKO under normal chow (Data not shown). We also found downregulation
586 of *Ppia* and *Nr1h4* pathways, which suppress lipogenesis in the liver [44,45] (Fig.2D; Fig.S9B). The
587 representative genes for inhibition of lipogenesis, such as *Sdc4*, *Rorα*, are significantly elevated in
588 ApoE$^{-/-}$ Liver-DKO (Fig.2E, 2F), and the lipogenic *Pparγ* is significantly diminished in ApoE$^{-/-}$
589 Liver-DKO (Fig2E, 2F). Likewise, under normal chow, we also discovered downregulated of
590 lipogenic pathways in Liver-DKO, such as *Pparγ* and *Ppia* pathways [44,46] (Data not shown). The

591 metabolites analysis by MEBOCOST algorithm showed enhanced communication interactions for
592 cholesterol/LDLR and cholesterol/Rorα pathways in HNF4α^{hi} hepatocytes in ApoE$^{-/-}$ Liver-DKO
593 (Fig.3G), and resulted in lower intensity of cholesterol in ApoE$^{-/-}$/Liver-DKO mice (Fig.2I).
594 However, we found no significantly difference for the mean expression of *Rorα* gene between
595 ApoE$^{-/-}$ and ApoE$^{-/-}$ Liver-DKO (Fig.2H). Similarly, We also found significant elevated
596 communication interactions for cholesterol/LDLR and cholesterol/Rorα pathways in Alb^{hi} HNF4α
597 ^{hi} hepatocytes in Liver-DKO under normal chow, and with higher mean expression of *Rorα* gene
598 in Liver-DKO (Data not shown), which promote the cholesterol clearance. Intriguingly, we found
599 significantly lower mean abundance of cholesterol but higher abundance of uridine diphosphate
600 glucose (UDPG) as intermediate metabolite for glycogenesis in HNF4α^{hi} hepatocytes in ApoE$^{-/-}$
601 Liver-DKO (Fig.2I), suggests elevated glycogenesis in the ApoE$^{-/-}$/Liver-DKO mice. Similarly,
602 we also found lower mean abundance of cholesterol but higher abundance of uridine diphosphate
603 glucose (UDPG) as intermediate metabolite for glycogenesis in Alb^{hi} HNF4α^{hi} hepatocytes in
604 Liver-DKO under normal chow (Data not shown).
605
606 **Elevated Lipogenic Gene Expression but Diminished Glycogenic Gene Expression in Alb^{hi}**
607 **HNF4α^{hi} Hepatocytes and with Lower CAD Protective Score in hPCSK9 D374Y Mutant.**
608
609 In addition to ApoE$^{-/-}$ atherosclerotic mouse model, we reanalyzed liver single cell RNA-seq data
610 from hPCSK9 D374Y mutation mice. PCSK9-D374Y gain-of-function mutant has a markedly
611 increased affinity for LDLR and promote its degradation [47]. As expected, we identified diminished
612 *Ldlr* expression in hPCSK9 D374Y mutants, especially in HC3_Alb^{hi} HNF4α^{hi} hepatocytes
613 (Fig.S13). Intriguingly, we found reduced proportion of HC3_Alb^{hi} HNF4α^{hi} hepatocytes in
614 hPCSK9 D374Y mutants (Fig.3A), and the HC1, HC2, and HC3 hepatocytes have been clustered
615 and evaluated by the expression of HNF4α and other hepatocyte markers (Fig.3B). Subsequently,
616 we found significantly lower CAD protective score in Alb^{hi} HNF4α^{hi} hepatocytes in hPCSK9
617 D374Y mutant than control. Intriguingly, the CAD protective score in both control and hPCSK9
618 D374Y mutant is positively correlated with HNF4α expression level, with highest CAD protective
619 score in HC3_Alb^{hi} HNF4α^{hi} hepatocytes among three different hepatocytes (Fig.3D). Especially,
620 we discovered significantly diminished HNF4α expression and with dramatically elevated epsin1
621 expression in HC3_Alb^{hi} HNF4α^{hi} hepatocytes in hPCSK9 D374Y mutant (Fig.3C, Fig.S13).
622 Consequently, lipogenic genes, such as *Acly* and *Fasn*, are significantly induced in hPCSK9
623 D374Y mutant (Fig.S14A), suggests activated lipogenesis in hPCSK9 D374Y mutant. On the
624 opposite, glycogenic genes, such as *Gys2*, *Ugp2*, are potently inhibited in hPCSK9 D374Y mutant
625 (Fig.S14B), indicates diminished glycogenesis in hPCSK9 D374Y mutant. Almost all the
626 apolipoprotein genes, such as *Apoa1*, *Apoa2*, *Apoa4*, *Apob*, *Apoc1*, *Apoc2*, and *Apoc3*, are
627 dramatically inhibited in hPCSK9 D374Y mutant (Fig.S12), reveals diminished LDL cholesterol
628 transportation for its clearance.
629
630 **Diminished Low-density Lipoprotein Particle Clearance and Glycogen Biosynthesis and**
631 **Hindered Alb^{hi} Hepatocytes to Alb^{hi} HNF4α^{hi} Hepatocytes Transition in the Liver of**
632 **hPCSK9 D374Y Mice**
633
634 Mechanistically, by Gene Ontology (GO) analysis, the pathways for the regulation of low-density
635 lipoprotein particle clearance and the regulation of glycogen biosynthetic process are significantly
636 downregulated for enrichment in hPCSK9 D374Y mutant (Fig.3G), while the pathways involved

637 in regulation of glycolytic process are significantly enriched that upregulated in hPCSK9 D374Y
638 mutant (Fig.3F), suggests diminished low-density lipoprotein clearance and inhibited glycogenesis
639 in hPCSK9 D374Y mutant. The further metabolites analysis by MEBOCOST algorithm showed
640 weakened communication interactions for cholesterol/LDLR and cholesterol/Rorα pathway in Alb
641 ^{hi} HNF4α ^{hi} Hepatocytes in hPCSK9 D374Y mutant (Fig.3H, 3J). Consequently, we found
642 significantly higher mean abundance of cholesterol but lower abundance of uridine diphosphate
643 glucose (UDPG) as intermediate metabolite for glycogenesis in Alb ^{hi} HNF4α ^{hi} in hPCSK9
644 D374Y (Fig.3I).
645
646 Subsequently, the pseudotime trajectory analysis showed that significantly inhibited cell fate
647 transition from HC1_lipogenic Alb ^{hi} hepatocytes to glycogenic HC3_Alb ^{hi} HNF4α ^{hi} in hPCSK9
648 D374Y mutant than control (Fig.3E). Correlate to this transition, lipogenic genes, such as *Acly*,
649 *Fasn*, show elevated fatty acid synthesis in the hepatocytes in hPCSK9 D374Y mutant (Fig.S14A),
650 while show diminished expression of apolipoprotein genes, such as *Apoa1*, *Apoa2*, *Apoa4*, *Apob*,
651 *Apoc1*, *Apoc2*, and *Apoc3*, suggest impaired low-density lipoprotein cholesterol clearance in
652 hPCSK9 D374Y mutant (Fig.S12). The glycogenic genes exhibit diminished expression, such as
653 *Gys2*, *Ugp2*, indicate inhibited glycogenesis in the hepatocytes in hPCSK9 D374Y mutant
654 (Fig.S14B). RNA velocity and CellRank analyses supported these dynamic shifts, demonstrating
655 an inhibited propensity for hepatocyte differentiation towards a glycogenic state in the presence of
656 elevated hepatic epsins in hPCSK9 D374Y (Data not shown). This transition is likely a
657 pathological mechanism in hPCSK9 D374Y mutant by inhibition of glycogenesis and enhanced
658 lipid synthesis, contributing to the hyperlipidemia in hPCSK9 D374Y mutant.
659
660
661 **Elevated LDLR Expression in the Liver of Liver Specific Epsins Deficiency Mice and**
662 **Diminished LDLR Expression in the Liver from WD-fed Mice**
663
664 Western blot analysis of liver tissue lysates from both WT and Liver-DKO mice revealed elevated
665 LDLR expression in Liver-DKO , and the absence of Epsin1 and Epsin2 expression in Liver-DKO
666 (Fig.4A). The protein levels of LDLR in WT and Liver-DKO have been quantified (Fig.4A).
667 Intriguingly, we found significantly diminished LDLR expression in the livers of western diet
668 (WD)-fed WT mice compared to normal diet (ND)-fed WT mice (Fig.4B). However, we
669 discovered that both Epsin1 and Epsin2 proteins are dramatically elevated in the livers of WD-fed
670 WT mice compared with ND-fed WT mice (Fig.4B). The protein levels of LDLR in both ND-fed
671 WT and WD-fed WT have been quantified (Fig.4B). In addition to WB analysis, we performed
672 immunofluorescence (IF) analysis of liver cryosections from both WT and Liver-DKO mice. We
673 found elevated LDLR immunofluorescence signal in the liver of Liver-DKO (Fig.4C,4D).
674 Notably, the LDLR immunofluorescence signal in the liver from WD-fed WT is markedly
675 diminished compared with ND-fed WT (Fig.4C,4D). However, the LDLR immunofluorescence
676 signal intensity in WD-fed Liver-DKO is partially maintained compared with ND-fed Liver-DKO
677 (Fig.4C,4D), suggests epsins deficiency in the liver prevention of the degradation of LDLR under
678 western diet treatment. The LDLR immunofluorescence signal intensity have been quantified
679 (Fig.4D). The absence of both Epsin1 and Epsin2 immunofluorescence signals in the livers of
680 Liver-DKO mice compared to WT mice (Fig.4C).
681

682 **Liver-deficiency of Epsins Inhibits Atherosclerotic Lesion Formation and Macrophage**
683 **Accumulation**
684
685 *En face* Oil Red O staining of aortas from ApoE $^{-/-}$ and ApoE $^{-/-}$ / Liver-DKO mice fed a WD
686 revealed significantly diminished atherosclerotic lesion in ApoE $^{-/-}$ / Liver-DKO mice compared
687 with ApoE $^{-/-}$ mice (Fig.5A). The lesion areas of aortic root in both ApoE $^{-/-}$ and ApoE $^{-/-}$ / Liver-
688 DKO mice have been quantified (Fig.5A). In addition, aortic roots cryosections from both ApoE $^{-}$
689 $^{/-}$ and ApoE $^{-/-}$ / Liver-DKO mice were stained with Oil Red O (ORO), and we found significantly
690 reduced lesion size in ApoE $^{-/-}$ / Liver-DKO mice than ApoE $^{-/-}$ mice (Fig.5B). We also discovered
691 significantly diminished CD68 immunofluorescence signals in ApoE $^{-/-}$ / Liver-DKO mice than
692 ApoE $^{-/-}$ mice, indicating fewer macrophage accumulation in the atherosclerotic lesions (Fig.5B).
693 We further measured plasma triglyceride (TG) and cholesterol levels in WD-fed WT and Liver-
694 DKO mice injected with PCSK9-AAV8, and we detected significantly reduced TG and cholesterol
695 levels in WD-fed Liver-DKO; PCSK9-AAV8 mice compared to WD-fed WT; PCSK9-AAV8
696 mice (Fig.5C). In addition, we also measured plasma cholesterol level from both ApoE $^{-/-}$ and
697 ApoE $^{-/-}$ / Liver-DKO mice under either ND or WD treatment, and we found significantly
698 diminished plasma cholesterol in ApoE $^{-/-}$ / Liver-DKO mice compared to ApoE $^{-/-}$ mice (Fig.5D).
699 Oil Red O staining of liver cryosections were performed in both ApoE $^{-/-}$ and ApoE $^{-/-}$ / Liver-DKO
700 mice, we found significantly reduced hepatic lipids in the livers of ApoE $^{-/-}$ / Liver-DKO mice
701 compared to ApoE $^{-/-}$ mice (Fig.5E).
702
703 **LDLR is Resistant to PCSK9-induced Proteasomal Degradation in Liver-DKO Mice and**
704 **LDLR Directly Binds to Epsin1 UIM Domain.**
705

706 Western blot (WB) analysis of liver tissue harvested from WT and Liver-DKO mice injected with
707 PCSK9-AAV8 virus ($2x10^{11}$ genomes) revealed LDLR was markedly degraded by PCSK9
708 administration in WT, but not in Liver-DKO livers (Fig.6A). The protein levels of LDLR in WT
709 and Liver-DKO mice were quantified, with significantly enhanced LDLR expression in the liver
710 from Liver-DKO mice (Fig.6A). In addition to liver tissue lysate analysis, we also performed WB
711 analysis of lysate from primary hepatocytes isolated from WT and Liver-DKO mice, treated with
712 PCSK9, cycloheximide (CHX) and MG132. We found PCSK9-induced LDLR degradation
713 occurred independent of new protein synthesis (in the presence of CHX) but was blocked by either
714 loss of epsins or proteasomal inhibitor MG132 (Fig.6B). The protein levels of LDLR were
715 quantified, with significantly higher LDLR expression in the hepatocytes from Liver-DKO under
716 either with or without MG132 treatment (Fig.6B). To study the interaction between LDLR and
717 Epsin1, we performed anti-epsin1 co-immunoprecipitation (co-IPs) analysis. We found LDLR
718 directly binds epsin1 in WT, but not in Liver-DKO primary hepatocytes (Fig.6C). To further study
719 which epsin1 motif can bind to LDLR, we transfected different FLAG-tagged epsin1 deletion
720 mutants plasmids into HepG2 cells (Fig.6D), including pcDNA (empty plasmid), full length epsin1
721 plasmid, epsin1-ΔENTH plasmid, epsin1-ΔUIM plasmid, epsin1-DPW/NPF plasmid. Intriguingly,
722 we found LDLR can specific bind to both the full length epsin1 and epsin1-ΔENTH, but not bind
723 to epsin1-ΔUIM and epsin1-DPW/NPF, indicating the epsin1-UIM domain is the binding motif
724 for the interaction between epsin1 and LDLR (Fig.6E). In addition, we discovered that
725 significantly diminished ubiquitinated LDLR in the liver lysate from Liver-DKO by testing
726 ubiquitin expression after LDLR antibody for immunoprecipitation (IP) (Fig.6F). In summary, by

727 preventing PCSK9-triggered LDLR degradation, hepatic epsin depletion enhances LDL-C
728 clearance and ameliorates dyslipidemia in atherosclerosis (Fig.8).

729

730 **Nanoparticle-mediated Delivery of Epsins siRNAs Potently Inhibits Lesion Development,**
731 **Reduces Foam Cell Formation, and Decreases Cholesterol and TG Levels in ApoE$^{-/-}$ Mice.**

732 To explore the therapeutic potential of targeting hepatic epsins, we employed nanoparticle-
733 encapsulated siRNAs specifically targeting epsins in the liver. Therapeutically, we applied
734 galactose targeted - nanoparticles (NPs) with epsin1/2 siRNA (Fig.7E) to inject ApoE $^{-/-}$ mice
735 under WD-treatment, control siRNA NPs were injected to WD-fed ApoE $^{-/-}$ mice as the control.
736 Before injection of siRNA NPs into ApoE $^{-/-}$ mice, we have performed cytometry to test the
737 efficiency of Gal-targeted Cy5.5-siRNA NPs and non-targeted Cy5.5-siRNA NPs in THLE-3 cells.
738 We found significantly higher uptake efficiency in Gal-targeted Cy5.5-siRNA NPs compared to
739 non-targeted Cy5.5-siRNA NPs in THLE-3 (Fig.7F). Western blots of liver lysates isolated from
740 WD-fed ApoE $^{-/-}$ mice (8 weeks) that treated with control or epsins siRNA NPs revealed
741 dramatically diminished epsin1 and epsin2 protein expression, indicating the highly efficiency of
742 epsins siRNA NPs for knockdown of epsin1 and epsin2 proteins (Fig.7G). *En face* ORO staining
743 of aortas from control siRNA NP-treated or epsin1/2 siRNA NP treated ApoE $^{-/-}$ mice fed a WD
744 revealed significantly diminished atherosclerotic lesion in epsin1/2 siRNA NP treated ApoE $^{-/-}$
745 mice compared with control siRNA NPs ApoE $^{-/-}$ mice (Fig.7A). The lesion areas of aortic root in
746 both control siRNA NPs treated ApoE $^{-/-}$ mice and epsin1/2 siRNA NPs treated ApoE $^{-/-}$ mice have
747 been quantified (Fig.7A). In addition, aortic roots from control siRNA NPs treated ApoE $^{-/-}$ or
748 epsin1/2 siRNA NP treated ApoE $^{-/-}$ mice were stained with Oil Red O or the CD68 macrophage
749 marker CD68. We found significantly reduced lesion size in epsin1/2 siRNA NP treated ApoE $^{-/-}$
750 mice than control siRNA NPs treated ApoE $^{-/-}$ mice (Fig.7B). We also discovered significantly
751 diminished CD68 immunofluorescence signals in epsin1/2 siRNA NP treated ApoE $^{-/-}$ mice than
752 control siRNA NPs treated ApoE $^{-/-}$ mice, indicating fewer macrophage accumulation in the
753 atherosclerotic lesions in epsin1/2 siRNA NP treated ApoE $^{-/-}$ mice (Fig.7B). We further measured
754 plasma triglyceride (TG) and cholesterol levels in both control siRNA NPs treated ApoE $^{-/-}$ mice
755 and epsin1/2 siRNA NPs treated ApoE $^{-/-}$ mice, and we detected significantly reduced TG (Fig.7C)
756 and cholesterol levels (Fig.7D) in epsin1/2 siRNA NP treated ApoE $^{-/-}$ mice compared to control
757 siRNA NPs treated ApoE $^{-/-}$ mice. These findings suggest that targeting liver epsins presents a
758 novel and promising therapeutic strategy for the treatment of atherosclerosis.

759 In summary, our results demonstrate that liver-specific epsins depletion significantly inhibits
760 atherogenesis and reduces lipid levels in a mouse model of atherosclerosis. The observed
761 phenotypic changes are associated with transcriptional reprogramming of hepatocytes, lipogenic
762 Alb ^{hi} Hepatocytes to glycogenic HNF4α ^{hi} Hepatocytes, enhanced LDL-C clearance pathways,
763 and improved lipid metabolism. Mechanistically, the deficiency of liver epsins protect LDLR from
764 PCSK9-triggered degradation. By targeting liver epsins with nanoparticle-encapsulated siRNAs,
765 it has highly efficacious at inhibiting dyslipidemia and impeding atherosclerosis. These findings
766 highlight the potential of targeting hepatic epsins as a therapeutic strategy for the treatment of
767 atherosclerosis and related cardiovascular diseases.

768

769 **Discussion**
770
771 Our previous studies have elucidated an atheroprone function of epsins in both endothelial cells[4],
772 macrophages[17,18], and vascular smooth muscle cells[48] due to significantly elevated inflammation
773 in the atherosclerotic plaque. However, atherosclerosis is initiated from the abnormal
774 accumulation of lipid in the subendothelial layer of the arterial wall for hyperlipidemia [49]. The
775 liver is the central organ for the control of lipid homeostasis[50]. The processes of de-novo
776 lipogenesis (DNL) taking place in the liver and hepatic lipid metabolism are critical for regulation
777 of the levels and distribution of lipids throughout the body [20]. LDLR is expressed in the liver that
778 is essential to clearance of circulating LDL-C that play protective roles in prevention of
779 atherosclerosis [13,51]. PCSK9 is dominantly expressed in the liver, and PCSK9 binds to LDLR that
780 promote LDLR degradation [52-54]. Currently, PCSK9 antibody-based therapeutic to reduce
781 circulating levels of LDL have been developed by several drug companies [55,56]; however, the
782 mechanistic details of PCSK9-mediated LDLR degradation remain insufficiently understood.
783
784 In this study, we identified significantly lower plasma cholesterol and triglyceride in ApoE$^{-/-}$ /
785 Liver-DKO mice or WD-fed Liver-DKO mice injected with PCSK9-AAV8 than those in ApoE$^{-/-}$
786 controls or WD-fed WT mice (Fig.5C, 5D). Intriguingly, the plasma cholesterol and triglyceride
787 levels in epsins deficient in other different cell types, such as endothelial cell, macrophage, and
788 vascular smooth muscle cells[4,17,18,48], do not have significantly differences when comparing with
789 ApoE$^{-/-}$ controls, indicating epsins in the hepatocytes participate in lipogenesis, which have been
790 validated with significantly diminished gene expression that involved in lipogenesis in ApoE$^{-/-}$ /
791 Liver-DKO mice (Fig.1D, 1E). The liver is the main organ that regulate circulating LDL-C
792 homeostasis by LDLR for LDL-C clearance [19]. Our single cell RNA sequencing data showed that
793 significantly elevated genes that are enriched in low-density lipoprotein particles and triglyceride-
794 rich lipoprotein particles clearance gene ontology (GO) in the hepatocytes in ApoE$^{-/-}$ / Liver-DKO
795 mice (Fig.2A), which is consistent to its reduced plasma cholesterol and triglyceride. Subsequently,
796 we also showed evidences that with enhanced communication score between LDLR and
797 cholesterol in the hepatocytes from ApoE$^{-/-}$ / Liver-DKO mice by MEBOCOST analysis (Fig.2G-
798 I), indicating enhanced capacity of low-density lipoprotein cholesterol (LDL-C) clearance by
799 LDLR in ApoE$^{-/-}$ / Liver-DKO mice. Consequently, we found significantly reduced atherosclerotic
800 lesion area in ApoE$^{-/-}$ / Liver-DKO mice than those in in ApoE$^{-/-}$ controls (Fig.5A, 5B). In addition
801 to diminished lipogenic genes expression, the enhanced UDPG communication score in HNF4α^{hi}
802 hepatocytes in ApoE$^{-/-}$ / Liver-DKO mice that resulted in elevated UDPG metabolite level promote
803 hepatic glycogenesis (Fig.2I). Chen *et al.* recently reported that hepatic glycogenesis inhibits
804 lipogenesis[57]. Consequently, the enhanced UDPG metabolite levels in the liver inhibits fatty acid
805 synthesis that could also contribute to reduced cholesterol and triglyceride in plasma in ApoE$^{-/-}$ /
806 Liver-DKO mice.
807
808 Currently, almost all studies involved in human liver single cell RNA-seq analysis are in the
809 context of chronic liver diseases, such as nonalcoholic fatty liver disease (NAFLD) [58,59], or acute
810 liver failure (ALF) [60]. Unfortunately, no single cell RNA-seq study for dissecting of human liver
811 transcriptome for patients in the context of coronary artery disease or other cardiovascular diseases,
812 and most single cell RNA-seq studies for patients in the context of coronary artery disease are for
813 exploring the transcriptome differences for atherosclerotic plaques [61,62]. Therefore, it is impossible
814 to compare our liver single cell RNA-seq data with liver single cell RNA-seq data from human

815 patients with coronary artery disease. However, the recently published article explored liver
816 transcriptome by single cell RNA-seq for hPCSK9-D374Y mice with emphasized analysis on
817 Kupffer cells [63], this dataset empower us to analyze heterogeneity of hepatocytes in the liver
818 between hPCSK9-D374Y mice and controls. The hPCSK9-D374Y mutation potently elevates the
819 affinity between PCSK9 and LDLR interaction, and further promote the degradation of LDLR [64].
820 In this study, we reanalyzed the liver single cell RNA-seq dataset by emphasizing the analysis in
821 the context of hepatocytes from hPCSK9-D374Y mice[63]. Intriguingly, in the hepatocytes of
822 hPCSK9-D374Y mice, we discovered diminished glycogenic genes expression but elevated
823 lipogenic genes expression in hPCSK9-D374Y mice, results in diminished glycogenesis and
824 activated lipogenesis that is consistent with lower CAD protective score in hPCSK9-D374Y mice,
825 especially for HC3_Alb^{hi} HNF4α^{hi} hepatocytes (Fig.3D, Fig.S14). Therefore, there are highly
826 phenotypic similarities between hPCSK9-D374Y mice and ApoE$^{-/-}$ mice. Mechanistically, we
827 identified significantly elevated epsin1 expression in hPCSK9-D374Y mice that would contribute
828 to downregulated LDL particles and VLDL particles clearance by reduction of LDLR expression
829 (Fig.3G, Fig.S13). Subsequently, we found diminished communication score between LDLR and
830 cholesterol in the hepatocytes from hPCSK9-D374Y mice by MEBOCOST analysis (Fig.3H-J),
831 which is consistent to serum cholesterol accumulation due to reduced hepatic LDLR levels in
832 hPCSK9-D374Y mice [65]. Similar to ApoE$^{-/-}$ mice, the decreased UDPG communication score in
833 glycogenic HC3_Alb^{hi} HNF4α^{hi} hepatocytes (Fig.3H, 3I), and together with diminished genes of
834 glycogenesis that further contribute to elevated lipogenesis[57]. Like to ApoE$^{-/-}$ mice, the diminished
835 tendency of cell fate transition from HC1_lipogenic Alb^{hi} hepatocytes into HC3_glycogenic Alb^{hi}
836 HNF4α^{hi} hepatocytes in hPCSK9-D374Y mice, which is consistent with its elevated lipogenic
837 genes and diminished glycogenic genes (Fig.S14). In summary, by comparison of ApoE$^{-/-}$ and
838 hPCSK9-D374Y mice, these two mouse model for atherosclerosis study shared similar hepatocyte
839 heterogeneity and the common pathological signaling pathways for inducing atherosclerosis or
840 dyslipidemia, which might be highly correlated with the common elevated epsins expression in
841 the liver that mediate LDLR degradation.
842
843 In this study, we firstly elaborated how liver epsins mediate the LDLR degradation that triggered
844 by PCSK9 in the liver (Fig.8). In liver epsins-deficient mice (Liver-DKO), significantly elevated
845 LDLR expression in the membrane of hepatocytes that empower upregulated LDL-C clearance
846 (Fig.4A, 4C), which is resistant to WD-induced espins mediated LDLR degradation (Fig.4C).
847 PCSK9 protein mediates LDLR protein degradation [66]. In this study, by injection of PCSK9-
848 AAV8 into both WT controls and Liver-DKO mice for PCSK9 overexpression, LDLR is
849 dramatically degraded in WT controls; however, the degradation of LDLR is significantly
850 inhibited in Liver-DKO mice (Fig.6A, 6B), which strongly supports that liver epsins are essential
851 for PCSK9-mediated LDLR degradation. Subsequently, we discovered that epsin1 can directly
852 bind to LDLR protein that further trigger its degradation (Fig.6C). Our previous studies revealed
853 that epsins are critical adaptor proteins that involved in endocytosis [16,23,67-69]. To explore which
854 motif in epsin1 can specific bind to LDLR, such as ENTH, UIM, DPW and NPF (Fig.6D), FLAG-
855 tagged epsin1 deletion mutants plasmids, including pcDNA control, full length epsin1 plasmid,
856 epsin1-ΔENTH plasmid, epsin1-ΔUIM plasmid and epsin1-DPW/NPF plasmid have been
857 transfected into HepG2 cells. Specifically, LDLR binds to UIM motif only but not binds to other
858 motifs (Fig.6E), the ubiquitin-interacting motif (UIM) in epsins facilitated ubiquitination mediated
859 protein degradation[70]. Consequently, diminished LDLR expression in the liver due to the
860 interaction between LDLR and epsin1 UIM motif for the activation of ubiquitination of LDLR

861 facilitate to its degradation in WT controls, but not in Liver-DKO mice. In addition, we revealed
862 diminished ubiquitinated LDLR in the liver lysate in Liver-DKO by LDLR antibody
863 immunoprecipitation (IP) assay, consequently, higher LDLR expression in the input lysate in
864 Liver-DKO mice than WT controls (Fig.6F), supporting the loss of epsins enhances the stability
865 of LDLR. MG132 proteasome inhibitors blocked the degradation of LDLR by inhibition of
866 ubiquitination [71]. We further isolated primary hepatocytes from both WT and Liver-DKO for
867 PCSK9, cycloheximide (CHX) and proteasomal inhibitor MG132 treatment, identified that
868 PCSK9-induced LDLR degradation occurred independent of new protein synthesis, similar to
869 MG132 treatment, and LDLR degradation was blocked by loss of epsins in the liver. In summary,
870 epsins play gatekeeping roles in the PCSK9-mediated ubiquitination-driven LDLR degradation
871 that by interaction between epsin1 UIM motif and LDLR. Therefore, the liver epsins might as
872 potential targets to treatment of dyslipidemia or further atherosclerosis by protecting hepatic
873 LDLR from degradation.

874 The liver is the primary organ of lipid nanoparticles accumulation following intravenous
875 administration [72,73], and lipid nanoparticle-mediated RNAs or siRNAs delivery holds great
876 potential to treat liver diseases [74,75]. In this study, we engineer the hybrid siRNA NPs for better
877 targeting of hepatocytes *in vivo* by surface modification with carbohydrate ligands (*e.g.* galactose)
878 that can recognize the asialoglycoprotein receptor (ASGPR) predominately expressed on
879 hepatocytes and minimally expressed by non-hepatic cells [36,37]. Finally, targeting liver epsins with
880 lipid nanoparticle encapsulated siRNAs that with highly efficacious at inhibiting dyslipidemia and
881 impeding atherosclerosis. We discovered significantly reduced atherosclerotic lesion in epsin1/2
882 siRNA NPs injected mice comparing to control NPs group (Fig.7A, 7B). As expected, we detected
883 significantly lower cholesterol and triglyceride levels in epsin1/2 siRNA NPs injected group than
884 control NPs group (Fig.7C, 7D). Therefore, we have tested the therapeutic efficiency for treatment
885 of atherosclerosis by targeting liver epsins in mice. However, in this study, the lack of therapeutic
886 data from large animals will be insufficient for evaluation of the efficiency by targeting liver epsins
887 for inhibiting atherosclerotic progression. To fill in the gaps, in future, we will test the efficiency
888 of epsin1/2 siRNA NPs targeting liver epsins in large animals, such as rabbit [76] and pig[77] for
889 atherosclerotic regression studies. It has been widely applied for rabbit model to investigate
890 familial hypercholesteromia (FH), and hypercholesteromia rabbits have very high LDL-C level
891 due to dysfunction of LDLR, also with severe atherosclerosis [12,78]. By targeting epsins in the liver
892 in hypercholesteromia rabbit with epsin1/2 siRNA NPs, we will measure the plasma LDL-C level
893 and atherosclerotic lesion between control NPs group and epsin1/2 siRNA NPs group.

894

895 In this study, mechanistically, we identified significantly higher hepatocyte nuclear factor 4α
896 (HNF4α) expression in ApoE$^{-/-}$ /Liver-DKO mice than ApoE$^{-/-}$ (Fig.1D-F), and HNF4α is reported
897 as critical transcription factor that modulation of lipid homeostasis [79]. The hepatic HNF4α
898 deficiency cause severe hepatic lipid accumulation, and overexpression of hepatic HNF4α lowers
899 plasma cholesterol levels [79]. In addition, the accumulation of hepatic glycogen is disrupted by loss
900 of hepatic HNF4α [80]. Intriguingly, we presented higher lipogenic genes expression in Alb^{hi}
901 hepatocytes than HNF4α^{hi} hepatocytes, while higher glycogenic genes expression in HNF4α^{hi}
902 hepatocytes than Alb^{hi} hepatocytes (Fig.S11). The higher percentage of glycogenic HNF4α^{hi}
903 hepatocytes but with lower lipogenic Alb^{hi} hepatocytes proportion in ApoE$^{-/-}$ /Liver-DKO mice
904 than ApoE$^{-/-}$ (Fig.2A), which contribute to reduced cholesterol and triglyceride in plasma in ApoE^{-}

905 $^{/-}$ / Liver-DKO mice. Coincidently, the cardiovascular disease (CAD) protective score is positive
906 associated with hepatic HNF4α expression in ApoE$^{-/-}$ / Liver-DKO mice, indicating glycogenic
907 HNF4α^{hi} hepatocytes are protective that attributable mainly to the inhibition of lipogenesis. Parviz
908 *et al.* and Wu *et al.* demonstrated that HNF4α is essential for hepatic glycogen synthesis, and
909 hepatic HNF4α deletion induces significantly impairment of hepatic glycogen accumulation in the
910 liver [80,81]. In addition to glycogenesis, Bonzo *et al.* demonstrated that genetic deletion of HNF4α
911 cause steatosis [82], and both Xu *et al.* and Yang *et al.* clarified that overexpression of HNF4α
912 significantly ameliorate hepatic steatosis by reducing of hepatic triglycerides and free fatty acids
913 (FFA) [83,84]. In this study, we discovered that significantly diminished hepatic and serum lipids in
914 ApoE$^{-/-}$ /Liver-DKO, but with elevated genes expression that involved in glycogenesis, indicating
915 upregulated hepatic glycogenesis suppress lipogenesis in the liver that is consistent to the recently
916 report that hepatic glycogenesis antagonizes lipogenesis [57]. Chen *et al.* demonstrated that elevated
917 UDPG mediated glycogenesis that repressed the cleavage of premature SREBP1 and SREBP2 into
918 mature SREBP1 and SREBP2, resulted in diminished hepatic lipogenesis [57]. In this study,
919 MEBOCOST analysis revealed elevated UDPG metabolite, as intermediate of glycogenesis, in
920 HNF4α^{hi} hepatocytes in ApoE$^{-/-}$ /Liver-DKO, which promote hepatic glycogenesis that inhibition
921 of hepatic lipogenesis. Intriguingly, there is a significantly higher tendency of cell fate transition
922 from lipogenic Alb^{hi} hepatocytes into glycogenic HNF4α^{hi} hepatocytes in ApoE$^{-/-}$ /Liver-DKO
923 than ApoE$^{-/-}$ (Fig.S1 B-F), suggests the activated glycogenesis and inhibited lipogenesis in the liver
924 in ApoE$^{-/-}$ /Liver-DKO. As HNF4α^{hi} hepatocytes are positively regulation of hepatic glycogenesis
925 [80,81], in addition to elevated LDLR expression, the elevated hepatic glycogenesis and inhibited
926 hepatic lipogenesis is a novel casual factor that contribute to the diminished atherosclerotic plaque
927 in ApoE$^{-/-}$ /Liver-DKO mice.
928
929 In summary, in our study, we firstly demonstrated how hepatic epsins in mediating PCSK9-driven
930 LDLR degradation (Fig.8). In the absence of hepatic epsins, PCSK9-mediated LDLR degradation
931 is significantly repressed, and higher LDLR expression in the liver that promotes the LDL-C
932 clearance in ApoE$^{-/-}$ /Liver-DKO mice and further inhibition of atherosclerotic plaque progression.
933 In the presence of hepatic epsins, LDLR specially binds to the epsin1 UIM motif that further be
934 processed for PCSK9-driven ubiquitination for proteosome degradation in ApoE$^{-/-}$ mice, which
935 accelerated the LDL-C accumulation and promote the atherosclerotic plaque progression.
936 Mechanistically, we elaborated that elevated pathways involved in LDL particle clearance and
937 diminished genes of de novo lipogenesis in ApoE$^{-/-}$ /Liver-DKO. Especially, we firstly proposed
938 that the cell fate transition from lipogenic Alb^{hi} hepatocytes into glycogenic HNF4α^{hi} hepatocytes
939 might be a novel protective mechanism for combating atherosclerosis in ApoE$^{-/-}$ /Liver-DKO.
940 Finally, for therapeutic study, we synthesized lipid nanoparticles (LNP) encapsulated epsins
941 siRNAs for treatment of WD-induced atherosclerotic ApoE$^{-/-}$ mice, which achieved significantly
942 inhibited dyslipidemia and impeded atherosclerotic plaque progression. However, as the
943 potentially therapeutic novel target for atherosclerosis, therapeutic studies on mice are not
944 sufficient for convincing its medical application. In future, we will further evaluate the efficiency
945 of LNP encapsulated epsins siRNAs in larger animals, such as rabbit or pig, for inhibition of
946 dyslipidemia and atherosclerotic plaque progression.
947
948
949 **Conclusion and Perspective**
950

In this study, we discovered significantly elevated epsin1 and epsin2 expression in both WD-fed mice and atherosclerotic patients, but with dramatically diminished expression of LDLR protein in the liver from WD-fed mice and fatty liver disease patients. To study the roles of liver epsins in atherosclerosis, we specific deleted liver epsin1 and epsin2 using albumin Cre (Liver-DKO) on an ApoE $^{-/-}$ background. We discovered that WD-induced atherosclerosis was significantly inhibited, along with diminished blood cholesterol and triglyceride levels in ApoE $^{-/-}$ Liver-DKO mice.

Mechanistically, scRNA-seq analysis on hepatocyte-derived data revealed elevated pathways involved in LDL particle clearance under WD treatment in ApoE$^{-/-}$ /Liver-DKO mice, which was coupled with diminished plasma LDL-C levels. Further analysis using the MEBOCOST algorithm revealed enhanced communication score between LDLR and cholesterol, suggesting elevated LDL-C clearance in the ApoE$^{-/-}$ Liver-DKO mice. In addition, we showed that loss of epsins in the liver upregulates of LDLR protein level. We further showed that epsins bind LDLR via the ubiquitin-interacting motif (UIM), and PCSK9-triggered LDLR degradation was abolished by depletion of epsins, preventing atheroma progression.

Intriguingly, scRNA-seq analysis revealed the activated cell fate transition from lipogenic Alb ^{hi} hepatocytes to glycogenic HNF4α ^{hi} hepatocytes in the liver of ApoE$^{-/-}$ Liver-DKO mice, which is consistent with its diminished lipogenic genes expression but elevated glycogenic genes expression. The CAD protective score in HNF4α ^{hi} hepatocytes is higher than Alb ^{hi} hepatocytes, which is positively correlated with HNF4α expression level in ApoE$^{-/-}$ Liver-DKO mice. In addition to ApoE$^{-/-}$ mice, analysis of hepatocyte-derived data from hPCSK9-D374Y mice revealed similar pathological pathways involved in atherosclerosis or dyslipidemia as WD-fed ApoE$^{-/-}$ mice, with significantly elevated epsins expression in both hPCSK9-D374Y and WD-fed ApoE$^{-/-}$ mice that mediated LDLR degradation.

Finally, our therapeutic strategy, which involved targeting liver epsins with nanoparticle-encapsulated epsins siRNAs, was highly efficacious at inhibiting dyslipidemia and impeding atherosclerosis. Targeting epsins in the liver may serve as a novel therapeutic strategy to treat atherosclerosis by suppression of PCSK9-mediated LDLR degradation. In future, targeting epsins in the liver using nanoparticle-encapsulated epsins siRNAs, we will test its efficiency at inhibiting of dyslipidemia and impeding atherosclerosis in larger animals, such as rabbit or pig.

Acknowledgments

We thank the imaging core at Boston Children's Hospital, and the Biopolymers Facility at Harvard Medical School for quality control analysis of DNA libraries prepared for scRNA-sequencing. We thank the animal core facility for the daily maintenance at Boston Children's Hospital.

Sources of Funding

This work was supported in part by NIH grants Nos. R01HL137229, R01HL1563626, R01HL158097, and R01HL158097 to HC.

Author contributions

B.Z., K.C., and H.C. conceived and designed the experiments. B.Z., K.C. performed most of the experiments. B.W. contributed to animal experiments. K.G. and K.C. analyzed the scRNA-seq data and performed bioinformatic work. M.M. and S.S. measured plasma cholesterol and

triglyceride. X.H. and J.S. prepared the galactose targeted nanoparticle-encapsulated epsins siRNAs (NPs). S.W. performed the mouse genotyping and colony maintenance. B.Z., K.G., K.L., D.B.C. K.C. and H.C. wrote and edited the article. All the authors reviewed and provided feedback on the article.

Disclosure

None.

Supplemental Material

Extended Methods
Major Resources Table
Nonstandard Abbreviations and Acronyms
Novelty and Significance
Supplemental Fig.1-14

References

1 Libby, P. *et al.* Atherosclerosis. *Nat Rev Dis Primers* **5**, 56, doi:10.1038/s41572-019-0106-z (2019).

2 Pahwa, R. & Jialal, I. in *StatPearls* (2024).

3 Zhu, B. *et al.* Two sides of the same coin: Non-alcoholic fatty liver disease and atherosclerosis. *Vascul Pharmacol* **154**, 107249, doi:10.1016/j.vph.2023.107249 (2023).

4 Dong, Y. *et al.* Epsin-mediated degradation of IP3R1 fuels atherosclerosis. *Nat Commun* **11**, 3984, doi:10.1038/s41467-020-17848-4 (2020).

5 Benito-Vicente, A. *et al.* Familial Hypercholesterolemia: The Most Frequent Cholesterol Metabolism Disorder Caused Disease. *Int J Mol Sci* **19**, doi:10.3390/ijms19113426 (2018).

6 Schaefer, J. R., Kurt, B., Sattler, A., Klaus, G. & Soufi, M. Pharmacogenetic aspects in familial hypercholesterolemia with the special focus on FHMarburg (FH p.W556R). *Clin Res Cardiol Suppl* **7**, 2-6, doi:10.1007/s11789-012-0041-y (2012).

7 Batty, M., Bennett, M. R. & Yu, E. The Role of Oxidative Stress in Atherosclerosis. *Cells* **11**, doi:10.3390/cells11233843 (2022).

8 Markin, A. M. *et al.* The Role of Cytokines in Cholesterol Accumulation in Cells and Atherosclerosis Progression. *Int J Mol Sci* **24**, doi:10.3390/ijms24076426 (2023).

9 Soehnlein, O. & Libby, P. Targeting inflammation in atherosclerosis - from experimental insights to the clinic. *Nat Rev Drug Discov* **20**, 589-610, doi:10.1038/s41573-021-00198-1 (2021).

10 Goldstein, J. L. & Brown, M. S. The LDL receptor. *Arterioscler Thromb Vasc Biol* **29**, 431-438, doi:10.1161/ATVBAHA.108.179564 (2009).

11 Bao, X. *et al.* Targeting proprotein convertase subtilisin/kexin type 9 (PCSK9): from bench to bedside. *Signal Transduct Target Ther* **9**, 13, doi:10.1038/s41392-023-01690-3 (2024).

1040 12 Lu, R. *et al.* Spontaneous severe hypercholesterolemia and atherosclerosis lesions in
1041 rabbits with deficiency of low-density lipoprotein receptor (LDLR) on exon 7.
1042 *EBioMedicine* **36**, 29-38, doi:10.1016/j.ebiom.2018.09.020 (2018).
1043 13 Zhao, H. *et al.* In Vivo AAV-CRISPR/Cas9-Mediated Gene Editing Ameliorates
1044 Atherosclerosis in Familial Hypercholesterolemia. *Circulation* **141**, 67-79,
1045 doi:10.1161/CIRCULATIONAHA.119.042476 (2020).
1046 14 Keeter, W. C., Carter, N. M., Nadler, J. L. & Galkina, E. V. The AAV-PCSK9 murine model
1047 of atherosclerosis and metabolic dysfunction. *Eur Heart J Open* **2**, oeac028,
1048 doi:10.1093/ehjopen/oeac028 (2022).
1049 15 Lee, R. G. *et al.* Efficacy and Safety of an Investigational Single-Course CRISPR Base-
1050 Editing Therapy Targeting PCSK9 in Nonhuman Primate and Mouse Models. *Circulation*
1051 **147**, 242-253, doi:10.1161/CIRCULATIONAHA.122.062132 (2023).
1052 16 Chen, H. *et al.* Epsin is an EH-domain-binding protein implicated in clathrin-mediated
1053 endocytosis. *Nature* **394**, 793-797, doi:10.1038/29555 (1998).
1054 17 Brophy, M. L. *et al.* Myeloid-Specific Deletion of Epsins 1 and 2 Reduces Atherosclerosis
1055 by Preventing LRP-1 Downregulation. *Circ Res* **124**, e6-e19,
1056 doi:10.1161/CIRCRESAHA.118.313028 (2019).
1057 18 Cui, K. *et al.* Epsin Nanotherapy Regulates Cholesterol Transport to Fortify Atheroma
1058 Regression. *Circ Res* **132**, e22-e42, doi:10.1161/CIRCRESAHA.122.321723 (2023).
1059 19 Duan, Y. *et al.* Regulation of cholesterol homeostasis in health and diseases: from
1060 mechanisms to targeted therapeutics. *Signal Transduct Target Ther* **7**, 265,
1061 doi:10.1038/s41392-022-01125-5 (2022).
1062 20 Sanders, F. W. & Griffin, J. L. De novo lipogenesis in the liver in health and disease: more
1063 than just a shunting yard for glucose. *Biol Rev Camb Philos Soc* **91**, 452-468,
1064 doi:10.1111/brv.12178 (2016).
1065 21 Pasula, S. *et al.* Endothelial epsin deficiency decreases tumor growth by enhancing VEGF
1066 signaling. *J Clin Invest* **122**, 4424-4438, doi:10.1172/JCI64537 (2012).
1067 22 Tessneer, K. L. *et al.* Genetic reduction of vascular endothelial growth factor receptor 2
1068 rescues aberrant angiogenesis caused by epsin deficiency. *Arterioscler Thromb Vasc Biol*
1069 **34**, 331-337, doi:10.1161/ATVBAHA.113.302586 (2014).
1070 23 Chen, H. *et al.* Embryonic arrest at midgestation and disruption of Notch signaling
1071 produced by the absence of both epsin 1 and epsin 2 in mice. *Proc Natl Acad Sci U S A*
1072 **106**, 13838-13843, doi:10.1073/pnas.0907008106 (2009).
1073 24 Hao, Y. *et al.* Integrated analysis of multimodal single-cell data. *Cell* **184**, 3573-3587
1074 e3529, doi:10.1016/j.cell.2021.04.048 (2021).
1075 25 Franzen, O., Gan, L. M. & Bjorkegren, J. L. M. PanglaoDB: a web server for exploration of
1076 mouse and human single-cell RNA sequencing data. *Database (Oxford)* **2019**,
1077 doi:10.1093/database/baz046 (2019).
1078 26 Jiang, S. *et al.* Cell Taxonomy: a curated repository of cell types with multifaceted
1079 characterization. *Nucleic Acids Res* **51**, D853-D860, doi:10.1093/nar/gkac816 (2023).
1080 27 Li, M. *et al.* DISCO: a database of Deeply Integrated human Single-Cell Omics data.
1081 *Nucleic Acids Res* **50**, D596-D602, doi:10.1093/nar/gkab1020 (2022).
1082 28 La Manno, G. *et al.* RNA velocity of single cells. *Nature* **560**, 494-498,
1083 doi:10.1038/s41586-018-0414-6 (2018).

1084 29 Bergen, V., Lange, M., Peidli, S., Wolf, F. A. & Theis, F. J. Generalizing RNA velocity to
1085 transient cell states through dynamical modeling. *Nat Biotechnol* **38**, 1408-1414,
1086 doi:10.1038/s41587-020-0591-3 (2020).
1087 30 Trapnell, C. *et al.* The dynamics and regulators of cell fate decisions are revealed by
1088 pseudotemporal ordering of single cells. *Nat Biotechnol* **32**, 381-386,
1089 doi:10.1038/nbt.2859 (2014).
1090 31 Cao, J. *et al.* The single-cell transcriptional landscape of mammalian organogenesis.
1091 *Nature* **566**, 496-502, doi:10.1038/s41586-019-0969-x (2019).
1092 32 Lange, M. *et al.* CellRank for directed single-cell fate mapping. *Nat Methods* **19**, 159-170,
1093 doi:10.1038/s41592-021-01346-6 (2022).
1094 33 Rongbin Zheng, Y. Z., Tadataka Tsuji, Xinlei Gao, Allon Wagner, Nir Yosef, Hong Chen, Lili
1095 Zhang, Yu-Hua Tseng, Kaifu Chen. MEBOCOST: Metabolite-mediated Cell
1096 Communication Modeling by Single Cell Transcriptome. doi:doi:
1097 https://doi.org/10.1101/2022.05.30.494067 (2022).
1098 34 Jin, S. *et al.* Inference and analysis of cell-cell communication using CellChat. *Nat*
1099 *Commun* **12**, 1088, doi:10.1038/s41467-021-21246-9 (2021).
1100 35 Wu, T. *et al.* clusterProfiler 4.0: A universal enrichment tool for interpreting omics data.
1101 *Innovation (Camb)* **2**, 100141, doi:10.1016/j.xinn.2021.100141 (2021).
1102 36 Sanhueza, C. A. *et al.* Efficient Liver Targeting by Polyvalent Display of a Compact Ligand
1103 for the Asialoglycoprotein Receptor. *J Am Chem Soc* **139**, 3528-3536,
1104 doi:10.1021/jacs.6b12964 (2017).
1105 37 Huang, K. W. *et al.* Galactose Derivative-Modified Nanoparticles for Efficient siRNA
1106 Delivery to Hepatocellular Carcinoma. *Biomacromolecules* **19**, 2330-2339,
1107 doi:10.1021/acs.biomac.8b00358 (2018).
1108 38 Tao, W. *et al.* siRNA nanoparticles targeting CaMKIIgamma in lesional macrophages
1109 improve atherosclerotic plaque stability in mice. *Sci Transl Med* **12**,
1110 doi:10.1126/scitranslmed.aay1063 (2020).
1111 39 Zhu, X. *et al.* Long-circulating siRNA nanoparticles for validating Prohibitin1-targeted
1112 non-small cell lung cancer treatment. *Proc Natl Acad Sci U S A* **112**, 7779-7784,
1113 doi:10.1073/pnas.1505629112 (2015).
1114 40 Aragam, K. G. *et al.* Discovery and systematic characterization of risk variants and genes
1115 for coronary artery disease in over a million participants. *Nat Genet* **54**, 1803-1815,
1116 doi:10.1038/s41588-022-01233-6 (2022).
1117 41 Kim, K. *et al.* RORalpha controls hepatic lipid homeostasis via negative regulation of
1118 PPARgamma transcriptional network. *Nat Commun* **8**, 162, doi:10.1038/s41467-017-
1119 00215-1 (2017).
1120 42 De Nardo, W. *et al.* Proteomic analysis reveals exercise training induced remodelling of
1121 hepatokine secretion and uncovers syndecan-4 as a regulator of hepatic lipid
1122 metabolism. *Mol Metab* **60**, 101491, doi:10.1016/j.molmet.2022.101491 (2022).
1123 43 Peet, D. J. *et al.* Cholesterol and bile acid metabolism are impaired in mice lacking the
1124 nuclear oxysterol receptor LXR alpha. *Cell* **93**, 693-704, doi:10.1016/s0092-
1125 8674(00)81432-4 (1998).
1126 44 Zhang, L., Li, Z., Zhang, B., He, H. & Bai, Y. PPIA is a novel adipogenic factor implicated in
1127 obesity. *Obesity (Silver Spring)* **23**, 2093-2100, doi:10.1002/oby.21208 (2015).

1128 45 Clifford, B. L. *et al.* FXR activation protects against NAFLD via bile-acid-dependent
1129 reductions in lipid absorption. *Cell Metab* **33**, 1671-1684 e1674,
1130 doi:10.1016/j.cmet.2021.06.012 (2021).
1131 46 Schadinger, S. E., Bucher, N. L., Schreiber, B. M. & Farmer, S. R. PPARgamma2 regulates
1132 lipogenesis and lipid accumulation in steatotic hepatocytes. *Am J Physiol Endocrinol*
1133 *Metab* **288**, E1195-1205, doi:10.1152/ajpendo.00513.2004 (2005).
1134 47 Lagace, T. A. *et al.* Secreted PCSK9 decreases the number of LDL receptors in
1135 hepatocytes and in livers of parabiotic mice. *J Clin Invest* **116**, 2995-3005,
1136 doi:10.1172/JCI29383 (2006).
1137 48 Beibei Wang, K. C., Bo Zhu, Yunzhou Dong, Donghai Wang, Bandana Singh, Yao Wei Lu,
1138 Hao Wu, Sudarshan Bhattacharjee, Eisa-Beygi Shahram, Scott Wong, Douglas B. Cowan,
1139 Mulong Du, Hong Chen. Epsins promote atherosclerosis through VSMC phenotypic
1140 modulation. doi:doi: https://doi.org/10.1101/2024.01.08.574714 (2024).
1141 49 Linton, M. F. *et al.* in *Endotext* (eds K. R. Feingold *et al.*) (2000).
1142 50 Alves-Bezerra, M. & Cohen, D. E. Triglyceride Metabolism in the Liver. *Compr Physiol* **8**,
1143 1-8, doi:10.1002/cphy.c170012 (2017).
1144 51 Go, G. W. & Mani, A. Low-density lipoprotein receptor (LDLR) family orchestrates
1145 cholesterol homeostasis. *Yale J Biol Med* **85**, 19-28 (2012).
1146 52 Lagace, T. A. PCSK9 and LDLR degradation: regulatory mechanisms in circulation and in
1147 cells. *Curr Opin Lipidol* **25**, 387-393, doi:10.1097/MOL.0000000000000114 (2014).
1148 53 Natarajan, P. & Kathiresan, S. PCSK9 Inhibitors. *Cell* **165**, 1037,
1149 doi:10.1016/j.cell.2016.05.016 (2016).
1150 54 Narasimhan, S. D. Beyond Statins: New Therapeutic Frontiers for Cardiovascular Disease.
1151 *Cell* **169**, 971-973, doi:10.1016/j.cell.2017.05.032 (2017).
1152 55 Robinson, J. G. *et al.* Efficacy and safety of alirocumab in reducing lipids and
1153 cardiovascular events. *N Engl J Med* **372**, 1489-1499, doi:10.1056/NEJMoa1501031
1154 (2015).
1155 56 Sabatine, M. S. *et al.* Evolocumab and Clinical Outcomes in Patients with Cardiovascular
1156 Disease. *N Engl J Med* **376**, 1713-1722, doi:10.1056/NEJMoa1615664 (2017).
1157 57 Chen, J. *et al.* Hepatic glycogenesis antagonizes lipogenesis by blocking S1P via UDPG.
1158 *Science* **383**, eadi3332, doi:10.1126/science.adi3332 (2024).
1159 58 Gribben, C. *et al.* Acquisition of epithelial plasticity in human chronic liver disease.
1160 *Nature* **630**, 166-173, doi:10.1038/s41586-024-07465-2 (2024).
1161 59 Fred, R. G. *et al.* Single-cell transcriptome and cell type-specific molecular pathways of
1162 human non-alcoholic steatohepatitis. *Sci Rep* **12**, 13484, doi:10.1038/s41598-022-
1163 16754-7 (2022).
1164 60 Matchett, K. P. *et al.* Multimodal decoding of human liver regeneration. *Nature* **630**,
1165 158-165, doi:10.1038/s41586-024-07376-2 (2024).
1166 61 Li, Y. *et al.* Single-Cell Transcriptome Analysis Reveals Dynamic Cell Populations and
1167 Differential Gene Expression Patterns in Control and Aneurysmal Human Aortic Tissue.
1168 *Circulation* **142**, 1374-1388, doi:10.1161/CIRCULATIONAHA.120.046528 (2020).
1169 62 Chou, E. L. *et al.* Aortic Cellular Diversity and Quantitative Genome-Wide Association
1170 Study Trait Prioritization Through Single-Nuclear RNA Sequencing of the Aneurysmal

1171 Human Aorta. *Arterioscler Thromb Vasc Biol* **42**, 1355-1374,
1172 doi:10.1161/ATVBAHA.122.317953 (2022).
1173 63 Di Nunzio, G., Hellberg, S., Zhang, Y. et al. Kupffer cells dictate hepatic responses to the
1174 atherogenic dyslipidemic insult. . *Nat Cardiovasc Res* **3**, 356–371,
1175 doi:https://doi.org/10.1038/s44161-024-00448-6 (2024).
1176 64 Timms, K. M. *et al.* A mutation in PCSK9 causing autosomal-dominant
1177 hypercholesterolemia in a Utah pedigree. *Hum Genet* **114**, 349-353,
1178 doi:10.1007/s00439-003-1071-9 (2004).
1179 65 Herbert, B. *et al.* Increased secretion of lipoproteins in transgenic mice expressing
1180 human D374Y PCSK9 under physiological genetic control. *Arterioscler Thromb Vasc Biol*
1181 **30**, 1333-1339, doi:10.1161/ATVBAHA.110.204040 (2010).
1182 66 Maxwell, K. N., Fisher, E. A. & Breslow, J. L. Overexpression of PCSK9 accelerates the
1183 degradation of the LDLR in a post-endoplasmic reticulum compartment. *Proc Natl Acad*
1184 *Sci U S A* **102**, 2069-2074, doi:10.1073/pnas.0409736102 (2005).
1185 67 Chen, H., Polo, S., Di Fiore, P. P. & De Camilli, P. V. Rapid Ca2+-dependent decrease of
1186 protein ubiquitination at synapses. *Proc Natl Acad Sci U S A* **100**, 14908-14913,
1187 doi:10.1073/pnas.2136625100 (2003).
1188 68 Chen, H., Slepnev, V. I., Di Fiore, P. P. & De Camilli, P. The interaction of epsin and Eps15
1189 with the clathrin adaptor AP-2 is inhibited by mitotic phosphorylation and enhanced by
1190 stimulation-dependent dephosphorylation in nerve terminals. *J Biol Chem* **274**, 3257-
1191 3260, doi:10.1074/jbc.274.6.3257 (1999).
1192 69 Chen, H. & De Camilli, P. The association of epsin with ubiquitinated cargo along the
1193 endocytic pathway is negatively regulated by its interaction with clathrin. *Proc Natl Acad*
1194 *Sci U S A* **102**, 2766-2771, doi:10.1073/pnas.0409719102 (2005).
1195 70 Oldham, C. E., Mohney, R. P., Miller, S. L., Hanes, R. N. & O'Bryan, J. P. The ubiquitin-
1196 interacting motifs target the endocytic adaptor protein epsin for ubiquitination. *Curr*
1197 *Biol* **12**, 1112-1116, doi:10.1016/s0960-9822(02)00900-4 (2002).
1198 71 Yan, H. *et al.* MG132, a proteasome inhibitor, enhances LDL uptake in HepG2 cells in
1199 vitro by regulating LDLR and PCSK9 expression. *Acta Pharmacol Sin* **35**, 994-1004,
1200 doi:10.1038/aps.2014.52 (2014).
1201 72 Bottger, R. *et al.* Lipid-based nanoparticle technologies for liver targeting. *Adv Drug Deliv*
1202 *Rev* **154-155**, 79-101, doi:10.1016/j.addr.2020.06.017 (2020).
1203 73 Sato, Y., Kinami, Y., Hashiba, K. & Harashima, H. Different kinetics for the hepatic uptake
1204 of lipid nanoparticles between the apolipoprotein E/low density lipoprotein receptor
1205 and the N-acetyl-d-galactosamine/asialoglycoprotein receptor pathway. *J Control*
1206 *Release* **322**, 217-226, doi:10.1016/j.jconrel.2020.03.006 (2020).
1207 74 Han, X. *et al.* Ligand-tethered lipid nanoparticles for targeted RNA delivery to treat liver
1208 fibrosis. *Nat Commun* **14**, 75, doi:10.1038/s41467-022-35637-z (2023).
1209 75 Zhang, J. *et al.* Liver-Targeted siRNA Lipid Nanoparticles Treat Hepatic Cirrhosis by Dual
1210 Antifibrotic and Anti-inflammatory Activities. *ACS Nano* **14**, 6305-6322,
1211 doi:10.1021/acsnano.0c02633 (2020).
1212 76 Fan, J. *et al.* Rabbit models for the study of human atherosclerosis: from
1213 pathophysiological mechanisms to translational medicine. *Pharmacol Ther* **146**, 104-119,
1214 doi:10.1016/j.pharmthera.2014.09.009 (2015).

1215 77 Hamamdzic, D. & Wilensky, R. L. Porcine models of accelerated coronary
1216 atherosclerosis: role of diabetes mellitus and hypercholesterolemia. *J Diabetes Res*
1217 **2013**, 761415, doi:10.1155/2013/761415 (2013).
1218 78 Shiomi, M. The History of the WHHL Rabbit, an Animal Model of Familial
1219 Hypercholesterolemia (II) - Contribution to the Development and Validation of the
1220 Therapeutics for Hypercholesterolemia and Atherosclerosis. *J Atheroscler Thromb* **27**,
1221 119-131, doi:10.5551/jat.RV17038-2 (2020).
1222 79 Yin, L., Ma, H., Ge, X., Edwards, P. A. & Zhang, Y. Hepatic hepatocyte nuclear factor
1223 4alpha is essential for maintaining triglyceride and cholesterol homeostasis. *Arterioscler*
1224 *Thromb Vasc Biol* **31**, 328-336, doi:10.1161/ATVBAHA.110.217828 (2011).
1225 80 Parviz, F. *et al.* Hepatocyte nuclear factor 4alpha controls the development of a hepatic
1226 epithelium and liver morphogenesis. *Nat Genet* **34**, 292-296, doi:10.1038/ng1175
1227 (2003).
1228 81 Wu, H. *et al.* A negative reciprocal regulatory axis between cyclin D1 and HNF4alpha
1229 modulates cell cycle progression and metabolism in the liver. *Proc Natl Acad Sci U S A*
1230 **117**, 17177-17186, doi:10.1073/pnas.2002898117 (2020).
1231 82 Bonzo, J. A., Ferry, C. H., Matsubara, T., Kim, J. H. & Gonzalez, F. J. Suppression of
1232 hepatocyte proliferation by hepatocyte nuclear factor 4alpha in adult mice. *J Biol Chem*
1233 **287**, 7345-7356, doi:10.1074/jbc.M111.334599 (2012).
1234 83 Yang, T. *et al.* Therapeutic HNF4A mRNA attenuates liver fibrosis in a preclinical model. *J*
1235 *Hepatol* **75**, 1420-1433, doi:10.1016/j.jhep.2021.08.011 (2021).
1236 84 Xu, Y. *et al.* Hepatocyte Nuclear Factor 4alpha Prevents the Steatosis-to-NASH
1237 Progression by Regulating p53 and Bile Acid Signaling (in mice). *Hepatology* **73**, 2251-
1238 2265, doi:10.1002/hep.31604 (2021).
1239
1240
1241
1242
1243
1244 **Figure legend:**
1245
1246 **Fig. 1: Single-cell RNA-sequencing reveals gene expression dynamics in Liver-DKO mice on**
1247 **an ApoE-/- background.** A: Schematic representation of the single-cell RNA-sequencing
1248 (snRNA-seq) process performed on liver tissues from ApoE$^{-/-}$ and ApoE$^{-/-}$/Liver-DKO mice. B:
1249 UMAP visualization illustrating the heterogeneity of hepatocyte cell populations indicating
1250 distinct clustering patterns of hepatocytes in ApoE$^{-/-}$/Liver-DKO mice compared to ApoE$^{-/-}$
1251 controls. C: Dot plot showing the expression of gene markers in respective sub-cell types. D-E:
1252 Elevated gene expression related to LDL particle clearance and decreased gene expression related
1253 to fatty acid synthesis in ApoE$^{-/-}$/Liver-DKO as compared to ApoE$^{-/-}$, shown through single-cell
1254 analysis (D) and real-time quantitative PCR (qPCR) (E). F: Elevated HNF4α expression level in
1255 Liver-DKO mice. Immunofluorescence stain of HNF4α ,Albumin in the liver from both WT and
1256 Liver-DKO mice (left), HNF4α is in red color, Albumin is in green color (marker of hepatocytes),
1257 and DAPI is used for nuclei stain. Quantification of HNF4α immunofluorescence signal intensity
1258 between WT and Liver-DKO (right). G: Western blot of HNF4α for the liver lysates from WT
1259 and Liver-DKO, beta-Actin is used as internal reference (left), the quantification of HNF4α. H:

Hnf4α expression increasing from HC1 Alb^{hi} to HC3 Alb^{hi} in both conditions $ApoE^{-/-}$ and $ApoE^{-/-}$/Liver-DKO. I: Coronary artery disease (CAD) protective score comparing $ApoE^{-/-}$/Liver-DKO to $ApoE^{-/-}$. **Note:** We used the two-tailed t- test to compare the samples in panel (E). expression in both WT and Liver-DKO (right). n=3, **p<0.01, ***p<0.001.

Fig. 2: Enhanced LDL particle clearance and LDLR-cholesterol communication elucidate improved LDL-C clearance and reduced atherogenesis. A-B: Gene Ontology (GO) analysis showing significantly enriched pathways for LDL particle clearance that are upregulated (A) and downregulated (B) in $ApoE^{-/-}$/Liver-DKO relative to $ApoE^{-/-}$. C-D: Illustration of LDLR-cholesterol communication pathways with increased signaling interactions (C) and decreased signaling (D) in $ApoE^{-/-}$/Liver-DKO relative to $ApoE^{-/-}$, indicating enhanced LDL-C particle clearance in $ApoE^{-/-}$/Liver-DKO. E-F: Elevated gene expression related to LDLR-cholesterol interactions and decreased gene expression related to fatty acid synthesis in $ApoE^{-/-}$/Liver-DKO mice, shown through single-cell analysis (E) and real-time quantitative PCR (qPCR) (F). G: Quantitative analysis demonstrating reduced blood cholesterol and triglyceride levels in $ApoE^{-/-}$/Liver-DKO mice, suggesting improved lipid metabolism and clearance. H: Relative receptor expression in $ApoE^{-/-}$/Liver-DKO compared to $ApoE^{-/-}$. i: Relative metabolite abundance in $ApoE^{-/-}$/Liver-DKO compared to $ApoE^{-/-}$. **Note:** We used the CellChat default method for the permutation test to calculate significant communication in panels (C) and (D). We also used the two-tailed t- test to compare the samples in panel (E).

Fig. 3: Single-cell RNA-sequencing reveals gene expression dynamics in PCSK9 D374Y mutated mice. A: UMAP visualization illustrating the heterogeneity of hepatocyte cell populations indicating distinct clustering patterns of hepatocytes in control mice compared to D374Y mutated. B: Dot plot showing the expression of gene markers in respective sub-cell types. C: Hnf4α expression increased from HC1 Alb^{hi} to HC3 Alb^{hi} in both control and D374Y mutated conditions. D: Coronary artery disease (CAD) protective score comparing D374 mutated to control. E: Pseudotime trajectory and RNA velocity analysis mapping the transition pathway from lipogenic Alb^{hi} hepatocytes (HC1 Alb^{hi}) to glucogenic $Hnf4\alpha^{hi}$ hepatocytes (HC3 Alb^{hi}) in control, in contrast to D374Y mutated. F-G: Gene Ontology (GO) analysis showing significantly enriched pathways for upregulated glycolytic process (F) and downregulated LDL particle clearance (G) and in D374Y mutated relative to control. H: Quantitative analysis demonstrating metabolite communication score in D374Y mutated mice compared to control. I: Relative metabolite expression abundance in D374Y mutation compared to control. J: Relative metabolite receptor expression abundance in D374Y mutated compared to control.

Fig. 4: Elevated LDLR expression in the liver of liver specific epsin deficiency mice and diminished LDLR expression in the liver of WD-fed mice. (A) Western blot (WB) analysis of liver tissue harvested from WT and Liver-DKO mice revealed elevated LDLR expression in Liver-DKO (left). Data quantification of LDLR expression (right) (n=3, *p< 0.05). (B) Western blot (WB) analysis of liver tissue harvested from WT (normal diet, ND) and WT (western diet, WD) mice showed diminished LDLR expression and elevated epsin1 and epsin2 expression in WT-WD (left). Data quantification of LDLR expression (right) (n=3, ***p<0.001). (C) Immunofluorescence (IF) analysis of liver cryosections from WT, Liver-DKO mice, and WT-WD

revealed elevated LDLR expression in Liver-DKO (left), but diminished LDLR expression in the liver from WD-fed WT mice (left), however, the diminished LDLR expression in the liver from WD-fed is inhibited in WD-fed Liver-DKO (left). Data quantification of LDLR, Epsin1, Epsin2 expression (right) (n=4, **p<0.01).

Fig.5: Liver-deficiency of epsins inhibits atherosclerotic lesion formation and macrophage accumulation. (A) *En face* ORO staining of aortas (top) from ApoE-/- or ApoE-/- / Liver-DKO mice fed a WD, and unpaired t-test (bottom) for the lesion areas (n=4, ***p< 0.001) (B) Aortic roots from WD-fed ApoE-/- or ApoE-/- Liver-DKO mice stained with ORO or the CD68 macrophage marker. Scale bars=500 um. (C) Plasma triglyceride (TG) and cholesterol levels in WD-fed WT and Liver-DKO mice treated with AAV8-PCSK9 (n=4, *<0.05) (D) Cholesterol in ApoE-/- and ApoE-/- Liver-DKO mice after 8 weeks on a WD (n=4, p*<0.05) (E) ORO staining of liver tissue (n=4).

Fig.6: LDLR is resistant to PCSK9-induced proteasomal degradation in Liver-DKO mice and Liver-DKO primary hepatocytes and directly bind to epsin1 UIM. (A) Western blot (WB) analysis of liver tissue harvested from WT and Liver-DKO mice injected with PCSK9-AAV8 virus revealed PCSK9-triggered LDLR degradation is inhibited in Liver-DKO mice (left). Data quantification (right) (n=3, **<0.01). (B) WB analysis of lysate from primary hepatocytes isolated from WT and Liver-DKO mice, treated with PCSK9, cycloheximide (CHX) and MG132 showed PCSK9-induced LDLR degradation occurred independent of new protein synthesis (in the presence of CHX) but was blocked by either loss of epsins or proteasomal inhibitor MG132 (left). Data quantification (right) (n=3, **p<0.01 vs lane 1, *p<0.05 vs lane 2). (C) Anti-epsin1 co-IPs showed LDLR directly binds epsin 1 in WT, but not Liver-DKO mouse primary hepatocytes (n=4). (D) Epsin deletion mutants and individual protein domains (E) LDLR antibody immunoprecipitation with lysates from HepG2 cell that were transfected by Flag-fused plasmids, including pcDNA full length epsin1, ΔENTH, ΔUIM, DPW/NPF. Anti-FLAG antibody was used for detect the binding between LDLR and epsin1 , ΔUIM is essential for LDLR bind to epsin1. F: LDLR antibody immunoprecipitation with lysates from liver tissues in both WT and Liver-DKO, Anti-ubiquitin antibody was used for detect the ubiquitinated LDLR between WT and Liver-DKO. Liver lysates from both WT and Liver-DKO were also used as Input control for testing anti-LDLR, Epsin1, Epsin2, and GAPDH antibodies.

Fig.7 Nanoparticles (NP) with epsin1/2 siRNA inhibits lesion formation and macrophage accumulation. (A) *En face* ORO staining of aortas (top) from control siRNA NP-treated ApoE$^{-/-}$ or epsin1/2 siRNA NP treated ApoE$^{-/-}$ mice fed a WD, and unpaired t-test (bottom) for lesion areas (n=4, ***p<0.001). (B) Aortic roots from control siRNA NP-treated ApoE$^{-/-}$ or epsin1/2 siRNA NP treated ApoE$^{-/-}$ mice were stained with ORO or the CD68 macrophage marker CD68. Scale = 500 um. (C) Plasma triglyceride (TG) levels in WD-fed ApoE-/- (WT) and epsin siRNA-nanoparticle (NP) treated mice (n=4, *p<0.05). (D) Cholesterol levels in WD-fed ApoE-/- (WT) and epsin siRNA-nanoparticle (NP) treated mice (n=4, *p<0.05). (E) Schematic of the targeted hybrid siRNA NP platform composed of a lipid-PEG shell with a targeting ligand and a PLGA core containing G0-C14/siRNA complexes (left). Synthesis of G0-C14 by reacting alkyl epoxides with polyamidoamine generation 0 (PAMAM, G0) with a ratio of 7:1 through ring-opening chemistry (right). We will synthesize G0-C14 analogs by changing the G0 to C14 ratio and the alkyl chain length. (F) Cytometry of uptake of Gal-targeted Cy5.5-siRNA NPs vs non-targeted

Cy5.5-siRNA NPs in THLE-3 cells. (G) Western blots of liver lysates isolated from WD-fed ApoE-/- mice (8 weeks) and treated with control or epsin siRNA NPs (0.75 nmoles) for 3 weeks (2 doses/week) (n=4).

Fig.8 Western diet (WD)-fed ApoE$^{-/-}$/Liver-DKO mice have elevated low-density lipoprotein cholesterol (LDL-C) clearance compared with WD-fed ApoE$^{-/-}$ mice that is attributable to promoted the cell fate transition from Alb^{hi} lipogenic hepatocytes to HNFα ^{hi} glycogenic hepatocytes. In the liver, the glycogenesis inhibits lipogenesis. Consequently, the progression of atherosclerotic plaques are significantly ameliorated in WD-fed ApoE$^{-/-}$ /Liver-DKO mice. Mechanistically, loss of epsins protein in the liver prevent ubiquitination-driven LDLR degradation. The expressed LDLR in hepatocyte cell membrane uptakes LDL-C from the circulation. In the presence of epsins protein in the liver (top), in WT mice, PCSK9 bind to LDLR, epsins protein mediate LDLR ubiquitination, and the ubiquitinated LDLR is directed to lysosomes for protein degradation. As a result, elevated circulating LDL-C due to PCSK9-mediated LDLR degradation. In the absence of epsins protein in the liver (bottom), in epsin1/2 Liver-DKO mice, PCSK9 bind to LDLR, but the LDLR ubiquitination is abolished thanks to the deficiency of epsins protein. The LDLR is directed to recycling endosomes, and LDLR protein can be recycled and back to the membrane of hepatocytes. As a result, diminished circulating LDL-C thanks to the recycling LDLR.

Fig.S1 Overview of animal models. A: Workflow of generation of *epsin1* $^{fl/fl}$, *epsin2* $^{-/-}$, Albumin Cre $^{+/-}$ (Liver-DKO), *epsin1* $^{+/+}$, and *epsin2* $^{+/+}$, Albumin Cre $^{+/-}$ as control group (WT). B: Workflow of generation of *epsin1* $^{fl/fl}$, *epsin2* $^{-/-}$, Albumin Cre $^{+/-}$, *Apoe* $^{-/-}$ (Liver-DKO / *Apoe* $^{-/-}$), and *epsin1* $^{+/+}$, *epsin2* $^{+/+}$, Albumin Cre $^{+/-}$, *Apoe* $^{-/-}$ as control group (WT / *Apoe* $^{-/-}$).

Fig.S2 Elevated epsin1 and epsin2 expression in the aorta from CAD patients, and recruitment of CD68 positive macrophages in the aorta from CAD patients that colocalization to both epsin1 and epsin2. A: Immunofluorescence co-stain of epsin1 and CD68 antibodies in aortas from both healthy control and CAD patients, epsin1 is in red color, CD68 is in green color, and DAPI is used for nuclei stain. The atherosclerotic lesion is encircled with dashed line in CAD patients. B: Immunofluorescence co-stain of epsin2 and CD68 antibodies in aortas from both healthy control and CAD patients, epsin2 is in red color, CD68 is in green color, and DAPI is used for nuclei stain. The atherosclerotic lesion is highlighted that below the dashed line in CAD patients. C: Quantification of epsin1 and epsin2 immunofluorescence signal intensity between healthy control and CAD patients. CD68 expression is highly colocalized with both epsin1 and epsin2 in CAD patients, and the overlay percentage between CD68 and epsin1 or CD68 and epsin2 are quantified. N=5, *** $p<0.001$.

Fig.S3 Elevated expression of epsin1 and epsin2 but diminished expression of LDLR protein in hepatocytes from the livers of NASH patients. A: Immunofluorescence staining of epsin1, epsin2 , LDLR and albumin protein in the livers of healthy control (left) and NASH patients (right). LDLR protein signals in green color, and albumin protein signals in red color, DAPI is used for nuclei stain. B: Quantification of epsin1, epsin2, LDLR immunofluorescence signal intensity in both healthy control and NASH patients. N=5, *** $p<0.001$.

Fig.S4 Diminished HNF4α expression level in NASH (Cirrhosis) patients. A: Immunofluorescence stain of HNF4α in the liver from both healthy control and cirrhosis patients (left), HNF4α is in green color, and DAPI is used for nuclei stain. Quantification of HNF4α immunofluorescence signal intensity between healthy control and cirrhosis patients (right). B: Western blot of HNF4α for the liver lysates from biopsy in both healthy control and NASH patients, beta-Actin is used as internal reference (left), the quantification of HNF4α expression in both healthy control and cirrhosis patients (right). C: Relative expression of HNF4α mRNA in both healthy control and NASH patients measured by RT-qPCR. N=3, * $p<0.05$, ** $p<0.01$, *** $p<0.001$.

Fig. S5: Single-cell RNA-sequencing reveals hepatocyte transition in Liver-DKO mice on an ApoE$^{-/-}$ background. A: A relatively high proportion of HC Hnf4α^{hi} in ApoE$^{-/-}$/Liver-DKO and a relatively high proportion of HC2 Alb^{hi} and HC3 Alb^{hi} of ApoE$^{-/-}$. B: Pseudotime trajectory and Rna velocity analysis mapping the transition pathway from lipogenic Alb^{hi} hepatocytes to glucogenic Hnf4α^{hi} hepatocytes in ApoE$^{-/-}$/Liver-DKO, in contrast to ApoE$^{-/-}$. C-E: CellRank analysis indicating more dynamic shifts from lipogenic Alb^{hi} hepatocytes to glucogenic Hnf4α^{hi} hepatocytes in ApoE$^{-/-}$/Liver-DKO compared to ApoE$^{-/-}$. CellRank probability calculation for hepatocyte sub-cell populations in ApoE$^{-/-}$ (C), and in ApoE$^{-/-}$/Liver-DKO (E). D-F: Violin plots show transition probabilities of initial to terminal states within hepatocyte sub-cell populations. in ApoE$^{-/-}$ controls (D), and in ApoE$^{-/-}$/Liver-DKO mice (F). **Note:** We used the two-sample proportion test to compare the cell's proportion in panel (A).

Fig.S6: Comprehensive cell type-specific gene markers and their corresponding expressions. A: UMAP visualization of ApoE$^{-/-}$/Liver-DKO cell populations compared to ApoE$^{-/-}$. B: Dot plot illustrating the percentage of cells expressing each gene marker corresponding to specific cell types in ApoE$^{-/-}$/Liver-DKO and ApoE$^{-/-}$ mice. The size of the dots represents the proportion of cells expressing the marker, while the color intensity indicates the expression level of the gene marker in each cell type.

Fig.S7: Diminished expression of lipogenic genes and elevated apolipoprotein genes are identified as indicators of inhibition of lipogenesis in HNF4α^{hi} hepatocytes. A: Feature plots show diminished expression of lipogenic genes in ApoE$^{-/-}$/Liver-DKO compared to ApoE$^{-/-}$. B: Shows gene expression dynamic with respect to pseudo time from Alb^{hi} to Hnf4 α^{hi} hepatocytes. The elevated HNF4α expression in HNF4α^{hi} hepatocytes is positively correlated to the diminished expression of Acaca and the elevated expression of Apoa4 and Apob in ApoE$^{-/-}$/Liver-DKO.

Fig.S8: Enhanced GO pathways enriched in plasma lipoprotein particle clearance and diminished glycolytic process in ApoE$^{-/-}$/Liver-DKO hepatocytes. A-C: CNET plots highlight the specific GO pathway enrichments related to genes upregulated in ApoE$^{-/-}$/Liver-DKO within the hepatocyte subtypes. D-G: CNET plots highlight the GO pathway enrichments related to genes downregulated in ApoE$^{-/-}$/Liver-DKO within the hepatocyte sub-populations. **Note:** The edge color represents different pathways, and the corresponding circle's number indicates the number of genes associated with the pathway.

Fig.S9: Enhanced Rorα-cholesterol and Sdc4-Fn1 communication pathways and diminished Bsg-Ppia and Nr1h4-AndrosteroneHSD17B6 communication pathways in ApoE$^{-/-}$/Liver-DKO hepatocytes. A: Chord plot highlights the specific Rorα-cholesterol and Sdc4-Fn1 communication related to genes and metabolites upregulated in ApoE$^{-/-}$/Liver-DKO. B: Chord plot exhibits the specific Bsg-Ppia and Nr1h4-AndrosteroneHSD17B6 communication associated to genes and metabolites downregulated in ApoE$^{-/-}$/Liver-DKO. **Note:** Edge and outer lower half-circle colors represent sender cell types, while inner lower and upper half-circle colors indicate receiver cell types.

Fig.S10: Elevated gene expression related to glycogenesis and diminished lipogenic gene expression in ApoE$^{-/-}$/Liver-DKO as compared to ApoE$^{-/-}$, shown through single-cell analysis and real-time quantitative PCR (qPCR) validation. A: Violin plots of gene expression related to glycogenesis (Gys2, Gck, Pgm1) and lipogenesis (Acly) and cholesterol clearance (Apoa2, Apob) in ApoE$^{-/-}$/Liver-DKO as compared to ApoE$^{-/-}$, shown through single-cell analysis B: Validation of genes expression involved in glycogenesis and lipogenesis by real-time quantitative PCR (qPCR) in the liver from both ApoE$^{-/-}$ and ApoE$^{-/-}$/Liver-DKO mice. N=3, * $p<0.05$, ** $p<0.001$, *** $p<0.0001$.

Fig.S11: Elevated gene expression related to glycogenesis and diminished lipogenic gene expression in different clustered hepatocytes, including HC1 Alb^{hi}, HC2 Alb^{hi}, HC3 Alb^{hi}, and HC HNF4α^{hi} in ApoE$^{-/-}$/Liver-DKO as compared to ApoE$^{-/-}$. A: Downregulated expression of lipogenic genes, such as Scd1, Acaca, but with upregulated expression apolipoprotein genes (Apoa4, Apob) in different clustered hepatocytes in the liver of ApoE$^{-/-}$/Liver-DKO, indicates diminished lipogenesis and elevated capacity for low-density lipoprotein clearance in the liver of ApoE$^{-/-}$/Liver-DKO. B: Upregulated expression of glycogenic genes, such as Pgm1, Gys2, and Ugp2, in different clustered hepatocytes in the liver of ApoE$^{-/-}$/Liver-DKO, reveals elevated glycogenesis in the liver of ApoE$^{-/-}$/Liver-DKO.

Fig.S12: Diminished apolipoprotein genes expression in hPCSK9-D374Y mutant compared with control. Downregulated expression of apolipoprotein genes, such as Apoa1, Apoa2, Apoa4, Apoc1, Apoc2, Apoc3 and Apob, in different clustered hepatocytes (HC1, HC2, HC3) in hPCSK9-D374Y mutant compared with control, indicates diminished low-density lipoprotein clearance in hPCSK9-D374Y mutant.

Fig.S13: Diminished HNF4α and elevated epsin1 expression in the different clustered hepatocytes in the liver from hPCSK9-D374Y mutant. Downregulated expression of genes involved in the transportation of low-density lipoprotein cholesterol and lipogenesis, such as Ldlr, Abca1, and genes participate in fatty acid metabolism (Sdc4) in the different clustered hepatocytes in the liver from hPCSK9-D374Y mutant, indicates the dyslipidemia in hPCSK9-D374Y mutant. Diminished HNF4α and Albumin expression in the different clustered hepatocytes (HC1, HC2, HC3) in the liver in hPCSK9-D374Y mutant, which negatively correlated to its elevated epsin1 expression.

Fig.S14: Elevated expression lipogenic genes and diminished glycogenic genes in the different clustered hepatocytes in the liver in hPCSK9-D374Y mutant. A: Upregulated expression of

genes involved in lipogenesis, such as Acly and Fasn, in the different clustered hepatocytes in the liver in hPCSK9-D374Y mutant. B: Downregulated expression of genes that participate in glycogenesis, such as Gys2 and Ugp2, in the different clustered hepatocytes in the liver in hPCSK9-D374Y mutant.

Fig.1

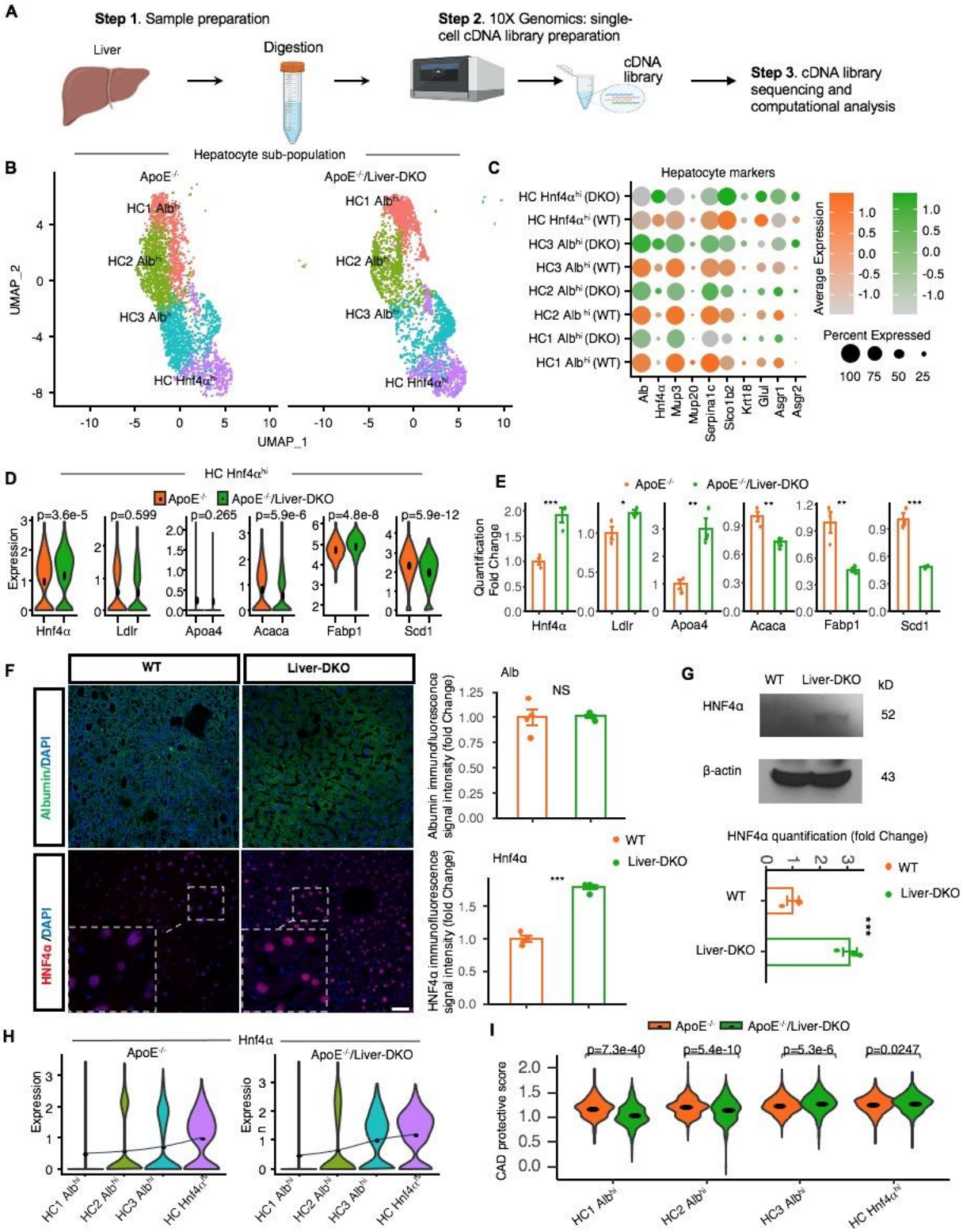
A
Step 1. Sample preparation
Liver
Digestion
Step 2. 10X Genomics: single-cell cDNA library preparation
cDNA library
Step 3. cDNA library sequencing and computational analysis
Hepatocyte sub-population
B
ApoE-/-
ApoE-/-/Liver-DKO
HC1 Albhi
HC2 Albhi
HC3 Albhi
HC Hnf4αhi
UMAP_2
UMAP_1
C
Hepatocyte markers
HC Hnf4αhi (DKO)
HC Hnf4αhi (WT)
HC3 Albhi (DKO)
HC3 Albhi (WT)
HC2 Albhi (DKO)
HC2 Albhi (WT)
HC1 Albhi (DKO)
HC1 Albhi (WT)
Alb
Hnf4α
Mup3
Mup20
Serpina1c
Slco1b2
Krt18
Glul
Asgr1
Asgr2
Average Expression
Percent Expressed
D
HC Hnf4αhi
ApoE-/-
ApoE-/-/Liver-DKO
p=3.6e-5
p=0.599
p=0.265
p=5.9e-6
p=4.8e-8
p=5.9e-12
Expression
Hnf4α
Ldlr
Apoa4
Acaca
Fabp1
Scd1
E
ApoE-/-
ApoE-/-/Liver-DKO
Quantification Fold Change
F
WT
Liver-DKO
Albumin/DAPI
HNF4α /DAPI
Alb
NS
Albumin immunofluorescence signal intensity (fold Change)
Hnf4α
HNF4α immunofluorescence signal intensity (fold Change)
G
WT
Liver-DKO
kD
HNF4α
52
β-actin
43
HNF4α quantification (fold Change)
H
Hnf4α
ApoE-/-
ApoE-/-/Liver-DKO
Expression
HC1 Albhi
HC2 Albhi
HC3 Albhi
HC Hnf4αhi
I
ApoE-/-
ApoE-/-/Liver-DKO
p=7.3e-40
p=5.4e-10
p=5.3e-6
p=0.0247
CAD protective score

Fig.2

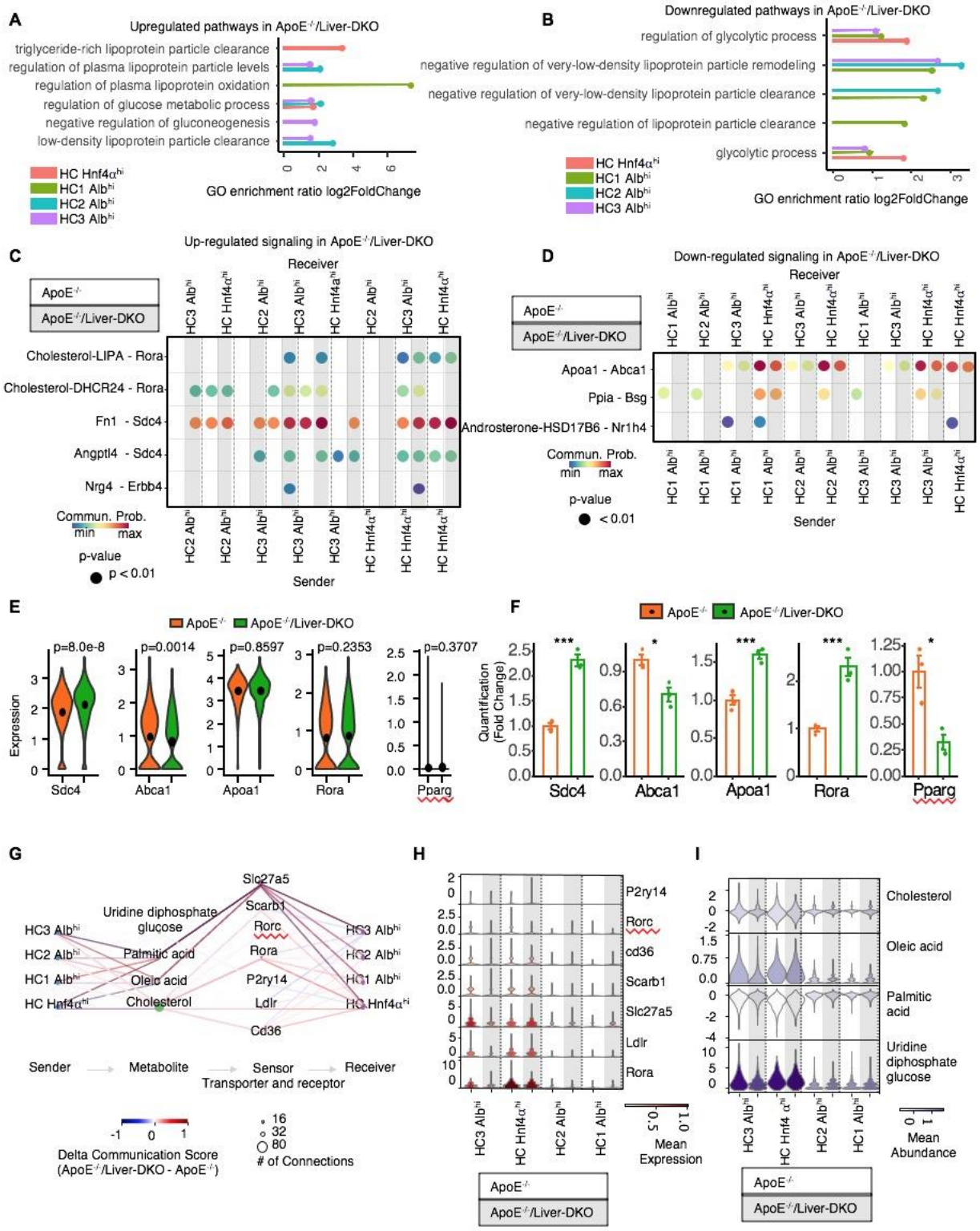
A
Upregulated pathways in ApoE-/-/Liver-DKO
triglyceride-rich lipoprotein particle clearance
regulation of plasma lipoprotein particle levels
regulation of plasma lipoprotein oxidation
regulation of glucose metabolic process
negative regulation of gluconeogenesis
low-density lipoprotein particle clearance
HC Hnf4α hi
HC1 Alb hi
HC2 Alb hi
HC3 Alb hi
GO enrichment ratio log2FoldChange
B
Downregulated pathways in ApoE-/-/Liver-DKO
regulation of glycolytic process
negative regulation of very-low-density lipoprotein particle remodeling
negative regulation of very-low-density lipoprotein particle clearance
negative regulation of lipoprotein particle clearance
glycolytic process
GO enrichment ratio log2FoldChange
C
Up-regulated signaling in ApoE-/-/Liver-DKO
Receiver
ApoE-/-
ApoE-/-/Liver-DKO
Cholesterol-LIPA - Rora
Cholesterol-DHCR24 - Rora
Fn1 - Sdc4
Angptl4 - Sdc4
Nrg4 - Erbb4
Commun. Prob.
min max
p-value
p < 0.01
Sender
D
Down-regulated signaling in ApoE-/-/Liver-DKO
Receiver
Apoa1 - Abca1
Ppia - Bsg
Androsterone-HSD17B6 - Nr1h4
Commun. Prob.
min max
p-value
< 0.01
Sender
E
ApoE-/-
ApoE-/-/Liver-DKO
p=8.0e-8
p=0.0014
p=0.8597
p=0.2353
p=0.3707
Expression
Sdc4
Abca1
Apoa1
Rora
Pparg
F
ApoE-/-
ApoE-/-/Liver-DKO
Quantification (Fold Change)
Sdc4
Abca1
Apoa1
Rora
Pparg
G
Slc27a5
Scarb1
Rorc
Rora
P2ry14
Ldlr
Cd36
Uridine diphosphate glucose
Palmitic acid
Oleic acid
Cholesterol
HC3 Alb hi
HC2 Alb hi
HC1 Alb hi
HC Hnf4α hi
Sender
Metabolite
Sensor
Receiver
Transporter and receptor
Delta Communication Score (ApoE-/-/Liver-DKO - ApoE-/-)
16
32
80
# of Connections
H
P2ry14
Rorc
cd36
Scarb1
Slc27a5
Ldlr
Rora
Mean Expression
ApoE-/-
ApoE-/-/Liver-DKO
I
Cholesterol
Oleic acid
Palmitic acid
Uridine diphosphate glucose
Mean Abundance
ApoE-/-
ApoE-/-/Liver-DKO

Fig.3

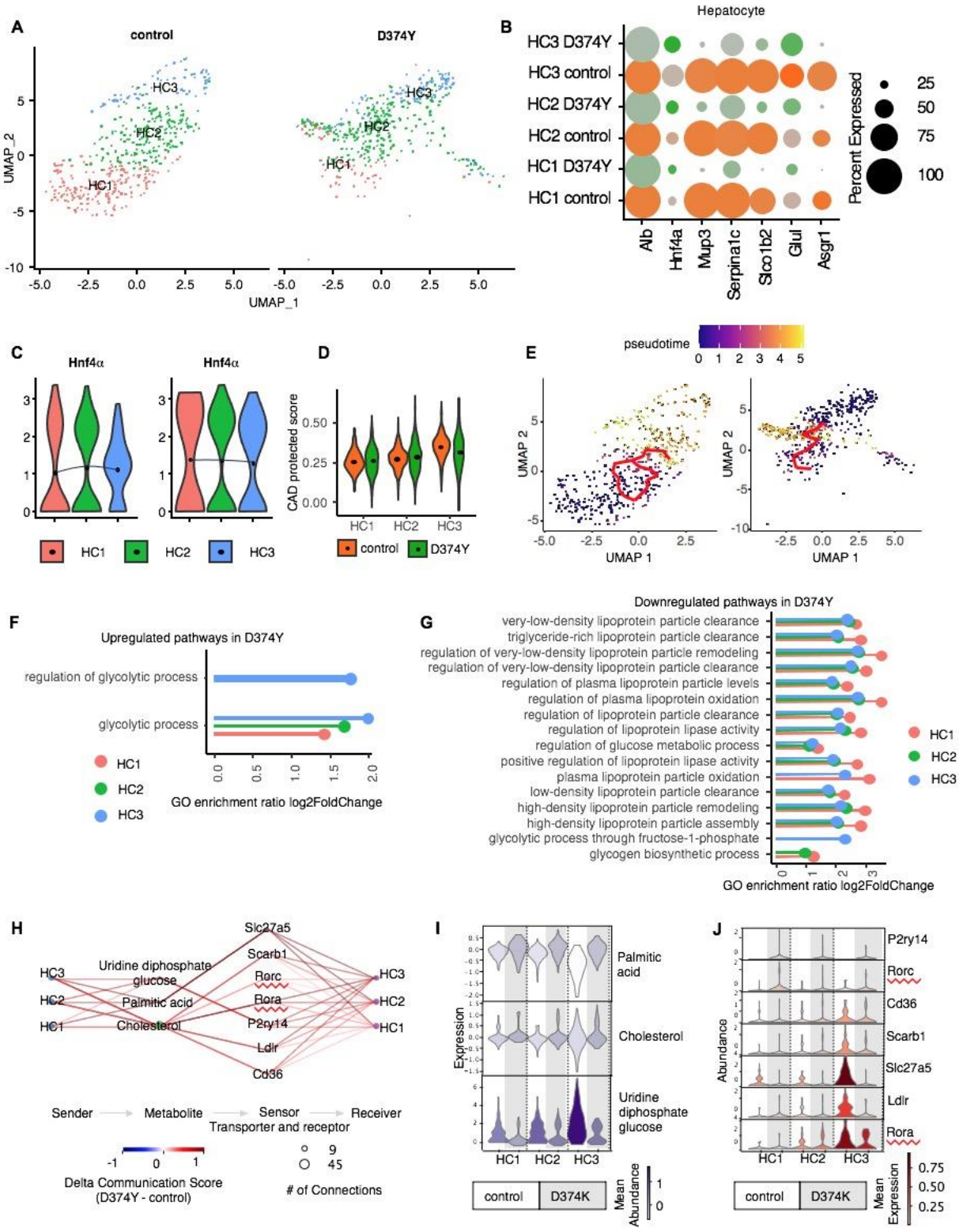
A
control
D374Y
HC3
HC2
HC1
UMAP_2
UMAP_1
B
Hepatocyte
HC3 D374Y
HC3 control
HC2 D374Y
HC2 control
HC1 D374Y
HC1 control
Alb
Hnf4a
Mup3
Serpina1c
Slco1b2
Glul
Asgr1
Percent Expressed
25
50
75
100
C
Hnf4α
Hnf4α
HC1
HC2
HC3
D
CAD protected score
HC1
HC2
HC3
control
D374Y
E
pseudotime
UMAP 2
UMAP 1
F
Upregulated pathways in D374Y
regulation of glycolytic process
glycolytic process
HC1
HC2
HC3
GO enrichment ratio log2FoldChange
G
Downregulated pathways in D374Y
very-low-density lipoprotein particle clearance
triglyceride-rich lipoprotein particle clearance
regulation of very-low-density lipoprotein particle remodeling
regulation of very-low-density lipoprotein particle clearance
regulation of plasma lipoprotein particle levels
regulation of plasma lipoprotein oxidation
regulation of lipoprotein particle clearance
regulation of lipoprotein lipase activity
regulation of glucose metabolic process
positive regulation of lipoprotein lipase activity
plasma lipoprotein particle oxidation
low-density lipoprotein particle clearance
high-density lipoprotein particle remodeling
high-density lipoprotein particle assembly
glycolytic process through fructose-1-phosphate
glycogen biosynthetic process
HC1
HC2
HC3
GO enrichment ratio log2FoldChange
H
HC3
HC2
HC1
Uridine diphosphate glucose
Palmitic acid
Cholesterol
Slc27a5
Scarb1
Rorc
Rora
P2ry14
Ldlr
Cd36
Sender
Metabolite
Sensor
Receiver
Transporter and receptor
Delta Communication Score (D374Y - control)
# of Connections
I
Expression
Palmitic acid
Cholesterol
Uridine diphosphate glucose
HC1
HC2
HC3
control
D374K
Mean Abundance
J
Abundance
P2ry14
Rorc
Cd36
Scarb1
Slc27a5
Ldlr
Rora
HC1
HC2
HC3
control
D374K
Mean Expression

1550
1551 **Fig.4**

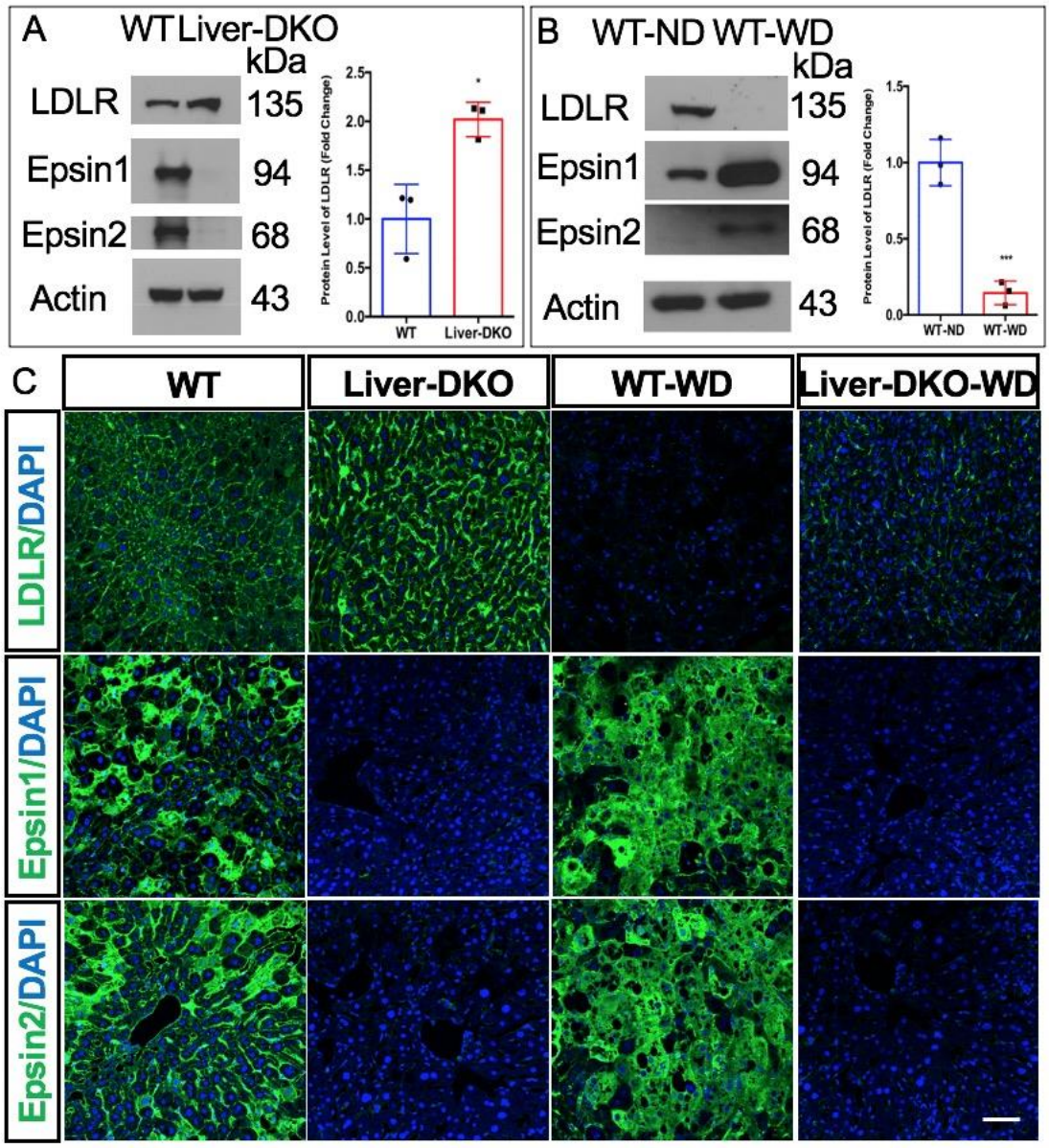

1552
1553
1554
1555

Fig.5

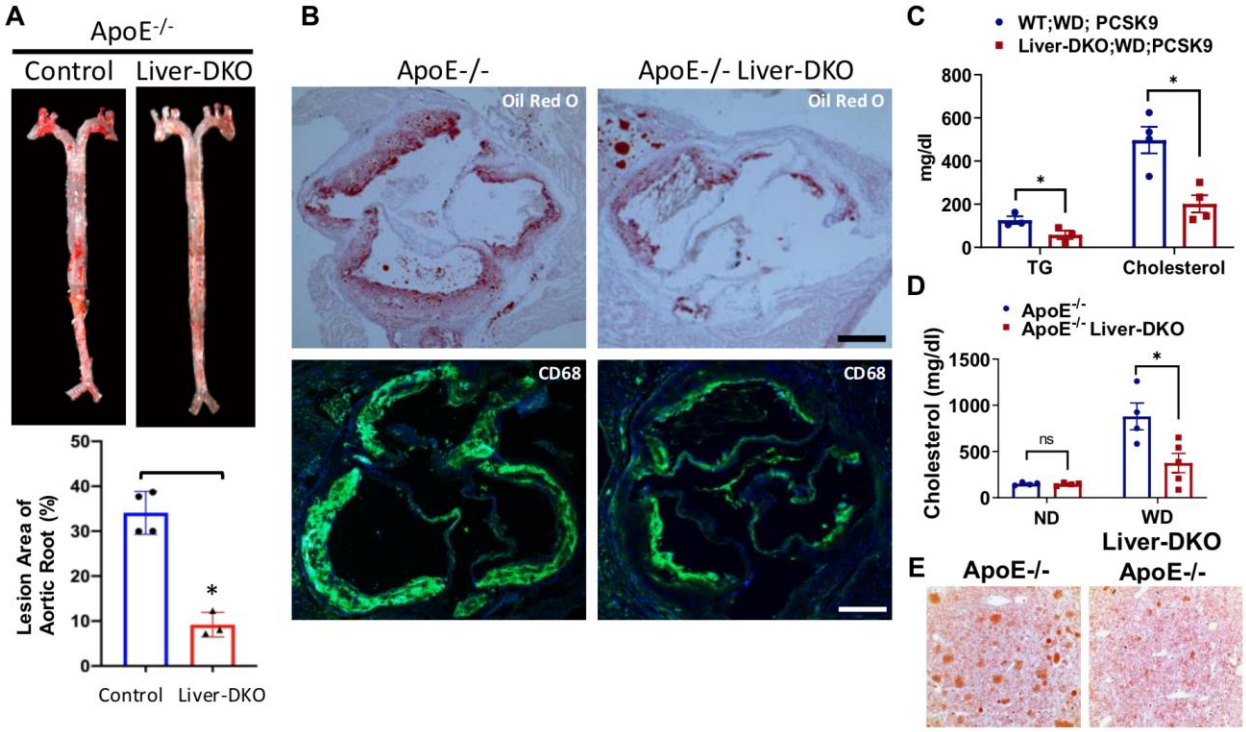
A
ApoE-/-
Control
Liver-DKO
Lesion Area of Aortic Root (%)
50
40
30
20
10
0
*
Control
Liver-DKO
B
ApoE-/-
ApoE-/- Liver-DKO
Oil Red O
Oil Red O
CD68
CD68
C
WT;WD; PCSK9
Liver-DKO;WD;PCSK9
mg/dl
800
600
400
200
0
*
*
TG
Cholesterol
D
ApoE-/-
ApoE-/- Liver-DKO
Cholesterol (mg/dl)
1500
1000
500
0
ns
*
ND
WD
E
ApoE-/-
Liver-DKO
ApoE-/-

1583
1584 **Fig.6**
1585

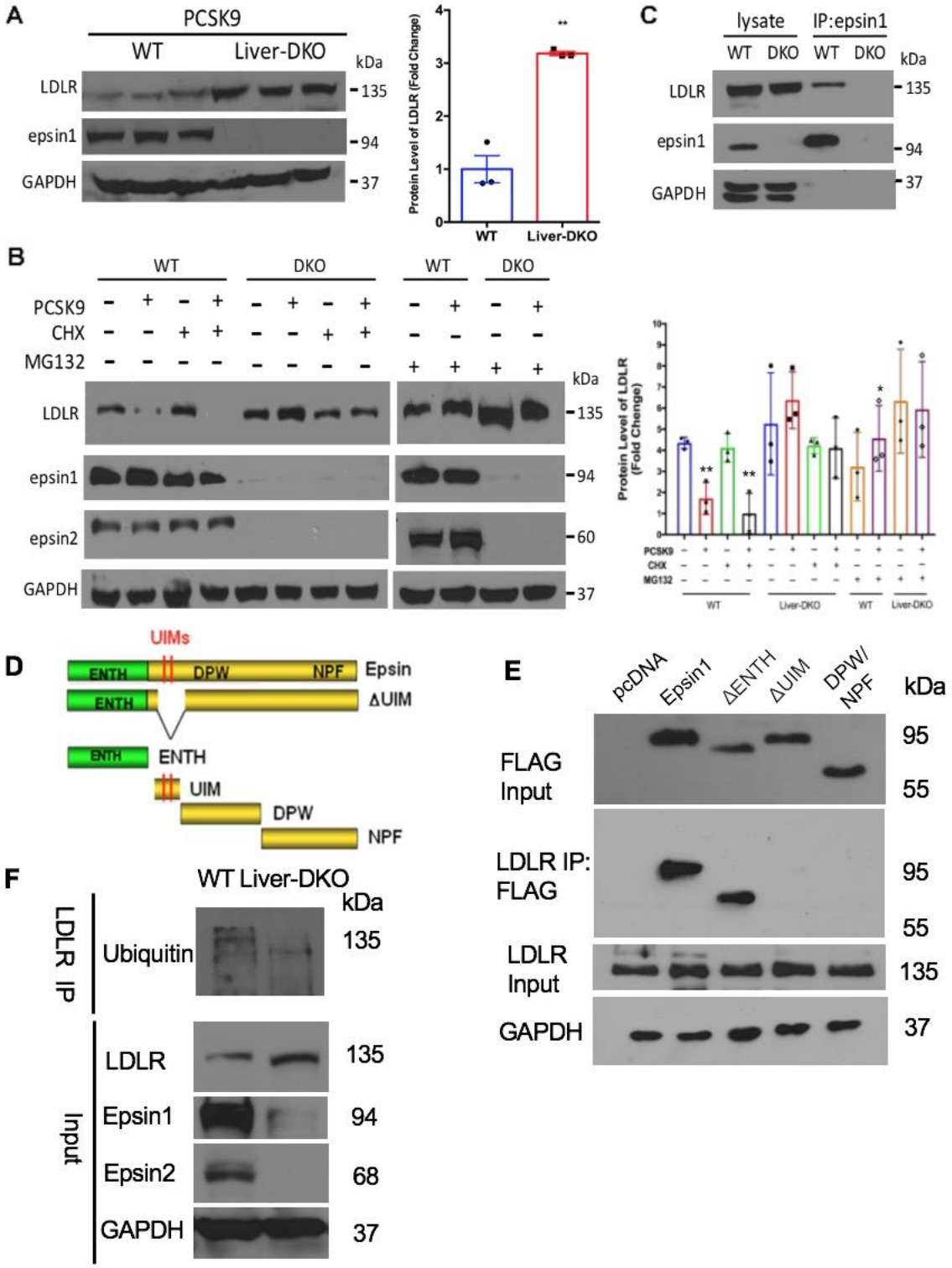

1586
1587
1588

Fig.7

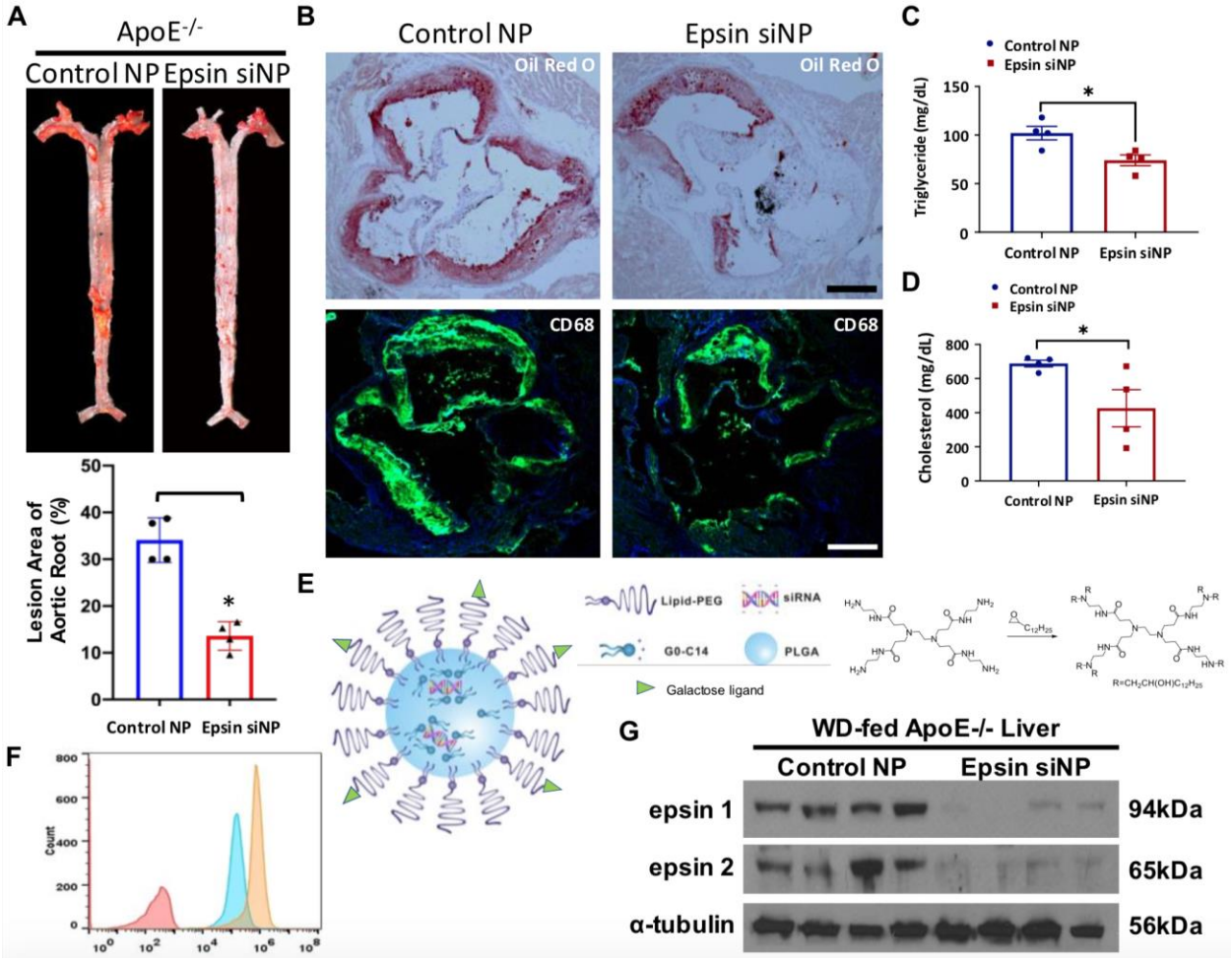
A
ApoE-/-
Control NP
Epsin siNP
Lesion Area of Aortic Root (%)
Control NP
Epsin siNP
B
Control NP
Epsin siNP
Oil Red O
CD68
C
Control NP
Epsin siNP
Triglyceride (mg/dL)
D
Cholesterol (mg/dL)
E
Lipid-PEG
siRNA
G0-C14
PLGA
Galactose ligand
F
Count
G
WD-fed ApoE-/- Liver
epsin 1
epsin 2
α-tubulin
94kDa
65kDa
56kDa

1610
1611 **Fig.8**

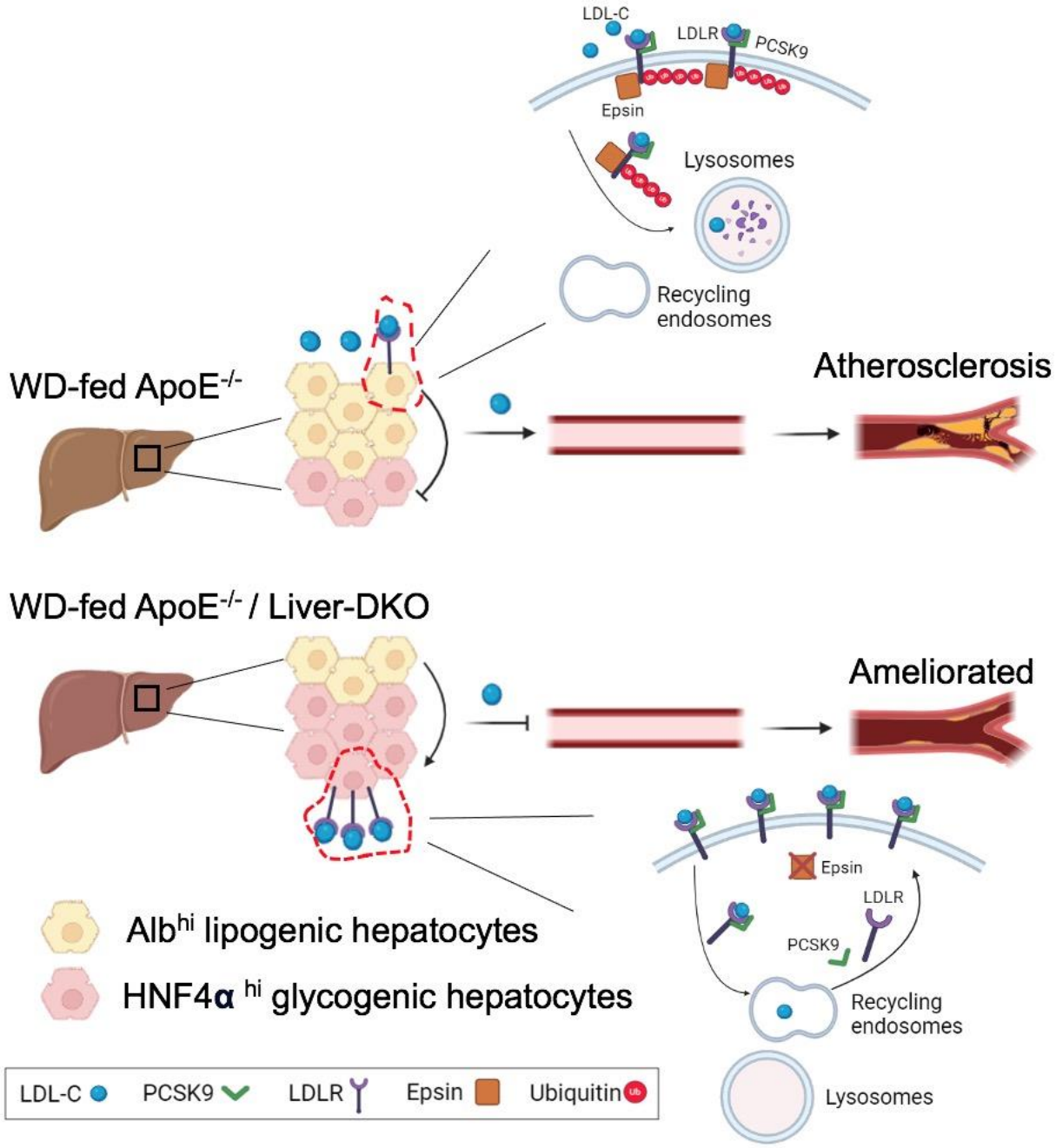

1612
1613
1614
1615
1616
1617
1618
1619
1620

1621 **Fig.S1**

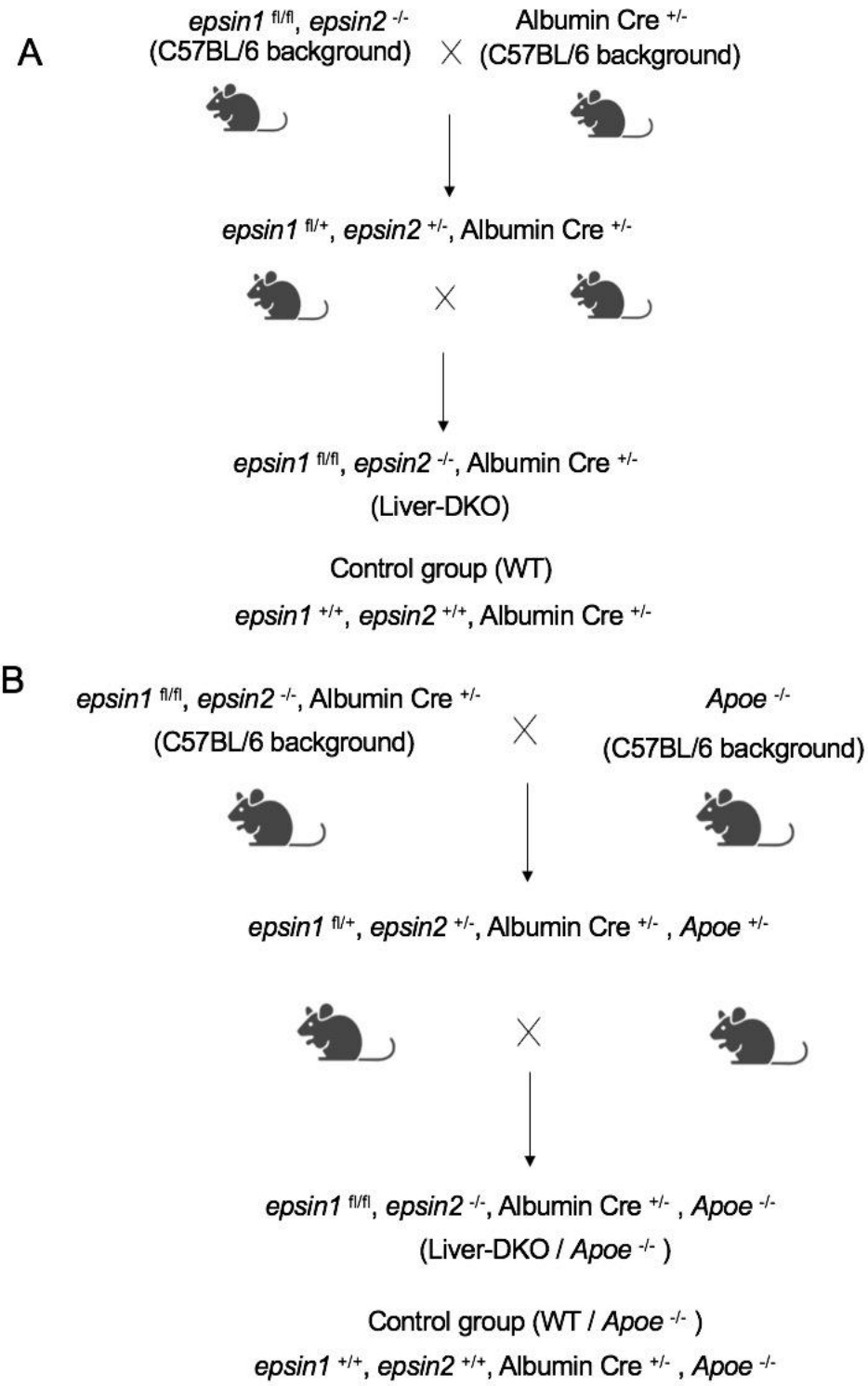

1622
1623
1624
1625

1626 **Fig.S2**

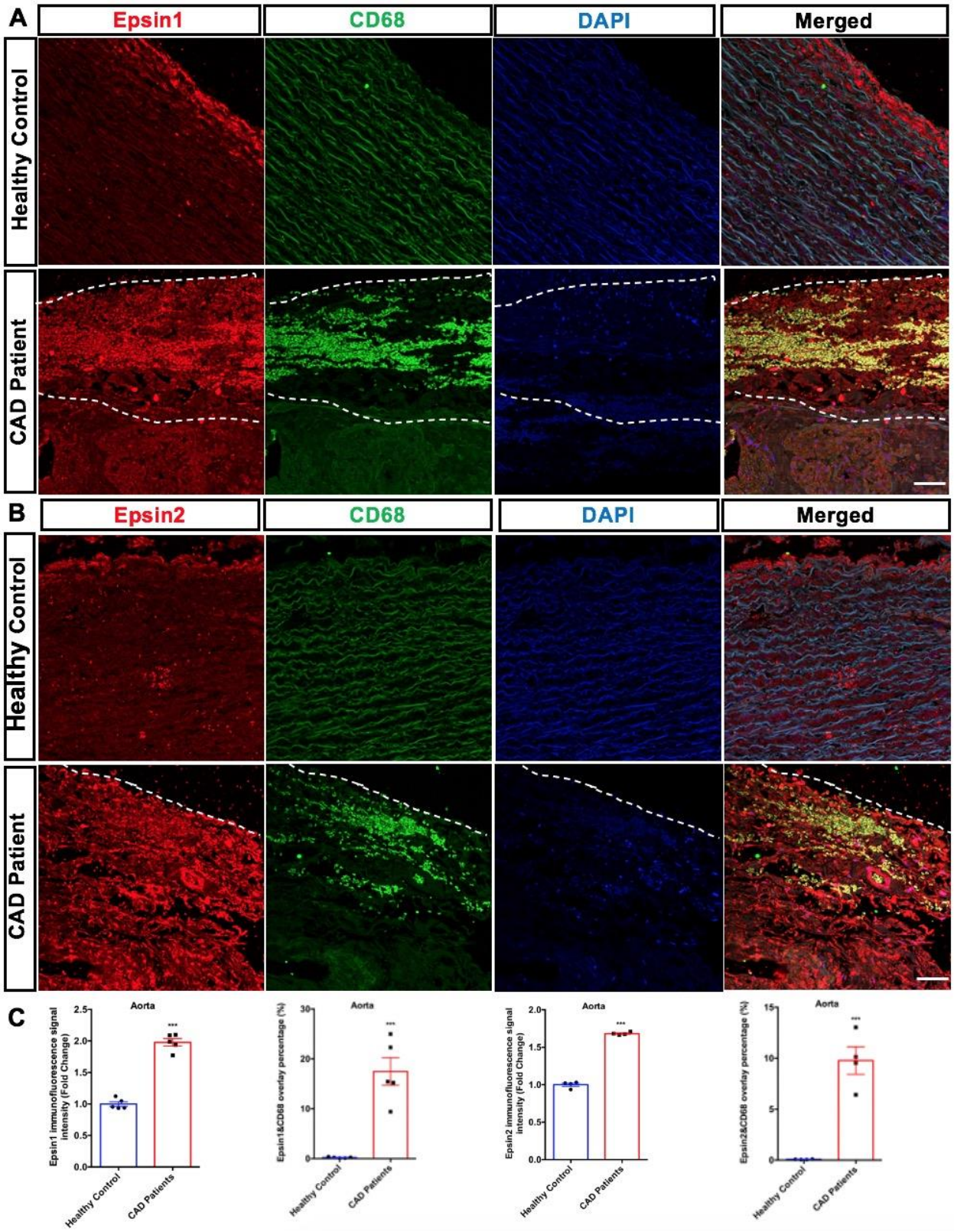

1627
1628
1629

1630
1631
1632 **Fig.S3**

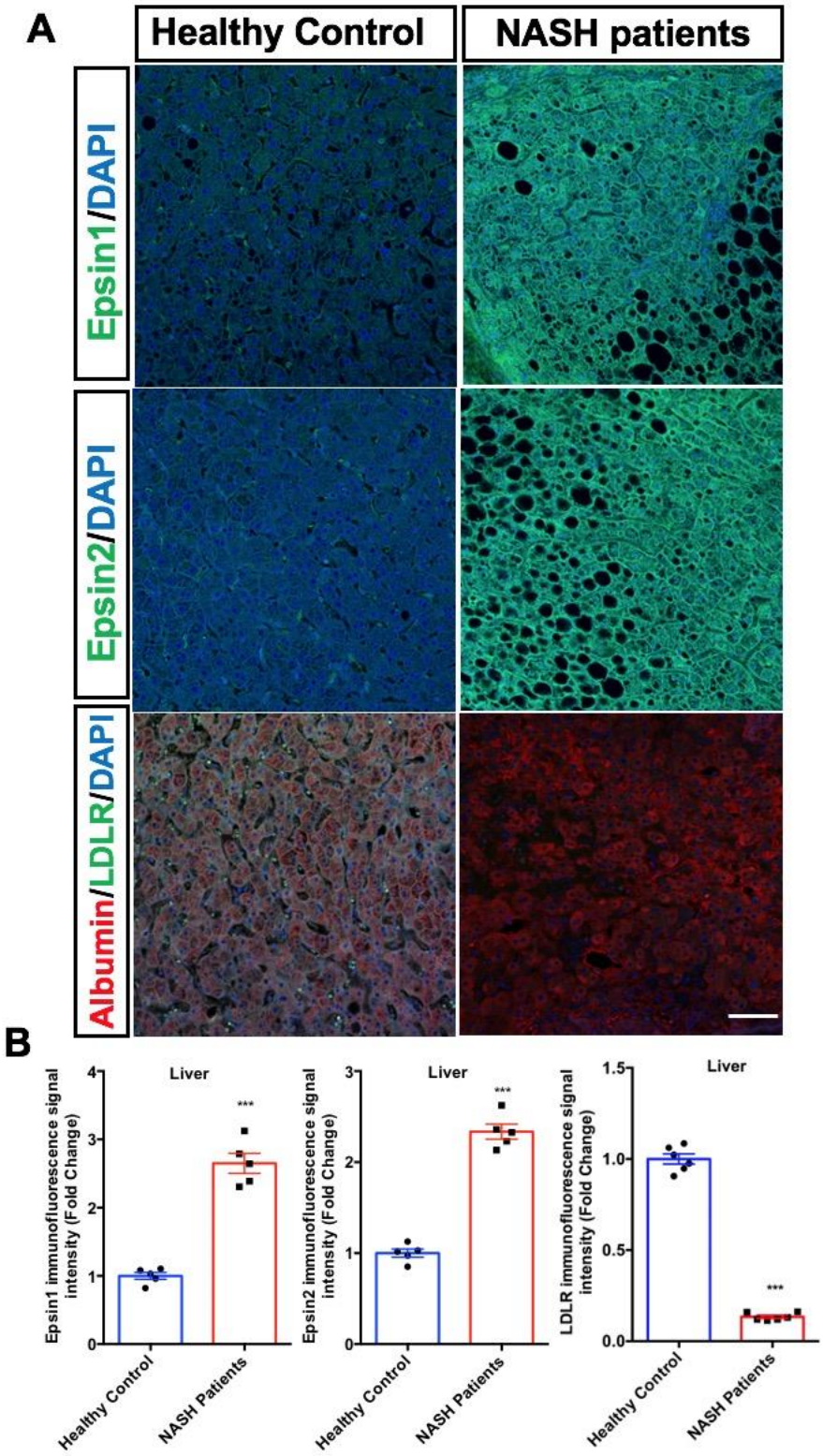

1633

1634
1635 **Fig.S4**

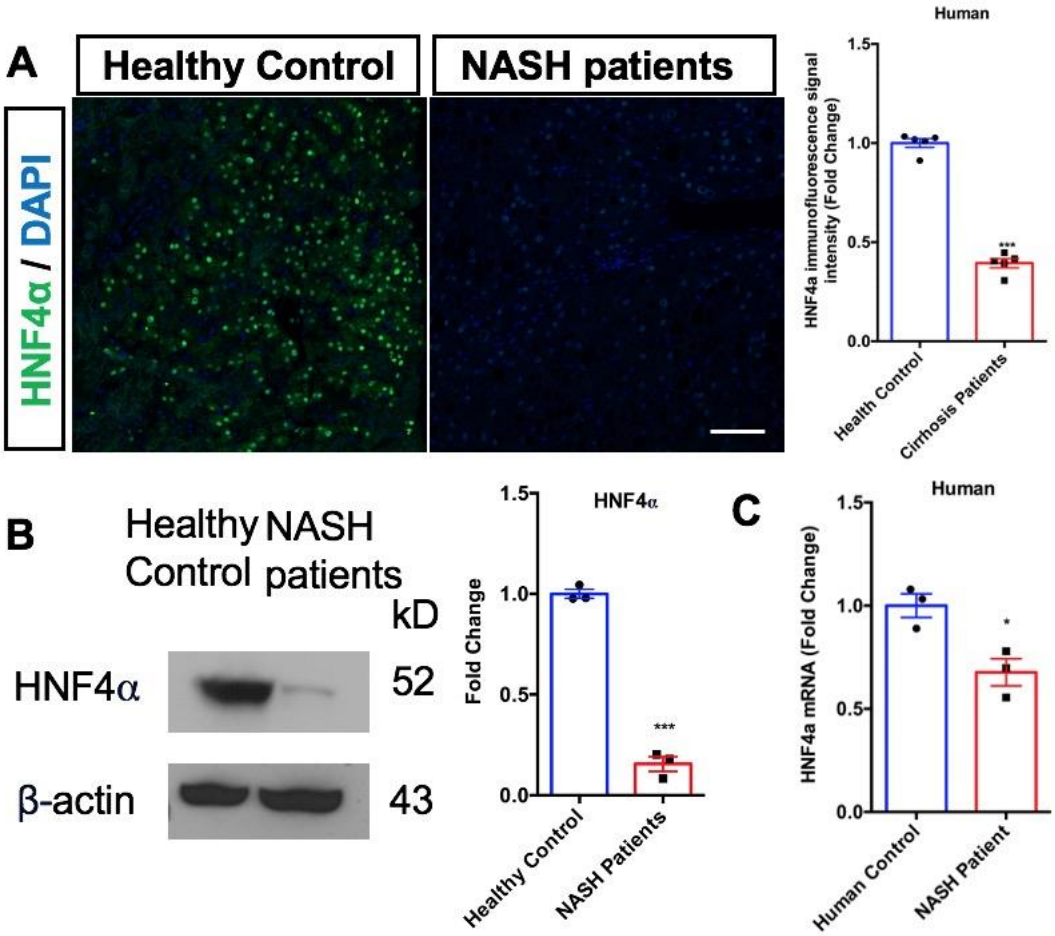

1636
1637
1638
1639
1640
1641
1642
1643
1644
1645
1646
1647
1648
1649
1650
1651
1652
1653
1654

Fig.S5

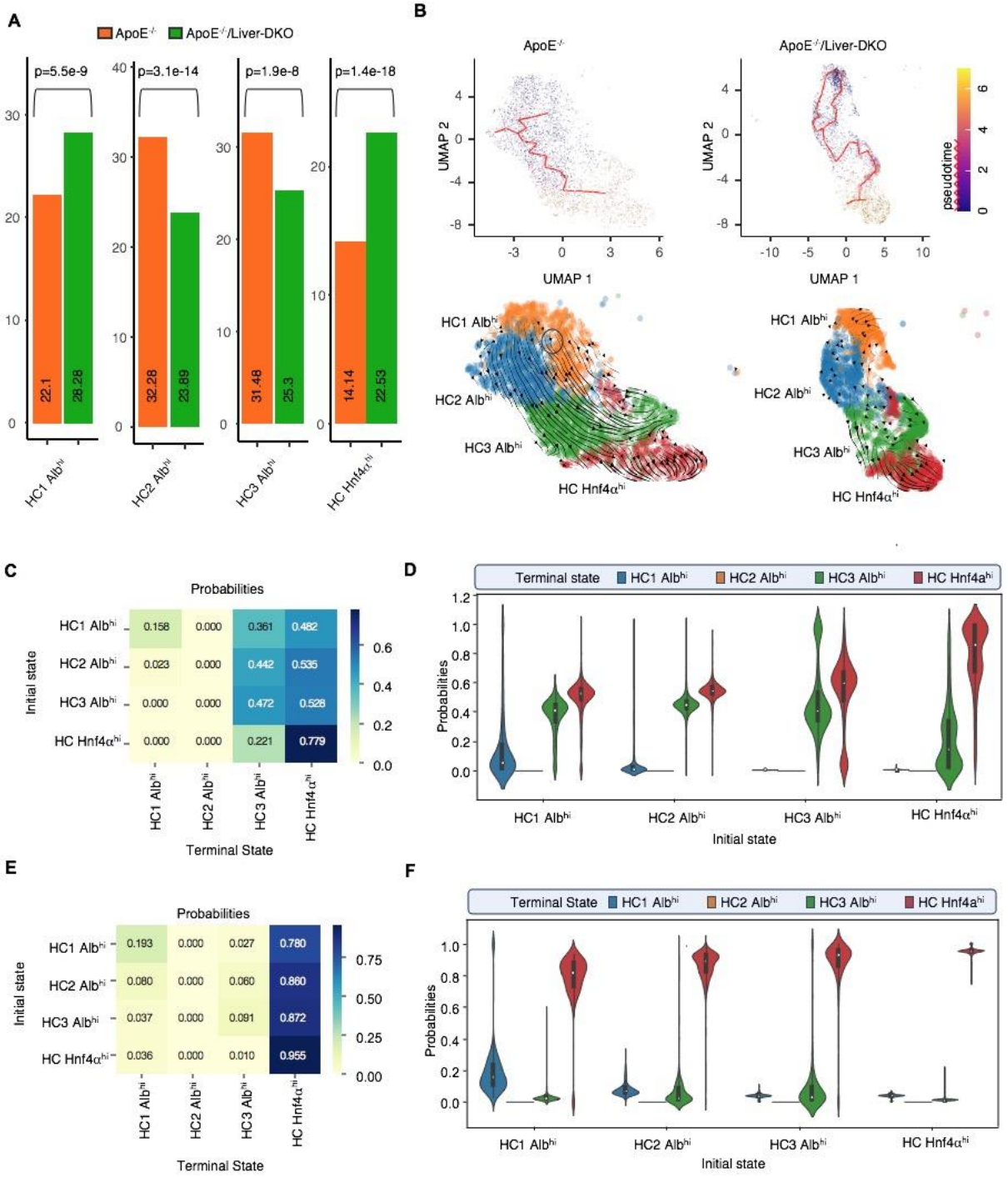
A
ApoE-/-
ApoE-/-/Liver-DKO
p=5.5e-9
p=3.1e-14
p=1.9e-8
p=1.4e-18
22.1
28.28
32.28
23.89
31.48
25.3
14.14
22.53
HC1 Alb^hi
HC2 Alb^hi
HC3 Alb^hi
HC Hnf4α^hi
B
ApoE-/-
ApoE-/-/Liver-DKO
UMAP 1
UMAP 2
pseudotime
C
Probabilities
Initial state
Terminal State
D
Terminal state
Probabilities
Initial state
E
Probabilities
Initial state
Terminal State
F
Terminal State
Probabilities
Initial state

Fig.S6

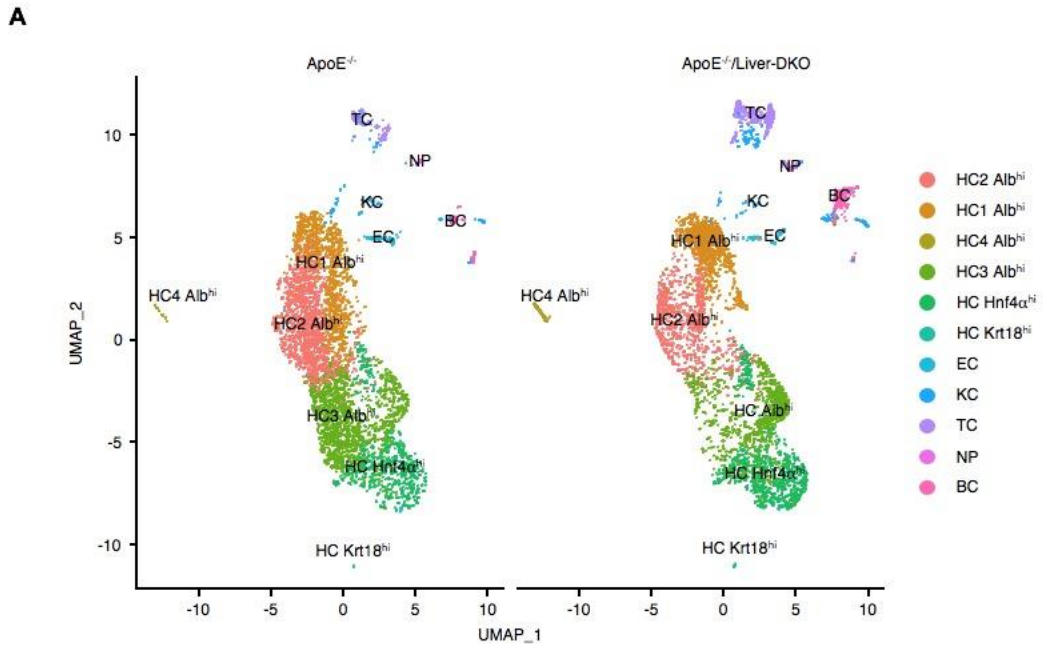
A
ApoE-/-
ApoE-/-/Liver-DKO
TC
NP
KC
BC
EC
HC1 Alb^hi
HC4 Alb^hi
HC2 Alb^hi
HC3 Alb^hi
HC Hnf4α^hi
HC Krt18^hi
UMAP_2
UMAP_1
HC2 Alb^hi
HC1 Alb^hi
HC4 Alb^hi
HC3 Alb^hi
HC Hnf4α^hi
HC Krt18^hi
EC
KC
TC
NP
BC

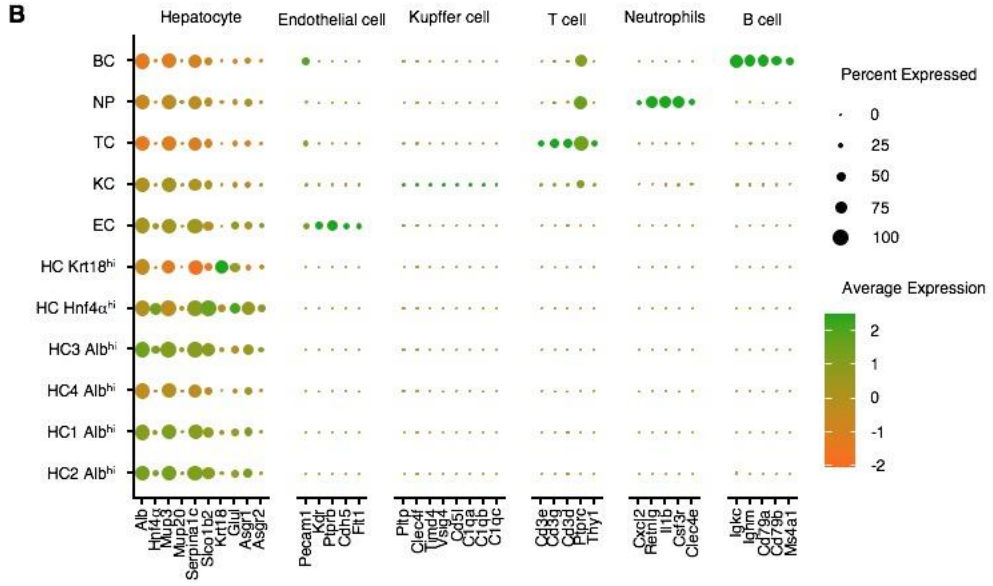
B
Hepatocyte
Endothelial cell
Kupffer cell
T cell
Neutrophils
B cell
BC
NP
TC
KC
EC
HC Krt18^hi
HC Hnf4α^hi
HC3 Alb^hi
HC4 Alb^hi
HC1 Alb^hi
HC2 Alb^hi
Alb
Hnf4α
Mup3
Mup20
Serpina1c
Slco1b2
Krt18
Glul
Asgr1
Asgr2
Pecam1
Kdr
Ptprb
Cdh5
Flt1
Ptprb
Clec4f
Timd4
Vsig4
Cd5l
C1qa
C1qb
C1qc
Cd3e
Cd3g
Cd3d
Ptprc
Thy1
Cxcl2
Retnlg
Il1b
Csf3r
Clec4e
Igkc
Igfm
Cd79a
Cd79b
Ms4a1
Percent Expressed
0
25
50
75
100
Average Expression
2
1
0
-1
-2

1675
1676 **Fig.S7**

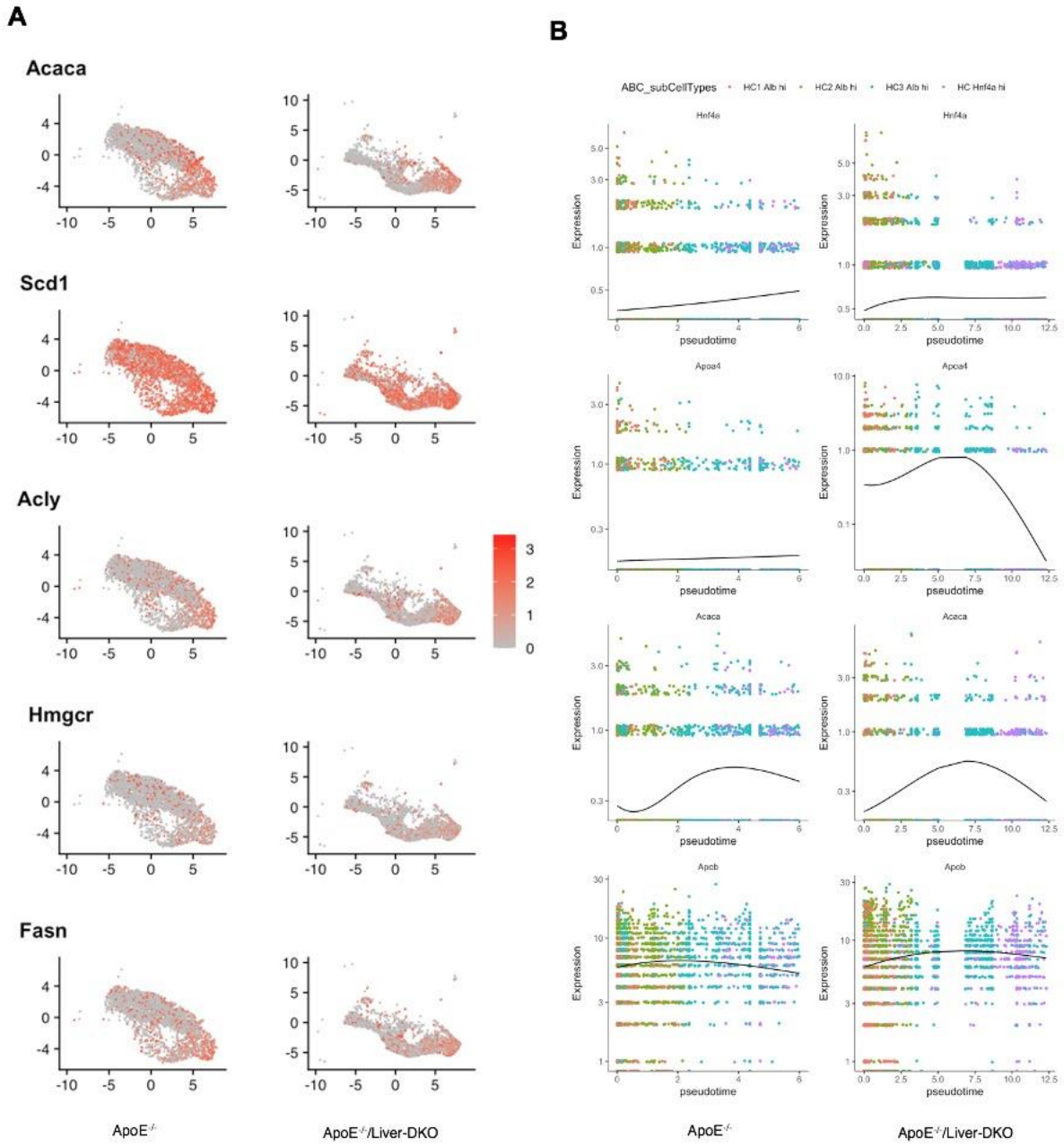

1677
1678
1679
1680
1681
1682
1683
1684
1685
1686

Fig.S8

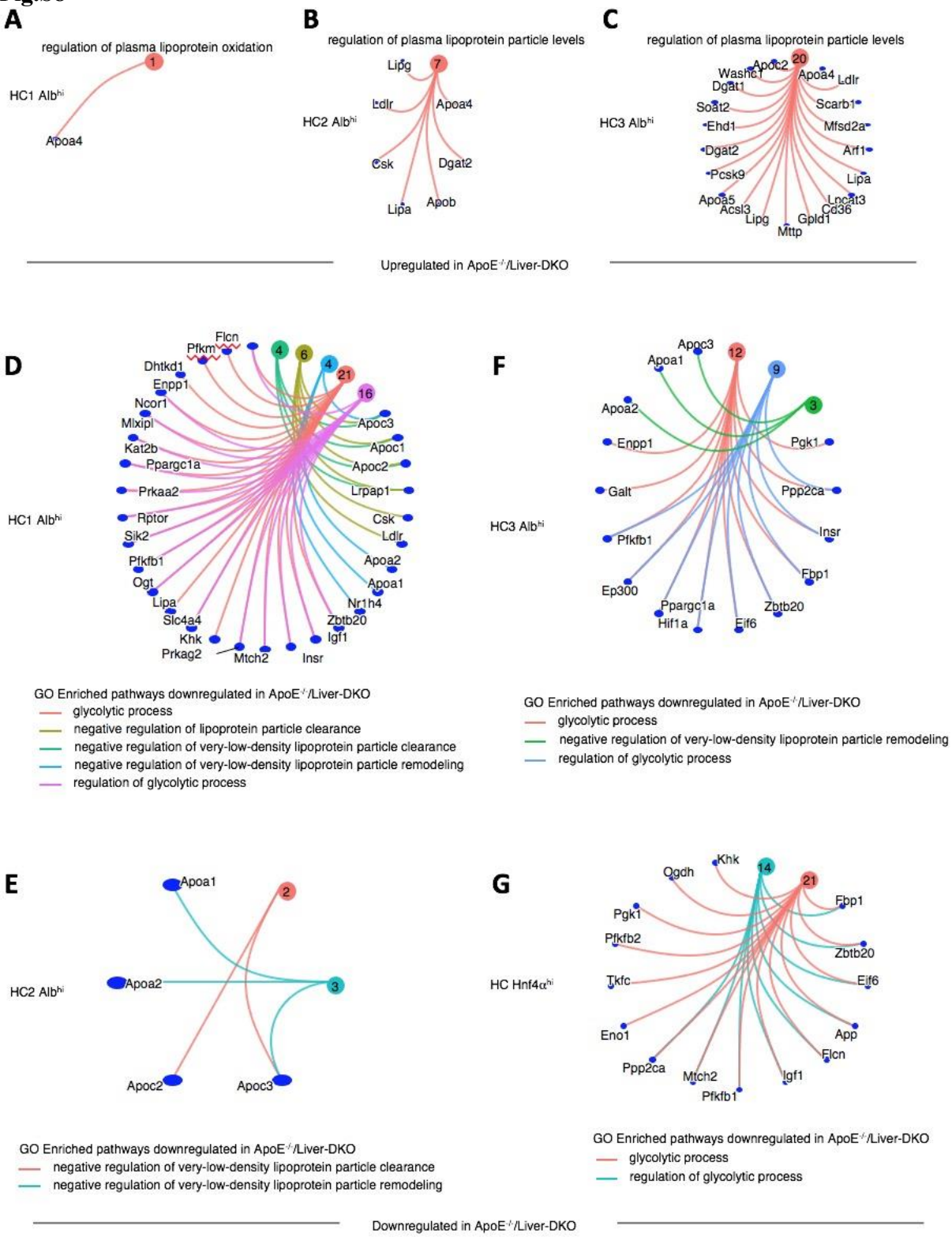
A
regulation of plasma lipoprotein oxidation
HC1 Alb^{hi}
Apoa4
B
regulation of plasma lipoprotein particle levels
HC2 Alb^{hi}
Lipg
Ldlr
Apoa4
Csk
Dgat2
Lipa
Apob
C
regulation of plasma lipoprotein particle levels
HC3 Alb^{hi}
Washc1
Apoc2
Apoa4
Ldlr
Dgat1
Soat2
Scarb1
Ehd1
Mfsd2a
Dgat2
Arf1
Pcsk9
Lipa
Apoa5
Lpcat3
Acsl3
Cd36
Lipg
Gpld1
Mttp
Upregulated in ApoE$^{-/-}$/Liver-DKO
D
HC1 Alb^{hi}
Flcn
Pfkm
Dhtkd1
Enpp1
Ncor1
Mlxipl
Kat2b
Ppargc1a
Prkaa2
Rptor
Sik2
Pfkfb1
Ogt
Lipa
Slc4a4
Khk
Prkag2
Mtch2
Insr
Igf1
Zbtb20
Nr1h4
Apoa1
Apoa2
Ldlr
Csk
Lrpap1
Apoc2
Apoc1
Apoc3
GO Enriched pathways downregulated in ApoE$^{-/-}$/Liver-DKO
glycolytic process
negative regulation of lipoprotein particle clearance
negative regulation of very-low-density lipoprotein particle clearance
negative regulation of very-low-density lipoprotein particle remodeling
regulation of glycolytic process
F
HC3 Alb^{hi}
Apoc3
Apoa1
Apoa2
Enpp1
Galt
Pfkfb1
Ep300
Ppargc1a
Hif1a
Eif6
Zbtb20
Fbp1
Insr
Ppp2ca
Pgk1
GO Enriched pathways downregulated in ApoE$^{-/-}$/Liver-DKO
glycolytic process
negative regulation of very-low-density lipoprotein particle remodeling
regulation of glycolytic process
E
HC2 Alb^{hi}
Apoa1
Apoa2
Apoc2
Apoc3
GO Enriched pathways downregulated in ApoE$^{-/-}$/Liver-DKO
negative regulation of very-low-density lipoprotein particle clearance
negative regulation of very-low-density lipoprotein particle remodeling
G
HC Hnf4α^{hi}
Khk
Ogdh
Pgk1
Pfkfb2
Tkfc
Eno1
Ppp2ca
Mtch2
Pfkfb1
Igf1
Flcn
App
Eif6
Zbtb20
Fbp1
GO Enriched pathways downregulated in ApoE$^{-/-}$/Liver-DKO
glycolytic process
regulation of glycolytic process
Downregulated in ApoE$^{-/-}$/Liver-DKO

Fig.S9

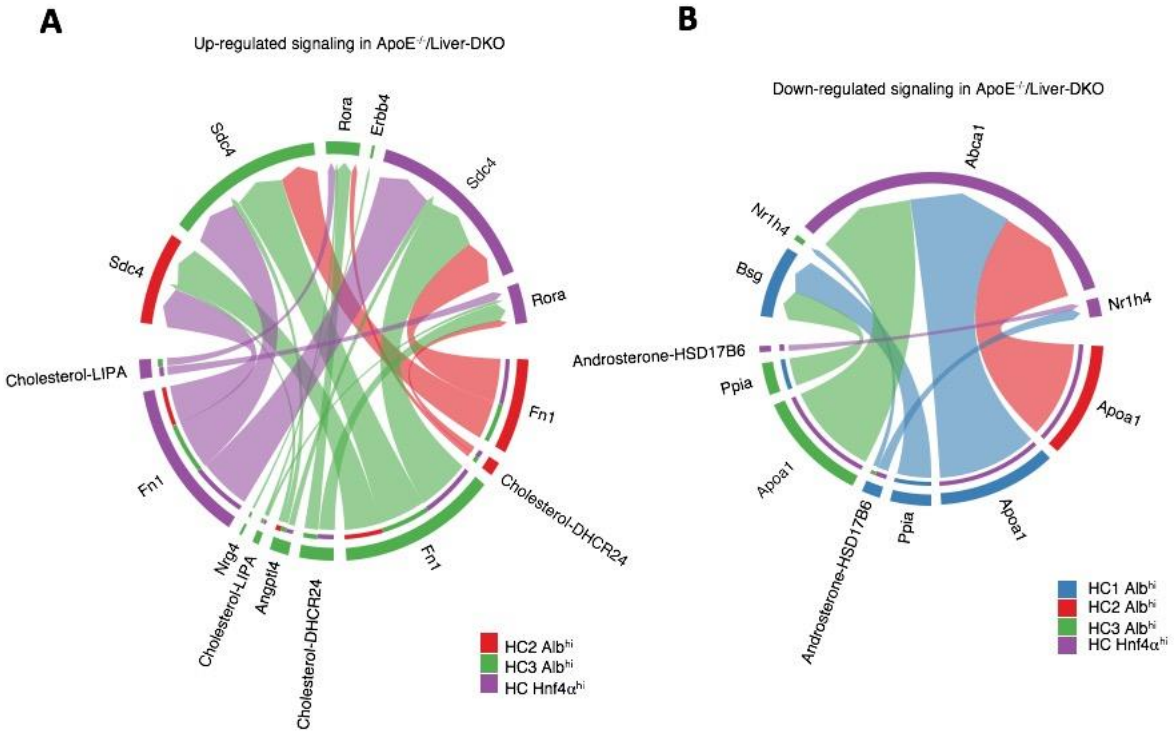
A
Up-regulated signaling in ApoE-/-/Liver-DKO
Sdc4
Rora
Erbb4
Sdc4
Sdc4
Rora
Cholesterol-LIPA
Fn1
Fn1
Cholesterol-DHCR24
Nrg4
Cholesterol-LIPA
Angptl4
Cholesterol-DHCR24
Fn1
HC2 Alb^hi
HC3 Alb^hi
HC Hnf4α^hi
B
Down-regulated signaling in ApoE-/-/Liver-DKO
Abca1
Nr1h4
Bsg
Nr1h4
Androsterone-HSD17B6
Ppia
Apoa1
Apoa1
Androsterone-HSD17B6
Ppia
Apoa1
HC1 Alb^hi
HC2 Alb^hi
HC3 Alb^hi
HC Hnf4α^hi

Fig.S10

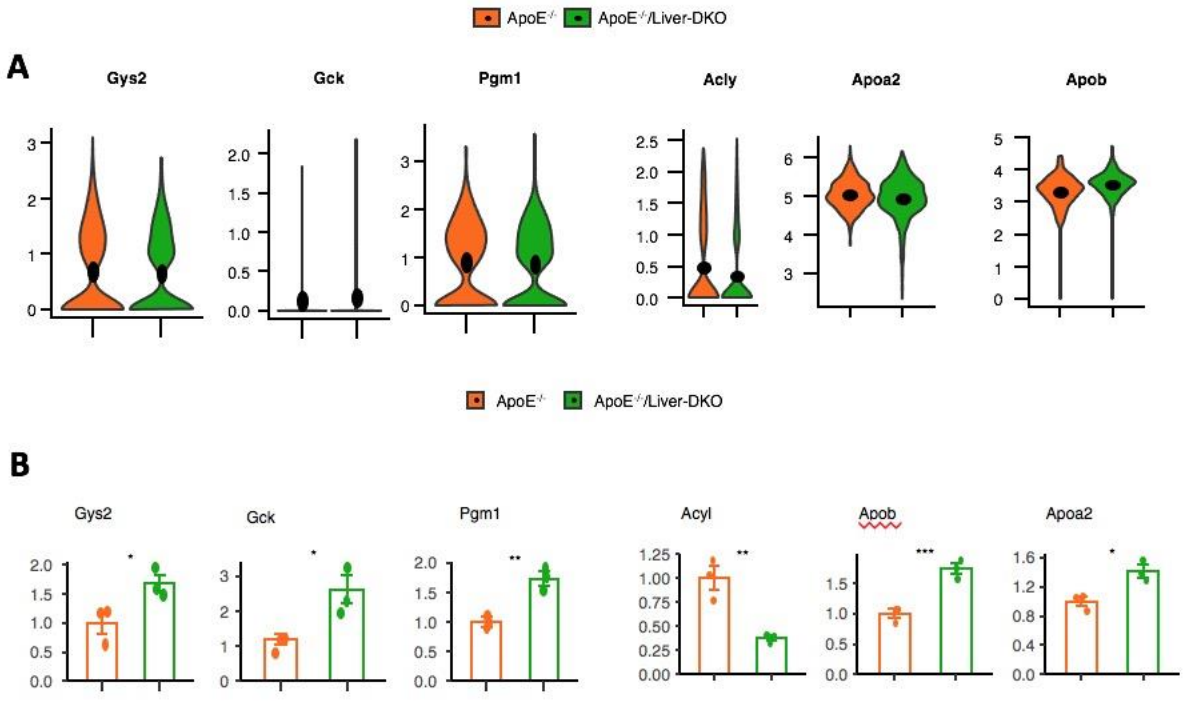
ApoE-/-
ApoE-/-/Liver-DKO
A
Gys2
Gck
Pgm1
Acly
Apoa2
Apob
ApoE-/-
ApoE-/-/Liver-DKO
B
Gys2
Gck
Pgm1
Acyl
Apob
Apoa2

1747
1748 **Fig.S11**

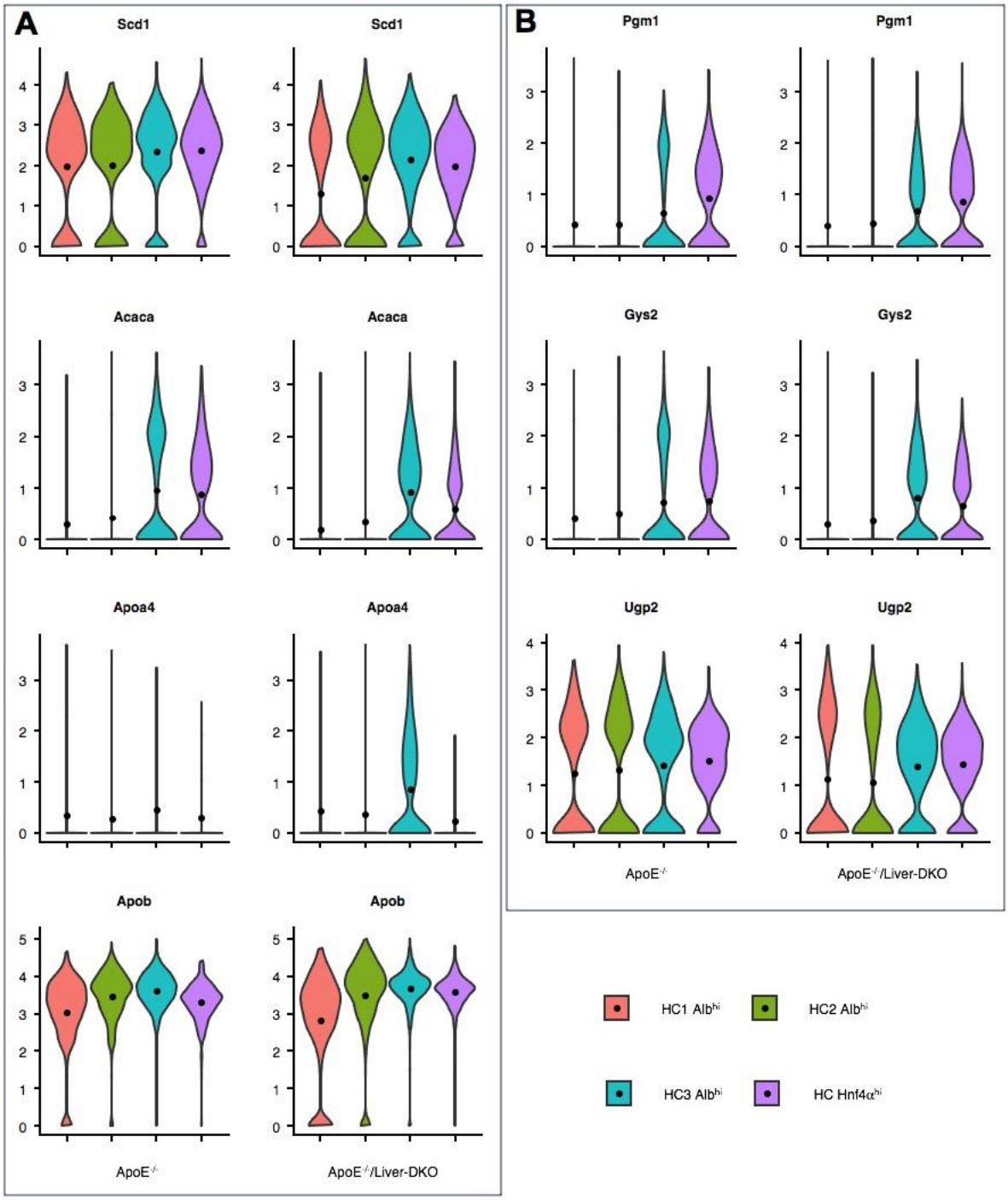

1749
1750
1751
1752
1753
1754
1755

Fig.S12

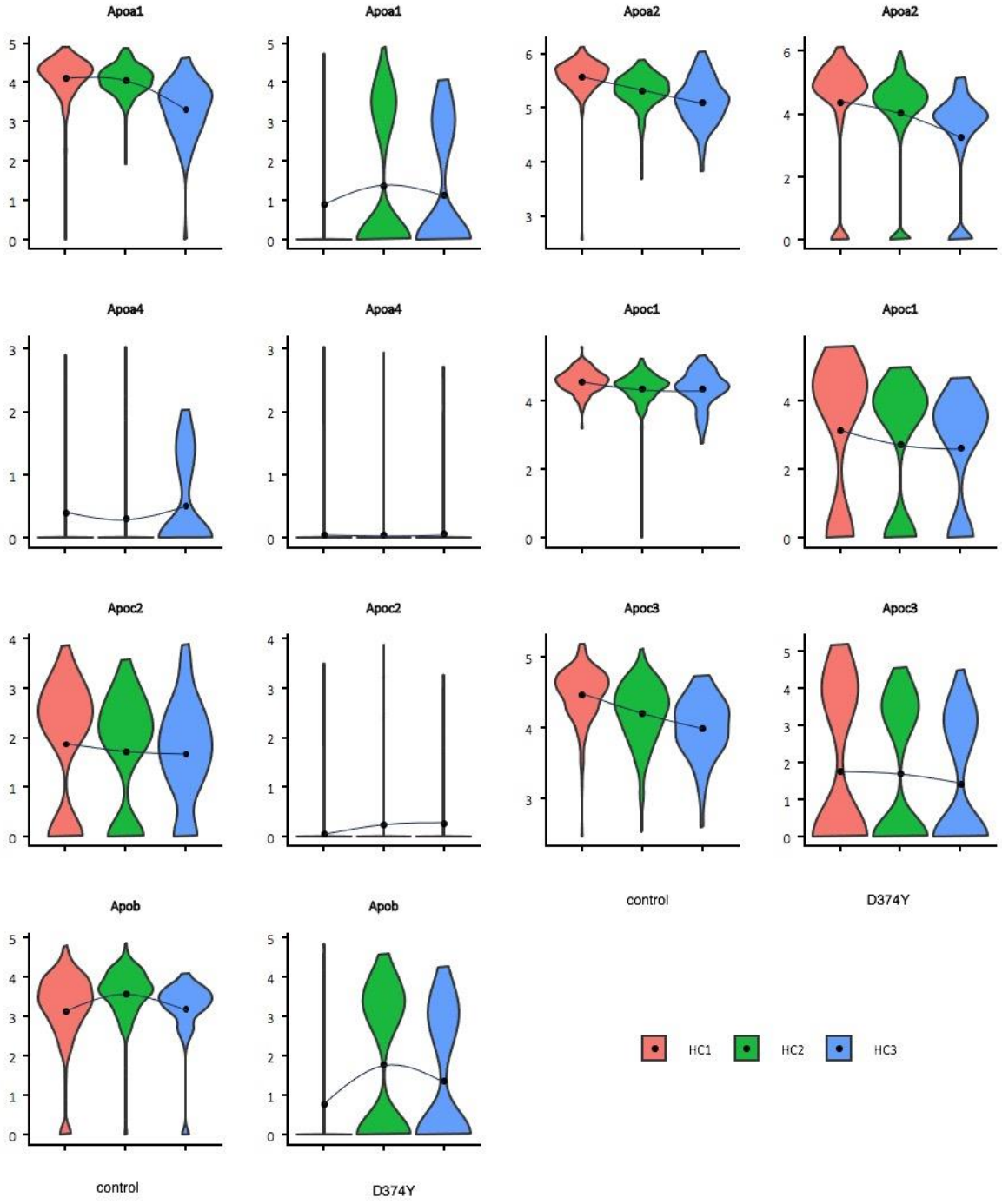
Apoa1
Apoa1
Apoa2
Apoa2
Apoa4
Apoa4
Apoc1
Apoc1
Apoc2
Apoc2
Apoc3
Apoc3
Apob
Apob
control
D374Y
control
D374Y
HC1
HC2
HC3

1764
1765 **Fig.S13**

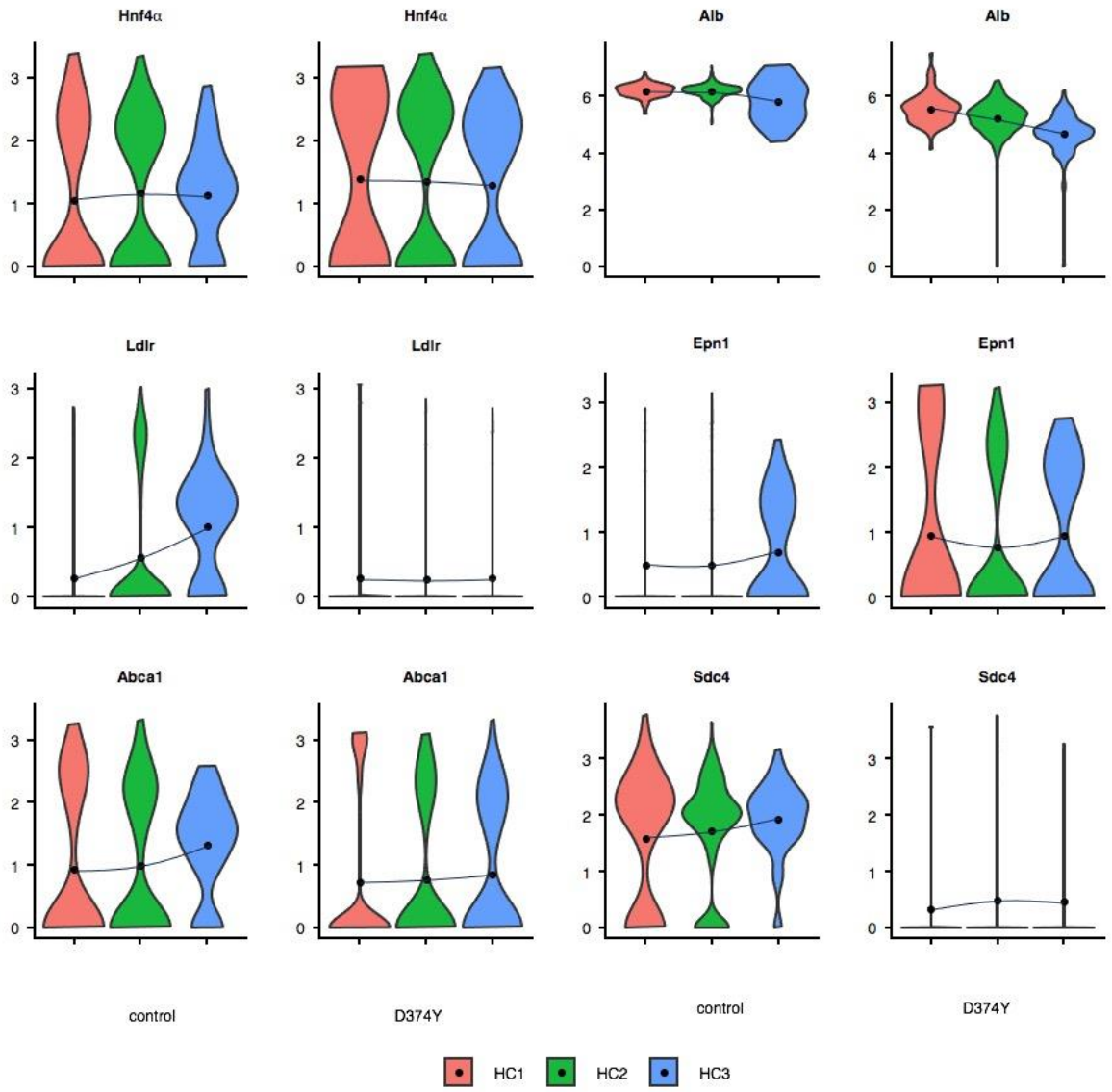

1766
1767
1768
1769
1770
1771
1772
1773
1774
1775
1776
1777
1778

1779
1780 **Fig.S14**

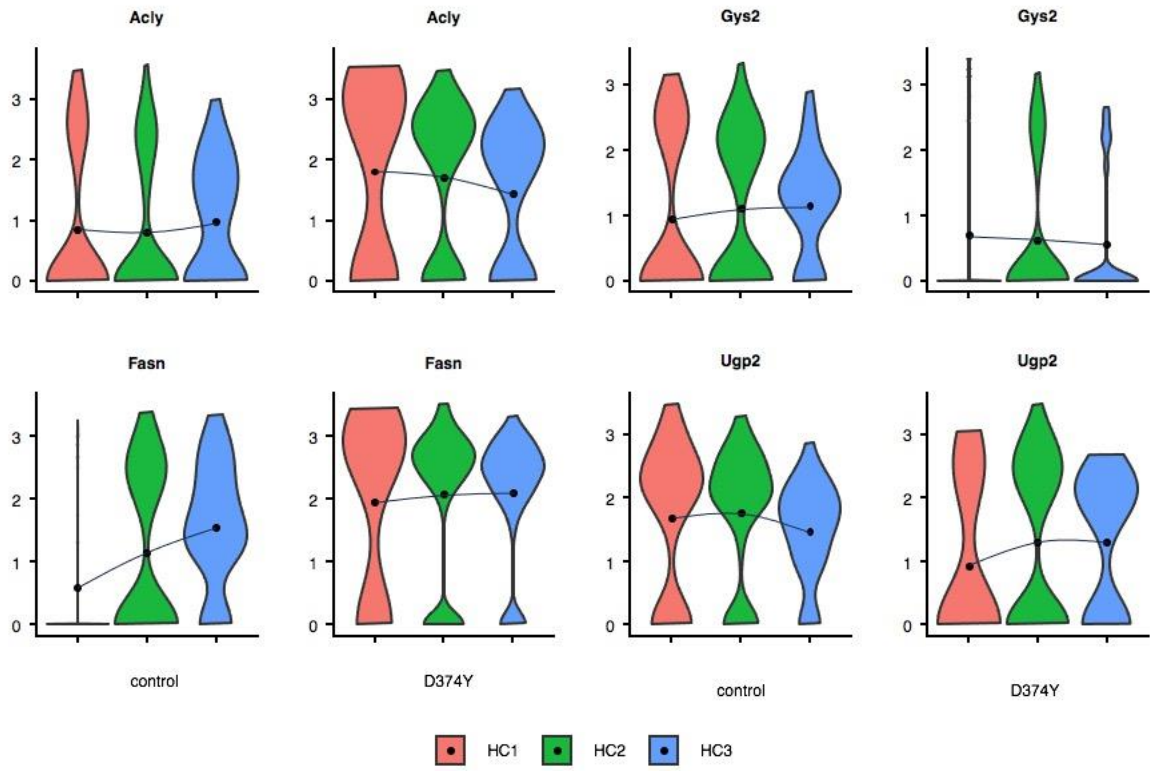

1781